2014-09-30

Performance of the Solar Thermal Hot Water System at the Southland Leisure Centre

Athaudage Dona, Nadeekangani

UNIVERSITY OF CALGARY

Performance of the Solar Thermal Hot Water System at the Southland Leisure Centre

by

Athaudage Dona Nadeekangani

A THESIS

SUBMITTED TO THE FACULTY OF GRADUATE STUDIES

IN PARTIAL FULFILMENT OF THE REQUIREMENTS FOR THE

DEGREE OF MASTER OF SCIENCE IN MECHANICAL ENGINEERING

GRADUATE PROGRAM IN MECHANICAL ENGINEERING

CALGARY, ALBERTA

SEPTEMBER, 2014

Abstract

Solar thermal water heating is a major application of renewable energy. Canada's renewable energy utilization is very low in fulfilling its hot water demands. Though Alberta has a good solar energy potential, it is seldom used. Possibly the biggest application is the solar thermal system with 150 evacuated tube collectors (ETCs) which was installed by the City of Calgary on the roof of the Southland Leisure Centre (SLC). The system pre-heats the swimming pool water. Expansions of City of Calgary's solar thermal water heating may well depend on the performance of the SLC system.

Important parameters of two collectors in the system were measured to compute efficiency during seven months. Among them, global solar radiation indicated the total energy received by the collectors. The wind speed and direction used to assess the convective heat transfer losses. Panel inlet and outlet temperatures and flow rate of working fluid provided the useful energy absorbed. Ambient temperature was recorded to estimate temperature rise of the collector. A data logger monitored the solar radiation and wind while a special purpose monitoring system collected temperatures and flow rate.

The efficiency of the collectors was computed based on steady and unsteady state energy balances. Experiment data were compared with the efficiency data measured by the Fraunhofer Institute (Germany) for the same collector type according to the appropriate international standard. Performance indicators were unsteady efficiency and the ratio of Unsteady/Steady terms in the energy equation. Unsteady state efficiency was very low compared to the international test standard and the ratio of Unsteady/Steady was very high. It was concluded that the operating efficiency of collectors is lower than the expected efficiency and the unsteady factors are dominant in the system.

Acknowledgements

I would like to thank my supervisor Dr. David Wood for giving me the opportunity to conduct this important research with City of Calgary, ENMAX and Southland Leisure Centre. With his valuable guidance and the financial support during my studentship I was able to complete this research successfully.

I also greatly appreciate former City of Calgary engineer Mr. Abbas Muhammad and current Engineer (Lead Green Associate) Tyler Yong, the maintenance staff of Southland Leisure Centre (Gary Lighfoot, Randy Spark, Fred) who made experiment continue for nearly 2 years. The Intern student Tiffany Ganster supported the data analysis in a difficult situation. The kind donation received from Siemens Canada, Building Technologies Division also resolved a costly installation and their prompt technical staff was always supportive. Thank you very much for all, including who did not mentioned by the name.

This research was funded by City of Calgary and ENMAX Corporation under Renewable Energy Chair Program.

Dedication

To my son and husband

Table of Contents

List of Tables

List of Figures and Illustrations

List of Symbols and Abbreviations

Symbol	Definition
A	Area of collector (m^2)
C_1	Heat loss coefficient at (T_m-T_a)=0
C_2	Temperature dependence of heat losses
C_3	Wind speed dependence of heat losses
C_4	Long wave irradiance dependence of heat losses
C_5	Effective thermal capacitance (kJ/K)
C_6	Wind speed dependence of zero loss efficiency
C_p	Specific heat capacity of working fluid (kJ/K.kg)
F'	Collector efficiency factor
$(\tau\alpha)_{en}$	Product of effective transmittance and absorptance at normal incidence
G	Global solar radiation on collector area
I_b	Beam radiation (W/m^2)
I_d	Diffuse radiation (W/m^2)
I	Global solar radiation (W/m^2)
$K_{\theta b}$	Incidence angle modifier for beam radiation
$K_{\theta d}$	Incidence angle modifier for diffuse radiation
$K_{\theta l}$	Incidence angle modifier for longitudinal component of beam radiation
$K_{\theta t}$	Incidence angle modifier for transverse component of beam radiation
$K_{\tau\alpha}(\theta)$	Incidence angle modifier

Symbol	Definition
$\dot{m}$	Mass flow rate of working fluid (kg/s)
$(MC)_e$	Effective heat transfer coefficient of collector structure
$\dot{Q}$	Rate of energy gain by working fluid
Q_u	Heat Gain (W/m^2)
T_a	Ambient temperature (°C)
$\overline{T}_a$	Absolute value of ambient temperature (K)
T_{abs}	Absorber temperature
T_m	Mean temperature of working fluid (°C)
T_{in}	Inlet temperature of manifold (°C)
T_{out}	Outlet temperature of manifold (°C)
u	Wind speed (m/s)
U_L	Convection coefficient
ΔU	Internal energy generation within the system

Greek Symbol	Definition
θ	Angle of incidence (°)
σ	Stefan Boltzmann constant
dT_m / dt	First order time derivative of mean temperature of working fluid
η	Efficiency of collector
η_0	Efficiency of collector at zero loss
η_{SS}	Efficiency of collector at steady state

Greek Symbol	Definition
η_{US}	Efficiency of collector at unsteady state
ε	Emissivity of glass
ϕ	Wind direction

Abbreviation	Definition
AB	Alberta
DHW	Domestic Hot Water
DMax-Rad	Daily Maximum Radiation
DTR	Daily Total Radiation
ETC	Evacuated Tube Collector
FPC	Flat Plate Collector
GHG	Green House Gas
HP ETC	Heat Pipe Evacuated Tube Collector
MAv-Rad	Monthly Average Radiation
SLC	Southland Leisure Centre
WG	Water in Glass

Chapter One: **INTRODUCTION**

1.1 Background

Solar energy is the radiant light and heat emitted from the sun. It is a source of energy and a promising alternative to fossil fuel based energy. Vast amount of freely available energy (wind energy, bio energy, and hydro energy) is created from solar energy and ranges of technologies are available to harness it. Solar energy can be harnessed either as a source of thermal energy when using solar thermal collectors, or direct electricity generation when using photovoltaic modules (Ghosh & Prelas, 2011).

The specific system studied in this research is a "solar thermal system". Solar thermal technology converts the sun's energy to heat (thermal energy) and its applications are hot water production, cooling and electricity (Simon & Aaron, 2008). Solar thermal systems have advantages compared to fossil fuel. They are 1) reduced utility bills by cutting fuel required to heat water/fluids, 2) reduced carbon footprint by reducing the amount of carbon-based greenhouse gases, 3) produce hot water even in winter for cold countries (Simon & Aaron, 2008).

Solar thermal collectors are the devices used for capturing solar radiation and transferring heat to the water or other heat transfer media in the system. Solar thermal collectors are available either in concentrating or non-concentrating formats (Kalogirou, 2014). Most commonly used non-concentrating types of collectors are unglazed, glazed flat-plate, and evacuated tube solar collectors (ETCs) (Walker, 2013). Parabolic trough collector is a concentrating type collector that uses tracking mounts, and focusing mirrors to concentrate solar energy (Walker, 2013).This study focuses on one category of ETCs, which is known as heat-pipe evacuated tube collector (HP ETC).

1.1.1 *Sun and Solar Radiation*

The sun is the source of solar energy and it is comprised of hot gaseous matter and measure 1.39×10^{9} m in diameter and 1.5×10^{11} m away from earth (Duffie & Beckman, 2013). Its interior temperature is about 15×10^{6} K (about 27×10^{6} ° F) (Duffie & Beckman, 2013). The fusion reaction in the sun releases the energy (high-energy gamma radiation) while forming helium atoms by combining two hydrogen atoms (Ghosh & Prelas, 2011). Solar radiation, which reaches the earth, is electromagnetic radiation (Ghosh & Prelas, 2011). The amount of solar energy reaching an area of a specific location on the surface of the earth at a specific time is called "insolation" (Ghosh & Prelas, 2011). The highest value of the insolation possible on the earth's surface is about $1000 W/m^2$ (Ghosh & Prelas, 2011) on a horizontal surface, on a clear day when sun is directly overhead. In later parts of the thesis, "solar radiation" will be used as a synonym for "insolation".

Incoming solar radiation that hits the upper atmosphere is partially reflected back to space while clouds, ocean and the earth absorb the rest. Total solar radiation that reaches a point on earth comprise of three components. The solar radiation that directly received on the earth is called the direct radiation and the radiation comes after scattering by air, dust, water, etc., is diffuse radiation (Duffie & Beckman, 2013). Some radiation hits the ground and reflects. This is called ground reflected radiation (Duffie & Beckman, 2013). The sum of the three refers to as global radiation (I). Figure 1.1 shows the each component of radiation.

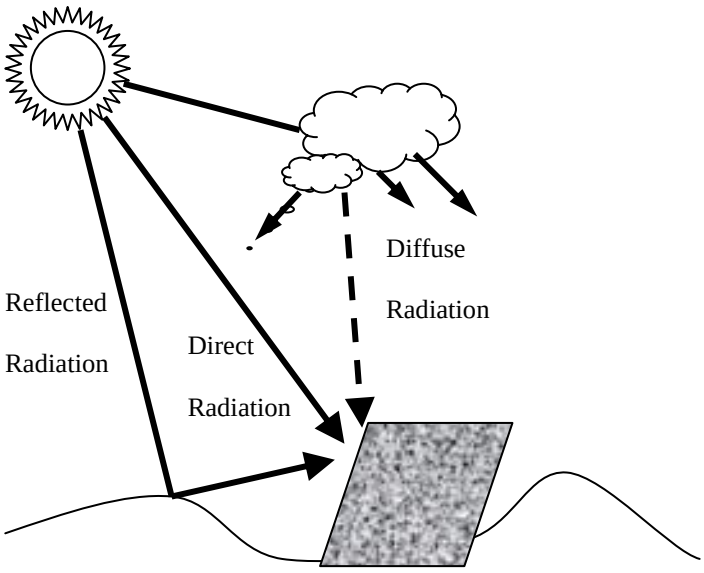

Figure 1.1: Direct, Diffuse and Reflected Radiation, Reproduced from (NREL,1992), Retrieved March 6, 2014 from: http://www.nrel.gov/docs/legosti/old/4856.pdf

When the incoming radiation hits the surface of an object it can only be reflected, transmitted, or absorbed by the surface. Three fractions are defined relative to the incoming radiation: reflectivity (ρ), transmissivity (τ) and absorptivity (α) and are used to represent the amount of radiation that reflected, transmitted and absorbed respectively (Duffie & Beckman, 2013). Another property of surface is the emissivity, that is the ability of the object to emit the received energy as thermal energy when compared to a blackbody at same temperature, and it is denoted by ε (Duffie & Beckman, 2013). These fractions and property will be used in chapter 2 for defining collector efficiency and in section 1.2, they will be related for a solar collector.

Another factor that limits the solar availability on earth surface is the relative motion of the earth. The relative motion of sun and earth causes for two effects. That is 1) the period of solar radiation received during a day, 2) the seasonal variation over the year.

Generally, during the day, more solar radiation received at midday than either during early morning or late afternoon. However, during the year, the amount of solar energy arriving at the earth's surface is different in different seasons. This seasonal effect or the amount of solar radiation received in different seasons varies with the geographical location. Therefore, the regions closest to equator receive highest solar radiation than the other areas and the seasonal variation over the year is low. However, high latitude parts of the earth including Canada experience pronounced seasonal variations (Four seasons) as well as daylight variations (long daytime in summer and short daytime in winter). This study will only focus on Canada's climate conditions and the solar availability.

Figure 1.2 describes the mean daily global insolation (MJ/m^2, kWh/m^2) in Canada and Alberta. According to Figure 1.2 the annual global insolation received by Calgary is about 4.2 kWh/m^2 to 5 kWh/m^2. (This was estimated based on annual global insolation at closest city to Calgary, Edmonton)

Also Canadian Forest Service, CanmetENERGY Photovoltaic systems group (2013) showed that the monthly global insolation (approximately) received by Calgary in June is 5.8 kWh/m^2 to 6.7 kWh/m^2, in July and August it is 5 kWh/m^2 to 5.8 kWh/m^2, and in Dec it is 2.5 kWh/m^2 to 3.3 kWh/m^2. In Jan and Feb it ranges from 4.2 kWh/m^2 to 5 kWh/m^2 and in March it is 5 kWh/m^2 to 5.8 kWh/m^2.According to (Canadian Forest Service, CanmetENERGY Photovoltaic systems group, 2013) insolation map, Calgary receives high insolation level compared to the rest of Canada.

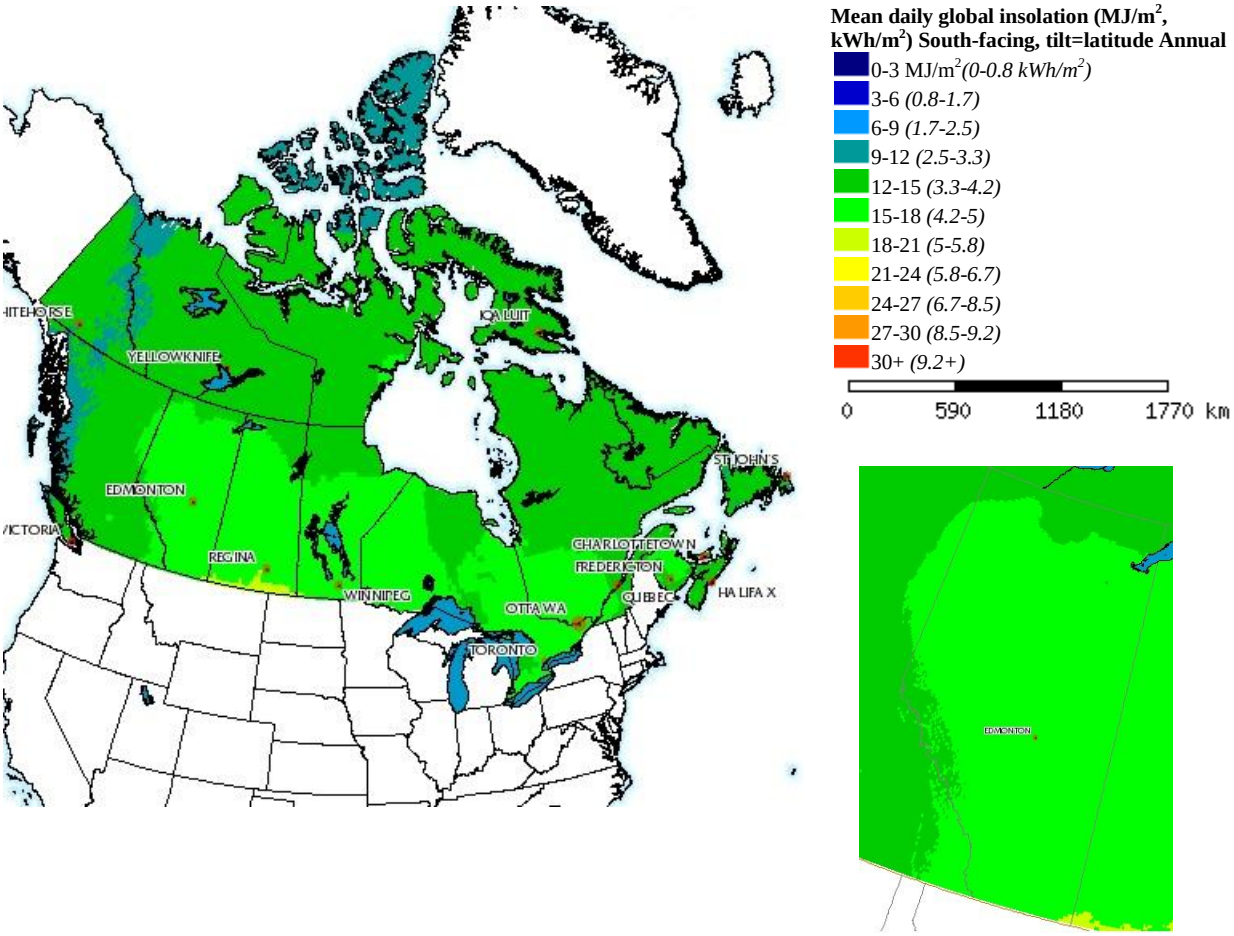

Alberta

Figure 1.2: Annual mean daily global insolation (MJ/m^2, kWh/m^2) in Canada and Alberta (Canadian Forest Service, CanmetENERGY Photovoltaic systems group, 2013). Retrieved October 14, 2013 from http://pv.nrcan.gc.ca/.

1.1.2 *Geometry of Earth and Solar Collector Positioning*

The geometry of earth influences the amount of solar energy absorbed by a solar collector. Solar collectors should be positioned properly to maximize solar gain. Following factors should be considered when positioning the collector.

Variation of Radiation Availability with Earth's Rotation

One earth's rotation around its axis is a day and this defines daytime and nighttime. As the earth rotates, solar radiation at any point on its surface rises to a maximum at solar noon. The solar noon of a location close to equator is around 12 noon and at a location far from equator changes during the year. On a clear day, the maximum solar harvest can be achieved at solar noon. Therefore, maximum solar gain occurs when the collector orientation follows the sun as it passes overhead from East to West during the day and when tracks variation of the sun's altitude. Sun tracking mechanisms are used to follow the sun path. However, tracking systems are expensive and rarely used on solar thermal systems, and will not be considered in this thesis.

Latitude

A solar collector placed on the ground with no tilt will receive the maximum radiation when the sun is directly overhead. However, the amount of radiation received by this collector will vary with the latitude, which is relevant to earth's spherical shape. Tilting to latitude angle will give best year-round performance and angles less than the latitude will provide bias production towards summer, which increases the yearly total radiation. Moreover, angles greater than the latitude will provide bias production in winter, which may be highly desirable in solar thermal systems.

Azimuth Effect

The azimuth is the angle of Sun's position from North (MacNish, 2008). It changes year around and the azimuth angle of Calgary changes from 0^0 to 80^0 (MacNish, 2008). Because of the azimuth angle effect, in northern hemisphere, solar collectors should point due South. Close to equator this can be different and at a location in southern hemisphere (below the equator) should point due north.

Earth Tilt

The earth's rotational axis is tilted at 23.45^0 from the plane of its orbit. At the northern summer solstice, northern half of the earth points towards the sun and has longer day times. In winter solstice, northern hemisphere points away from the sun and it creates shorter day times. Available solar hours changes with this daytime effect.

1.2 Solar Collector Characteristics

Convection and Conduction

Conduction and convection are the main heat transfer modes in the solar collector. These two modes transfer absorbed radiation to the working fluid as well as causes conduction and convection losses that result in lower heat gain by a collector (Duffie & Beckman, 2013). Estimation of heat losses and the amount of heat transferred can be found using analytical techniques as well as experimental methods (Duffie & Beckman, 2013).

The heat loss from solar collector exposed to outside wind is through forced convection. On calm days, the heat loss is through free convection, which is usually much less than forced convection (Duffie & Beckman, 2013).

Absorption, Reflectance, Transmittance

The transmission, reflection and absorption of solar radiation by various parts of a solar collector are important in determining collector performance (Duffie & Beckman, 2013). The transmission, reflection and absorption are functions of the incoming radiation, thickness and material properties (Duffie & Beckman, 2013). These three characteristics apply to the collector glass cover and the absorber (Duffie & Beckman, 2013).

Selective Surface

Solar collectors must have high absorptance for radiation in the solar energy spectrum (Duffie & Beckman, 2013).The absorbing surface should have low thermal losses from short wave radiation and low emittance for long wave radiation (Duffie & Beckman, 2013). A selective surface has high absorptance for short wave radiation and very low emittance for long wave radiation (Duffie & Beckman, 2013). The technology of preparing a selective surface has achieved by coating a substance with desired properties (Duffie & Beckman, 2013). Copper Oxides on Aluminum, Copper Oxide on Copper, Nickel-Zinc coating on galvanized iron are few examples (Duffie & Beckman, 2013).

1.3 Evacuated Tube Solar Collector (ETC)

Evacuated tube collectors are made of parallel rows of transparent glass tubes. Each tube contains an outer glass tube and an inner glass or metal tube attached to an absorber (William & Michael, 2001). Air is removed from the space between the two tubes to form a vacuum. This greatly increases the efficiency when the outside temperature is very cold. So ETCs are applicable for cold climate conditions (William & Michael, 2001).

Evacuated tube collectors have shown that the combination of a selective surface and an effective convection suppressor can result in good performance at high temperatures as well (Kalogirou, 2014).The vacuum envelope reduces convection and conduction losses, so the theses collectors can operate at higher temperatures than flat plate collectors (FPCs) (Kalogirou, 2014). Like FPCs, they collect both direct and diffuse radiation, but their efficiency is higher at low incidence angles (Kalogirou, 2014). This gives ETCs an advantage over flat plate collectors in terms of daylong performance (Kalogirou, 2014). In addition, ETCs can reach over 250 °C and are suitable for medium and high temperature hot water applications (Kalogirou, 2014).

They are available in two different types according to evacuated tube manufacturing technology: glass-glass and glass-metal. Glass- glass ETCs can be further categorized into three classes as direct flow, heat pipe and U-pipe as described by Kalogirou (2014) and William & Michael (2001). These are different from one another by the technology of moving the working fluid. The direct flow ETCs contain the working fluid in the glass tube, which absorbs the solar radiation. The U pipe ETCs have a U shape tube that contains the working fluid inside of glass tube and it absorbs heat (William & Michael, 2001). Heat pipe technology, as used at the Southland Leisure Centre, will be discussed in the next Section. Figure 1.3 shows a U shape and direct flow ETCs.

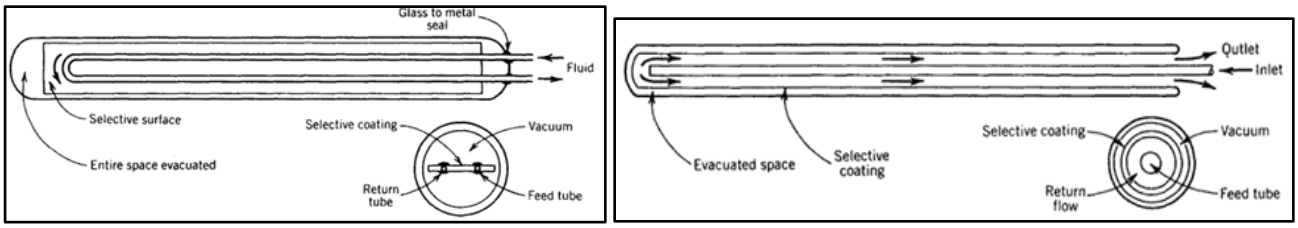

Figure 1.3: U Shape ETC (Left Side) and Direct Flow ETC (Right Side) (William & Michael, 2001)

1.4 Heat Pipe Evacuated Tube Collector (HP ETC)

In a heat pipe evacuated tube collector a sealed copper pipe (heat pipe) is bonded to a copper fin (absorber plate) that fills the evacuated glass tube.

Figure 1.4 a shows the components of a heat pipe evacuated tube. A small copper condenser is attached to the top of each heat pipe. These condensers are inserted into a super insulated heat exchanger chamber in the manifold at the top of the solar collector system (Mahjouri, n.d).

Figure 1.4 b) shows the components of a HP ETC.

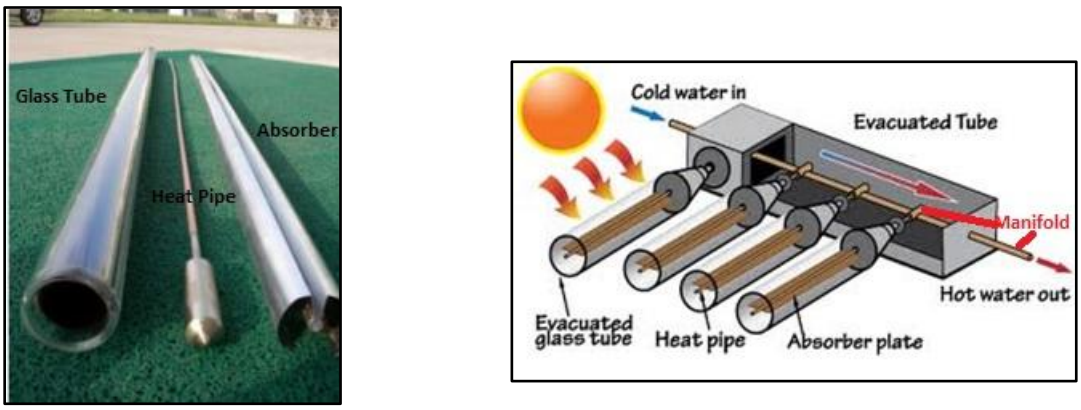

Figure 1.4: a) Inside of Heat Pipe Evacuated Tube (Jiangsu Sunrain Solar Energy, n.d.) (Left), b) Mainfold and Evacuated Tube (United state department of agriculture, n.d.) (Right).

The heat pipe is a closed container consisting of a capillary wick structure and a small amount of vaporizable fluid. The heat pipe employs an evaporating-condensing cycle, which accepts heat from an external source at the evaporator section (Bragg & Reid, n.d.) (Figure 1.5).

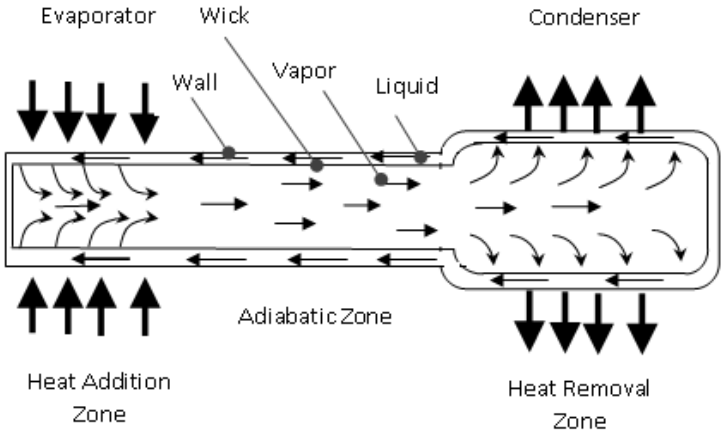

Figure 1.5: Heat Pipe Operation; Reproduced from: Bragg & Reid, (n.d)

This external heat source elevates the heat pipe's liquid to the boiling region (Bragg & Reid, n.d.), (Mahjouri, n.d.). The heat pipe liquid evaporates (latent heat) and then it releases latent heat by condensation at the condenser (heat sink) section. This process is repeated continuously by a gravity return feed mechanism of the condensed fluid back to the evaporator zone. Water, or water/ glycol mixture, flows through the manifold and cools the condenser (Mahjouri, n.d.).

1.5 Solar Thermal Water Heating Systems

Typical solar thermal systems consist of solar collectors, piping system and a storage tank. Solar collector is the main component and it converts solar radiation into heat. Then heat is pumped from the collectors to a heat exchanger using the piping system.

A very commonly used heat transfer media is water and antifreeze (usually Propylene Glycol.) in cold climate like Calgary's. It has low freezing point and the boiling point of a 50/50 mixture of Glycol and water rises sharply as the closed loop is pressurized. The method of pumping can be forced circulation (pump) or natural circulation (thermosyphon) (Simon & Aaron, 2008). Forced circulation systems are called active systems and natural circulation systems are called passive systems. Solar thermal systems are used for different applications such as domestic hot water systems, swimming pool/hot tub-heating systems, and space-heating systems and as combination (combi) systems of above three (Simon & Aaron, 2008).

The system studied in this research is a forced circulation system with heat pipe evacuated tube solar collectors and the application is combination of a swimming pool system and a domestic hot water system.

1.5.1 ***Swimming Pool Systems***

Solar thermal water heating systems are used for swimming pool heating for few reasons. Swimming pools require low water temperatures (29°C to 37°C) that most solar systems are capable of supplying (Bob, n.d.). In addition, solar thermal systems can provide the maximum output of hot water during the summer months when seasonal swimming pools are in use (Bob, n.d.).

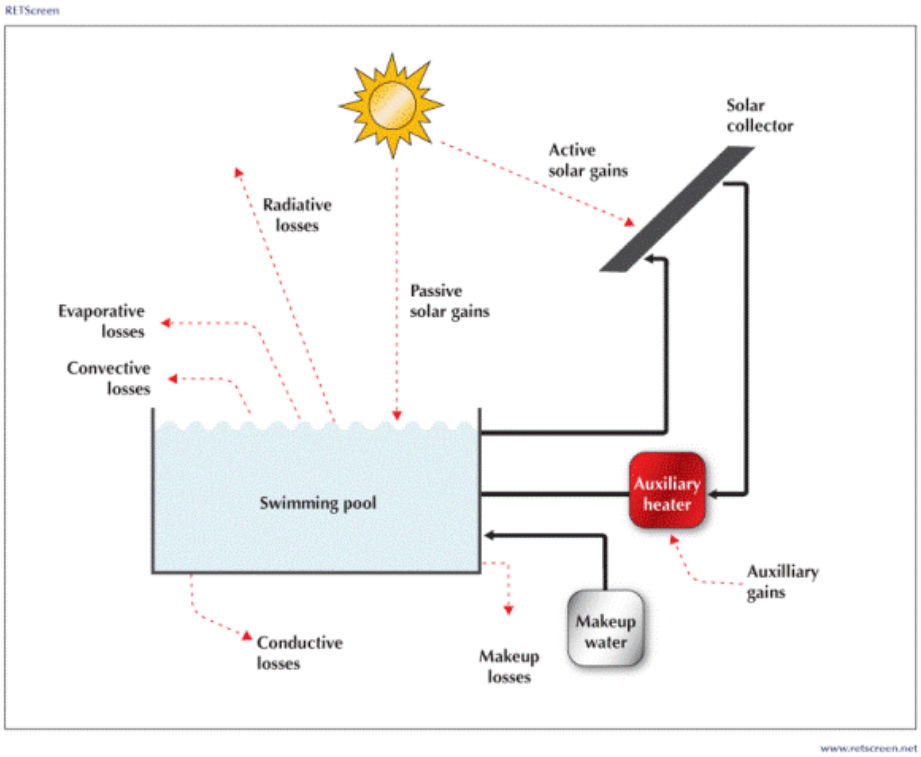

Figure 1.6: Solar Pool Heating System Schematic (RETScreen, 2008)

Solar thermal systems can be used for indoor and outdoor swimming pools (Simon & Aaron, 2008) as well as for small scale and large-scale swimming pools heating. In addition, they can be used as direct water heating or integrated with a heat exchanger. Integrated system with a heat exchanger has two loops and collector side loop consist of a working fluid that absorbs the

heat from the solar collector. Then it carries heat and transfers it to the pool water in the other loop.

1.5.2 *Domestic Hot Water (DHW) System*

Natural Resources Canada (2011) has showed that the domestic water heating energy intensity for Canadian households is 18.3 GJ/household in 2009. Electricity and natural gas are the major fuels use for domestic water heating. Natural gas used by the residential sector caused 30.4 metric tons (Mt) of green house gas (GHG) emission in 2010 and electricity used by residential sector caused 27.6 Mt of GHG emissions in 2010 (Natural Resources Canada, 2011). Solar thermal domestic hot water production is an alternative to reduce greenhouse gas emission by reducing electricity and natural gas use. A typical solar thermal domestic hot water system schematic is shown in Figure 1.7.

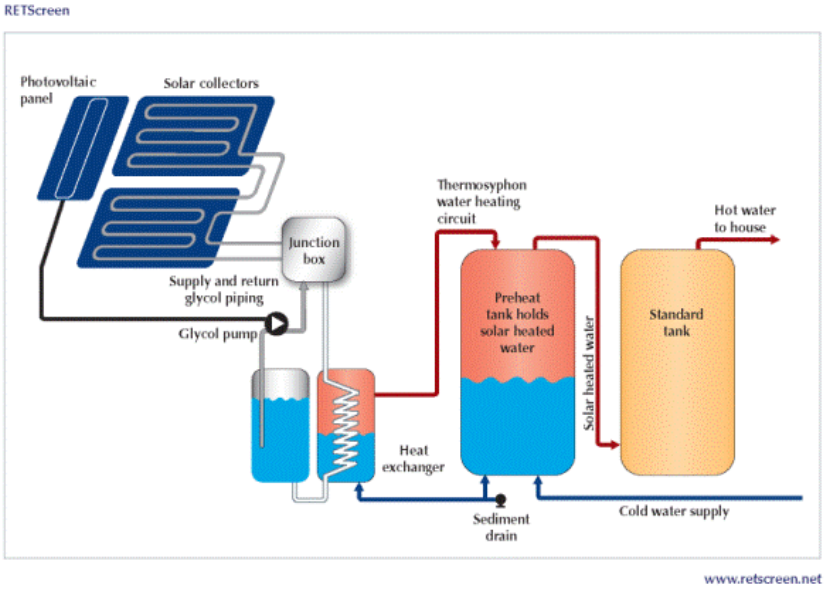

Figure 1.7 : Solar Hot Water System Schematic (RET Screen, 2008)

1.6 Heating Demand for a Canadian Solar Source

Eggertson (2005) has argued that homes in cooler climates require significant energy for winter heating and year-round water heating. The 2003 energy demand data showed that secondary energy use for the commercial / institutional sector is 1,182 PJ ($\times 10^{15}$ Joules) in Canada. Among them 644 PJ was for space heating and 76 PJ for water heating (Eggertson, 2005). He argued that 67% of Canada's energy use in the commercial and institutional sector could be met with heat produce from renewable energy sources (Eggertson, 2005).

In 2009, Canadian residential energy demand was 1,419 PJ ($\times 10^{15}$ Joules), and accounted for 14 % of total Canadian energy demand (National Energy Board Canada, 2011). 2009 data also showed Canada's cold climate caused 17 % of the residential energy consumption for water heating (National Energy Board Canada, 2011) and 8% of energy for the commercial/ institutional sector water heating (National Energy Board Canada, 2011).

Canadian residential and commercial sector yearly energy demand for water heating and space heating is considerably high. It is indicated by above 2003 and 2009 data. Only energy source, which satisfy this demand is the non-renewable source, fossil fuels. Solar thermal energy is a feasible solution that reduces fossil fuel consumption that ultimately reduces green house gas emissions in Canada. Figure 1.2 showed that Canada has high annual solar availability, which can be easily harness using solar thermal technologies. Solar thermal technology can be a successful solution to satisfy energy requirements for water heating.

1.7 Thesis Objectives and Approach

In 2010, City of Calgary implemented a large-scale solar thermal system at Southland Leisure Centre (SLC), Calgary, AB, Canada to provide hot water for the swimming pool and excess heat is used to provide domestic hot water. This system with 150 panels is a forced circulation-closed loop system with heat pipe evacuated tube collectors and working fluid is water/glycol mixture. Solar hot water system is combined with the existing boiler running hot water system that consumes electricity.

This is the first large scale solar thermal system in Calgary and City of Calgary is intending to implement similar systems in other leisure centres depending on the performance of solar thermal system in SLC. With this objective, city of Calgary and ENMAX desire to know the efficiency and performance of this first solar thermal system.

Testing equipments were setup in December 2011 to measure solar radiation, wind speed and direction, flow rate of water/glycol mixture through panels, temperature of inlet and outlet of two panels and the ambient temperature close to testing panels of this large solar thermal system. Measuring equipments included a pyranometer, anemometer, data logger, temperature sensors and a flow meter. Data will be analyzed to assess panel performance. The initial data collection period was 2 years. First year data is used to find the performance of heat pipe evacuated tube collectors at SLC.

In the first stage of the project, the following outcomes were expected:

1. Set up, commissioning and validation of the data monitoring system to measure collector efficiency parameters
2. Collect data from data monitoring systems
3. Analyze the collected data

In the second stage, collected first year data is used to estimate:

1. Steady state efficiency of evacuated tube collector
2. Unsteady state efficiency
3. Comparison of unsteady state efficiencies with International test standards

Chapter Two: **LITERATURE REVIEW ON SOLAR THERMAL COLLECTOR PERFORMANCE**

2.1 Introduction

The main objective of the project is to analyze efficiency of the HP ETCs working in the solar thermal system at SLC and then compare the calculated efficiencies with international test standards. The first part of literature review covers theoretical background of efficiency of ETCs and reducing the efficiency equation of solar thermal collectors to HP ETCs and International test standards especially available for HP ETCs.

The current literature was reviewed on:

1. Performance evaluation of evacuated tube collectors (ETCs)
2. Theoretical background for heat gain of heat pipe evacuated tube collectors (HP ETCs)
    I. Under steady state conditions
    II. Under unsteady state conditions

As a base for the data analysis of research, literature was reviewed on

3. International Standards available for performance evaluation of ETCs
4. International Standard procedures to calculate performance under
    I. Steady state conditions
    II. Unsteady state conditions

In the second part of the literature review, the studies conducted on large-scale solar thermal systems and the requirement for performance analysis of solar thermal systems in Alberta, Canada will be discussed.

2.2 Efficiency of Evacuated Tube Collectors

The efficiency of a solar thermal collector depends on the amount of solar radiation received by the collector and the amount of that energy converted into thermal energy by the collector. The amount of thermal energy produced by a collector reduces due to associated heat losses. The efficiency of evacuated tube collectors can be defined as rate of energy absorbed by working fluid or heat transfer media as thermal energy (Energy Output or Heat Gain) divided by rate of solar energy absorbed by collector (Energy Input) (Duffie & Beckman, 2013).The definition of efficiency, η, is

$$\eta = \frac{\dot{Q}}{AI} \tag{2.1}$$

Where $\dot{Q}$ is the rate of energy gained by the working fluid in the collector, I is global solar radiation falling on the aperture/absorber area and A is aperture area or absorber area of the collector (Duffie & Beckman, 2013).

2.3 Heat Gain of ETCs

The useful heat absorbed by an ETC is the amount of heat transfer to its working fluid. Section 1.3 described the different designs of ETCs and the technique of circulating working fluid within the collector. One main objective of this section is to derive the heat gain equation of HP ETC. The piping arrangement, which circulate the heat transfer media in a HP ETC is different from other ETC categories. As explained in Section 1.3 HP ETCs working fluid flows through the manifold and absorbs useful heat from the heat pipes' condenser bulbs or fins. The

amount of energy transferred through the ETC depends on various parameters and heat losses. Next Section will discuss the heat flow, parameters and associated heat losses of HP ETC.

2.4 Defining Variables of HP ETCs

The experiments conducted at SLC used two HP ETCs. Heat flows and variables in Figure 2.1 will be used to develop the heat gain model of HP ETCs. The open system with one fluid inlet and one outlet will be used to derive the equation (2.6) later in this chapter. Control volume was defined around two HP ETCs. Two collectors will gain a higher temperature rise across collectors than one collector and it will increase the accuracy of efficiency results. Two HP ETCs and its parameters are shown in Figure 2.1.This setup and parameters will be used in Chapter 4 for efficiency calculation.

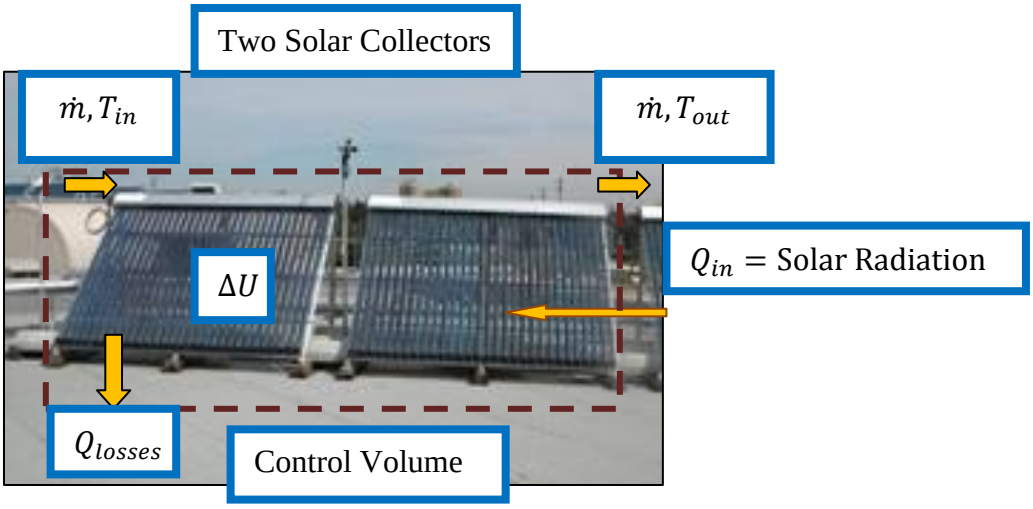

Figure 2.1: Selection of Control Volume

$Q_{in} = AI$ is the energy received by collectors as solar radiation, Q_{losses} is the associated conduction, radiation and convection losses in collector, $\dot{m}$ is the mass flow rate of the working fluid and ΔU is the internal energy generated within the system.

2.5 Heat Gain Model of Evacuated Tube Collector

Applications of solar collectors in controlled environment are rare. In most cases, collectors operate in dynamic environmental conditions or unsteady state conditions. The behavior of collector under dynamic conditions is also called transient behavior. The general equation of heat gain by any solar thermal collector during transient behavior is

$$Q_u = F'(\tau\alpha)_{en} K_{\theta b} I_b + F'(\tau\alpha)_{en} K_{\theta d} I_d - c_6 uI - c_1(T_m - T_a) - c_2(T_m - T_a)^2 - c_3 u(T_m - T_a) + c_4(E_L - \sigma \overline{T}_a^{\,4}) - c_5 \frac{dT_m}{dt} \quad (2.2)$$

Equation (2.2) is given by Fischer et al. (2004). Q_u is the rate of useful energy output (heat gain), F' is the collector efficiency factor, $(\tau\alpha)_{en}$ is the product of the effective transmittance and absorptance at normal incidence , $K_{\theta b}$ is the beam radiation incidence angle modifier, $K_{\theta d}$ is the diffuse radiation incidence angle modifier, I_b the beam radiation, I_d he diffuse radiation, u is the wind speed, I is the global solar radiation, T_m is the mean temperature of the collector which is assumed to be that of the working fluid, T_a is the ambient temperature, E_L is the power four of the absorber surface temperature multiplied by the Stefan-Boltzmann constant σ, ε is the emissivity of absorber surface, $\bar{T}_a$ is the ambient temperature in Kelvin, and dT_m/dt is the first order time derivative of the mean temperature of working fluid.

Equation (2.2) can be applied to an ETC to derive an equation for the efficiency of heat pipe ETC under unsteady conditions. The important terms, coefficients and parameters in equation (2.2) will be related to an ETC in following Sections. Further, the unsteady state heat gain of a HP ETC will be developed based on Equation (2.2).

2.5.1 *Collector Efficiency Factor (F′)*

Collector efficiency factor is the ratio of the actual useful energy gain to the useful gain that would result if the collector's absorbing surface had been at the local fluid temperature or working fluid inlet temperature (Duffie & Beckman, 2013).

If the collector's absorbing surface had been at fluid inlet temperate, heat absorbed by the collector will be delivered to the working fluid without losses and this is the maximum possible heat delivery of the collector (Duffie & Beckman, 2013).

2.5.2 *Effective Transmittance Absorptance Product (τα)*

Collector's absorber absorbs the solar radiation after it penetrates through the glass tube of ETC. However, not all solar radiation received by the collector reaches the absorber. A part of this radiation is reflected back to the sky and another component is absorbed by the glazing. The rest of it reaches the absorber.

Subtracting the summation of all the reflections in the glass cover from the total incoming radiation leaves the incident solar radiation absorbed by the absorber (Rabl, 1985). This is frequently called effective transmittance absorptance product and designated by ($\tau\alpha$) (Rabl, 1985). The product will be modified as effective transmittance absorptance product at normal incidence to calculate zero loss efficiency of collector.

2.5.2.1 Incidence Angle Modifier (K_Θ) for ETCs

Incidence Angle

One of the most important factors is the effect of the angle of incidence of the indented radiation on the collector surface. Incidence angle is the angle between the solar radiation striking the collector surface and the normal to the collector surface. Incidence angle is denoted by theta (Θ).

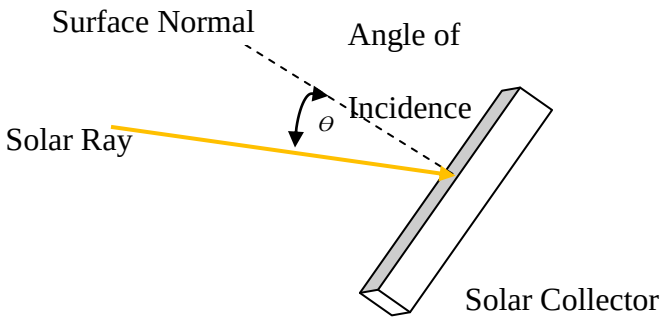

Figure 2.2: Angle of Incidence.

Incidence Angle Modifier

Incidence angle modifier is denoted by $K_{\tau\alpha}(\theta)$. The dependence of effective tramittance absorptance product ($\tau\alpha$) with the incidence angle of solar radiation is described by the incidence angle modifier. Two separate incidence angle modifiers are available for beam and diffuse radiation that discussed in Section 1.1.1. Two components those comes in different angles have two incidence angle modifies. $K_{\tau\alpha}(\theta_b)$ is the beam radiation incidence angle modifier and $K_{\tau\alpha}(\theta_d)$ is the diffuse radiation incidence angle modifier (Duffie & Beckman, 2013).

$K_{\tau\alpha}(\theta_b)$ is the ratio of effective transmittance absorption product at the actual angle of beam radiation to the effective transmittance absorption product at normal incidence. The incidence angle modifier for beam radiation incidence at angle θ_b is defined as $K_{\tau\alpha}(\theta_b) = \left((\tau\alpha)_b / (\tau\alpha)_n \right)$. $K_{\tau\alpha}(\theta_d)$ is the ratio of effective transmittance absorption product at some angle of diffuse radiation to the effective transmittance absorption product at normal incidence. The incidence angle modifier for diffuse radiation incidence at angle θ_d is defined as $K_{\tau\alpha}(\theta_d) = \left((\tau\alpha)_d / (\tau\alpha)_n \right)$ (Duffie & Beckman, 2013).

The beam radiation can be divided into two components based on the two projections of the incidence angle. They are called transversal and longitudinal directional radiation. θ_t is the transverse projection of incidence angle θ and $\theta_l$is longitudinal projection of incidence angle θ (Zambolin & Del Col, 2010).

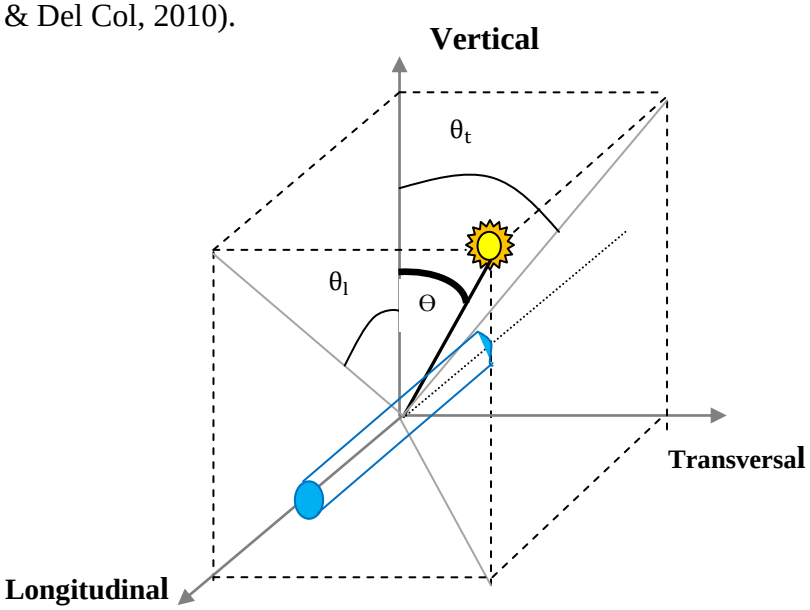

Figure 2.3: Transversal and Longitudinal Incidence Angle (Referred Ramon & Victor, 2012)

Incidence angle modifier for the transverse component of beam radiation is $K_{\theta t}(\theta_t, 0)$ and for longitudinal component of beam radiation is $K_{\theta l}(0, \theta_l)$. The total incidence angle modifier for beam radiation at incidence angle θ is the product of the two: $K_{\theta b}(\theta_t, \theta_l) = K_{\theta t}(\theta_t, 0) K_{\theta l}(0, \theta_l)$ (Zambolin & Del Col, 2010). The tubular shape of evacuated tube collectors has a strong influence from both modifiers.

2.5.3 *Components of Heat Gain Model*

2.5.3.1 Heat Gain

Short Wave Radiation

As explained in Section 1.1.1, the short wave solar radiation received by absorber has two components: the beam radiation (I_b) and diffuse radiation (I_d). The first two components of equation (2.2) $F'(\tau\alpha)_{en} K_{\theta b} I_b + F'(\tau\alpha)_{en} K_{\theta d} I_d$ are the energy gain by the working fluid from beam radiation and diffuse radiation. The fraction of beam radiation received in an incidence angle is $K_{\theta b} I_b$ .Part of the beam radiation is transmitted through glass cover and only part of transmitted radiation is absorbed by the absorber. The actual energy received by the heat pipe is $(\tau\alpha)_{en} K_{\theta b} I_b$. Heat is also lost while transferring to the working fluid due to heat transfer resistance of the collector. The actual energy received by the working fluid is $F'(\tau\alpha)_{en} K_{\theta b} I_b$ .Heat gain from diffuse radiation is $F'(\tau\alpha)_{en} K_{\theta d} I_d$, after including the same loss mechanisms that occur for beam radiation.

Long Wave Radiation

Part of the solar radiation received is long wave radiation with low frequency. The selective surface coating of a typical ETC absorber has lower emittance for the long wave radiation with an emissivity of ε <<< 1. If the glass covers are at ambient temperature, the rate of irradiative energy emission from absorber or rate of radiation heat loss of absorber can be written as $\varepsilon\sigma(T_{abs}^4 - \bar{T}_a^4)$ according to the Stefan Boltzmann law. T_{abs} is the absorber temperature in Kelvin. In equation (2.2) σT_{abs}^4 has expressed as E_L , the long wave irradiance (Fischer et al., 2004).

2.5.3.2 Thermal Heat Losses

Heat Generated within the System

ETCs are made of different parts as shown in Figure 1.4 and each part has different heat capacity. When a collector is operating, each collector component responds differently to a change in operating conditions and has a different temperature. Therefore, it is useful to consider an effective thermal capacity for the whole collector (ISO, 2010). A collector can usually be considered as a combination of masses, each at a different temperature (ISO, 2010).

Some energy received by the collector does not fully pass to the working fluid but goes to heat the collector parts. The different temperatures of different parts are difficult to determine. The temperature of the collector parts can be approximated from T_m the mean temperature of the working fluid (Rabl, 1985). The internal energy of the collector ΔU can be expressed as a function of effective thermal capacity $(MC)_e$ of the collector and the rate of change of mean

temperature, T_m. The heat generated within the system is $(MC)_{e.}\, {}^{dT_m}/_{dt}$. C_5 in equation (2.2) is $(MC)_e$. This internal energy generation term consist of two terms such as internal energy generated within the collector structure and the internal energy generation in the working fluid.

Convection Losses

Convection heat losses from a collector can be expressed as $U_L(T_{abs} - T_a)$ where U_L is the heat transfer coefficient. U_L can be assumed to have linear temperature dependence: $c_1 + c_2(T_{abs} - T_a)$ (Duffie & Beckman, 2013). The temperature dependent convection loss can be expressed as $[c_1 + c_2(T_{abs} - T_a)](T_{abs} - T_a) = c_1(T_{abs} - T_a) + c_2(T_{abs} - T_a)^2$ and absorber temperature can be approximated by the working fluid's mean temperature T_m (Duffie & Beckman, 2013).

Wind dependence of zero loss efficiency $F'(\tau\alpha)_{en}K_\theta I$ and convection loss [$U_L(T_m - T_a)$] of the collector has expressed in equation (2.2) using two terms, $-c_6uI$ and $-c_3u(T_m - T_a)$ (Zambolin & Del Col,2010). $-c_6uI$ is the component of linear dependant of $F'(\tau\alpha)_{en}$ with wind and this is dominant for unglazed collectors (Burch & Casey, 2009),(Zambolin & Del Col,2010). $-c_3u(T_m - T_a)$ is the linear wind dependent convection loss of U_L and this is also dominant for unglazed collectors (Burch & Casey, 2009),(Zambolin & Del Col,2010). ETCs are glazed collectors and these two terms can be neglected for glazed HP ETC.

2.6 Unsteady State Heat Gain of HP ETC

The general unsteady heat gain model is valid for all solar thermal collectors. The general equation (2.2) can be reduced for ETCs.

The reduction of equation (2.2) is based on following assumptions and limitations. Evacuated tube collectors are specially designed with a vacuum inside of tubes to reduce convection losses. Lower convection losses indicate lower $c_1(T_m - T_a) + c_2(T_m - T_a)^2$ in equation (2.3). Also glazed design of collector reduces wind dependence of $F'(\tau\alpha)_{en}$ and $U_{L,}$ that is $c_6 uI + c_3 u(T_m - T_a) \approx 0$. The Borosilicate outer glass tubes of evacuated tube have very high transmitivity. The absorber has a selective coating with high absorption. The absorber inside of the tube is made of Aluminum or Copper coating that can be assumed to have $\varepsilon \approx 0$. These absorber characteristics indicate very low long wave radiation loss so that $c_4(E_L - \sigma T_a^{\,4})$ can be neglected. The C_5 constant in equation (2.2) can be represented by $(MC)_e$ which indicates effective thermal capacity of the collector. The reduced Equation (2.2) is

$$Q_u = F^{'}(\tau\alpha)_{en} K_{\theta b} I_b + F^{'}(\tau\alpha)_{en} K_{\theta d} I_d - c_1(T_m - T_a) - c_2(T_m - T_a)^2 - (MC)_e \frac{dT_m}{dt} \qquad (2.3)$$

The heat absorbed by the working fluid (In this case water/glycol mixture) at steady state can be written as,

$$Q_u = \dot{m} C_p (T_{out} - T_{in}) \qquad (2.4)$$

Where C_p is the specific heat capacity of the working fluid at constant pressure. T_{out} and T_{in} are the inlet and the outlet temperatures of working fluid inside the manifold respectively. After substituting Q_u from equation (2.4) into (2.3) can be rewritten as

$$F^{'}(\tau\alpha)_{en} K_{\theta b} I_b + F^{'}(\tau\alpha)_{en} K_{\theta d} I_d - Losses = \dot{m} C_p (T_{out} - T_{in}) + (MC)_e \frac{dT_m}{dt} \qquad (2.5)$$

The component $F'(\tau\alpha)_{en} K_{\theta b} I_b + F^{'}(\tau\alpha)_{en} K_{\theta d} I_d$ in equation (2.5) is the energy delivered to working fluid without losing energy from convection or radiation. After subtracting convection and radiation losses from left hand side of the equation, the actual energy delivered to working fluid is

$$Q_u = \dot{m} C_p (T_{out} - T_{in}) + (MC)_e \frac{dT_m}{dt} \qquad (2.6)$$

The experiment in Section 3.8 will prove that the highest heat capacity of HP ETC is present in manifold and is due to the working fluid. In later parts of the thesis, $(MC)_{e.} {}^{dT_m}/_{dt}$ term of this equation will implies the internal energy generation within the working fluid in the manifold.

2.7 Steady State Heat Gain Model

A system can be described as a steady state if the properties of the control volume do not vary with time. Equation (2.2) can be reduced to the steady state heat gain equation after eliminating the time dependant internal energy generated within the system.

$$c_5 dT_m / dt = 0 \tag{2.7}$$

So that equation (2.6) becomes

$$Q_u = \dot{m} C_p (T_{out} - T_{in}) \tag{2.8}$$

2.8 Steady State Efficiency

Equation (2.1) is the definition of efficiency of evacuated tube collector. The steady state efficiency of heat pipe evacuated tube collector is

$$\eta_{SS} = \frac{\dot{m} C_p (T_{out} - T_{in})}{IA} \tag{2.9}$$

2.9 Unsteady State Efficiency

The unsteady state efficiency of heat pipe evacuated tube collector can be determined from equation (2.6) (Fischer et al., 2004). It is

$$\eta_{US} = \frac{(MC)_e \frac{dT_m}{dt} + \dot{m} C_p (T_{out} - T_{in})}{IA} \tag{2.10}$$

Equation (2.10) is valid only if following conditions are satisfied. The evacuated tube collector should be a heat pipe evacuated tube collector as discussed in Section 1.3. The design of heat pipe evacuated tube collector should have low convection and radiation losses. The

temperature of the collector can be approximated by the mean temperature of the working fluid inside of the manifold, so that the mean temperature can be approximated as $(T_{out} + T_{in})/2$. Also assumed, that the collector can be characterized as a single thermal node of mass M and the specific heat C, at a uniform temperature that is equal to the working fluid mean temperature T_m (Rabl, 1985).

2.10 Internaional Performance Standards for ETCs

Performance evaluation of solar thermal collectors or the efficiency evaluation of collector is an important task for decision-making. When comparing performance of two collectors made by two different manufactures, there can be a considerable difference. Implementing an accepted standard by an independent and professional organization will allow to document any variation of performance and will give confidence in the performance evaluation. Among them, European standard EN 12975 is the most accepted collector evaluation procedure for solar thermal collectors (Nielson, 2010).

Currently, there are number of different standards available for testing solar thermal collectors. First standard used for solar collector was US ASHRAE standard (93-77) and then the ISO 9806 series of standards was developed (Kovacs, 2012). The latest standard is EN 12975 (European Committee for Standards, 2013). However, there are several national standards available those developed outside Europe based on the ISO 9806 (Fisher et al. 2012). European standard, the most acceptable standard, contains amongst other things the guidelines to test solar thermal collectors at steady state (ISO, 2010) and unsteady state (Fischer et al., 2004).

2.11 Steady State Efficiency of HP ETC (According to International Standards)

2.11.1 *Solar Collector Testing Agency and Collector Manufacture*

The Fraunhofer Institute for Solar Energy Systems ISE (or Fraunhofer ISE) is one of institutes that conduct performance measurements of solar collectors based on international test standards. HP ETC collectors series (TZ58-1800-300) used at the SLC were tested by Fraunhofer ISE and results are shown in Figure 2.5. Following sections will discuss the test procedure, theoretical background and test results using EN 12975 (European Committee for Standards, 2013).

2.11.2 *International Standard EN 12975 Test for HP ETC (TZ58-1800-300)*

The performance testing of heat pipe evacuated tube collector TZ58-1800 series was performed in 2007 according to EN 12975 by the Fraunhofer institute to determine the efficiency of the HP ETCs manufactured by Jiangsu Sunrain Solar Energy co. Ltd, the supplier of the HP ETCs to the SLC (Jiangsu Sunrain Solar Energy, n.d). According to this report, the steady state performance of the collector was calculated based on following testing conditions.

Test Conditions (Jiangsu Sunrain Solar Energy, n.d.)

Test method: outdoor, steady state	Latitude: 48.0°
Collector tilt: tracked between 35°and 55°	Longitude: 7.8°
Collector azimuth: tracked	Mean irradiation: 936 W/m^2
Mean wind speed: 3 m/s	Mean flow rate: 66 kg/h
Working fluid: water	

Procedure

European Committee for Standards (2013) was used to select data for the steady state efficiency calculation. Clear day data was taken for the analysis. Collector testing period was selected based on the following requirements in EN 12975 (European Committee for Standards, 2013).

1. Wind Speed in the range of 2 m/s to 4 m/s
2. Solar noon (When highest solar radiation received)
3. Solar radiation data higher than 800 W/m^2
4. An even number of data points

Results

A TZ58-1800-30R collector with 30 tubes was tested in an outdoor test rig on a clear day as shown in Figure 2.4. Wind speed was measured using an anemometer and this testing day was selected as the wind speed was between 2m/s to 4m/s to reduce convective losses. The solar radiation has measured using the six pyranometers as shown in Figure 2.4 and solar availability on this day reached mean 936 W/m^2 , which exceeds the minimum requirement of 800 W/m^2 to perform a steady state test according to (European Committee for Standards, 2013). Water has used as working fluid, and it was circulated through testing collector and temperature rises across the collector was measured.

Figure 2.4: Instrumentation of HP ETC TZ58-1800-30R on Test Day ((Jiangsu Sunrain Solar Energy, n.d.)

Measurements taken during a test day in February 2007 are shown in table 1.

Table 1 : Measured Data for Efficiency Determination (Jiangsu Sunrain Solar Energy, n.d.); *G* is the global radiation represented by *I* earlier in this chapter. The units are W/m^2. t_{in} represents T_{in},t_e represents T_{out}, t_m represents T_m and t_a represents the T_a, η_a represents η.

G [W/m^2]	G_d/G [-]	m [kg/h]	t_{in} [°C]	t_e [°C]	$t_e - t_{in}$ [K]	t_m [°C]	t_a [°C]	$t_m - t_a$ [K]	$(t_m - t_a)/G$ [K m^2/W]	η_a [-]
980	0.14	67.7	6.79	15.38	8.60	11.08	9.88	1.21	0.0012	0.740
992	0.13	67.7	6.81	15.46	8.65	11.14	9.88	1.26	0.0013	0.736
969	0.11	67.7	6.84	15.39	8.55	11.12	11.14	-0.02	-0.0000	0.745
937	0.09	67.8	7.78	16.05	8.27	11.91	11.05	0.86	0.0009	0.745
944	0.08	67.8	7.82	16.06	8.24	11.94	11.27	0.67	0.0007	0.737
852	0.17	60.8	6.76	15.14	8.38	10.95	10.39	0.56	0.0007	0.745
843	0.16	60.9	6.78	15.11	8.33	10.95	10.50	0.44	0.0005	0.749
892	0.12	66.1	33.03	40.28	7.25	36.66	7.43	29.23	0.0328	0.666
898	0.12	66.0	33.08	40.42	7.34	36.75	7.75	29.00	0.0323	0.669
905	0.12	66.1	33.10	40.52	7.42	36.81	7.97	28.84	0.0319	0.671

Theoretical Background

The steady state heat gain model was used with second order convection losses. Ignoring the unsteady term, equation (2.3) gives

$$Q_u = F'(\tau\alpha)_{en} K_{\theta b} I_b + F'(\tau\alpha)_{en} K_{\theta d} I_d - c_1(T_m - T_a) - c_2(T_m - T_a)^2 \qquad (2.11)$$

When the heat gain is divided by the global solar radiation *G* that is (*I*), and the area of the collector *A*, the equation becomes the efficiency of the collector. The term $(F'(\tau\alpha)_{en} K_{\theta b} I_b + F'(\tau\alpha)_{en} K_{\theta d} I_d)/(GA)$ is non-dimensional and can be replaced by η_o the zero loss efficiency. After replacing the constants c_1/A and c_2/A with C_1 and C_2 respectively, the equation becomes a second order equation of (T_m-T_a):

$$\eta = \eta_0 - C_1 \frac{(T_m - T_a)}{G} - C_2 \frac{(T_m - T_a)^2}{G} \tag{2.12}$$

2.11.3 *Test Results for HP ETC (TZ58-1800 Series)*

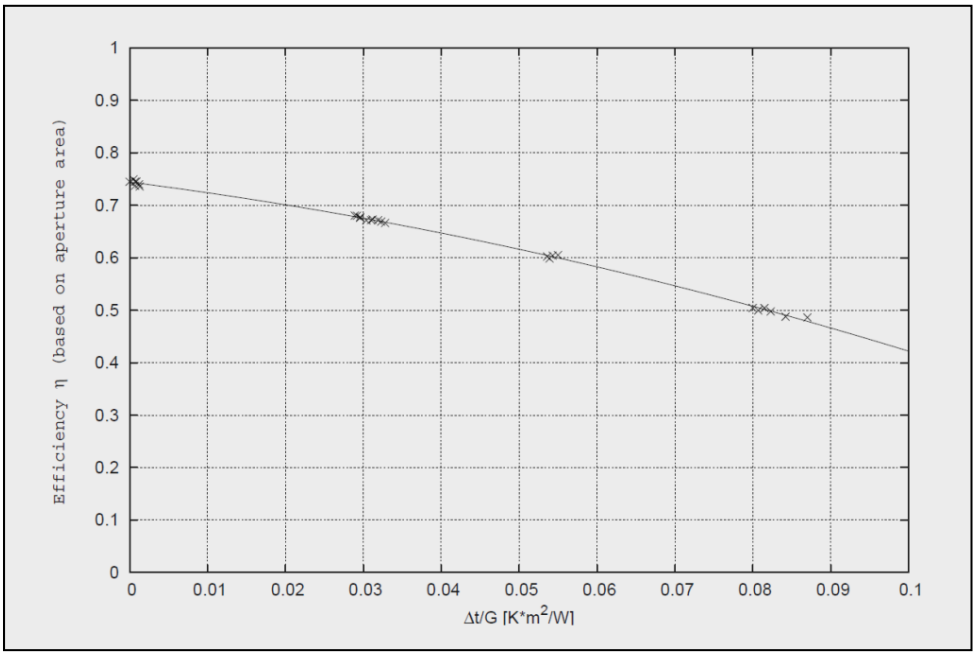

Figure 2.5: Efficiency vs. $(T_m\text{-}T_a)/G$ in (K.m^2/W) from Fraunhofer test results; (Jiangsu Sunrain Solar Energy, n.d.).

Figure 2.5 shows that the collector operates at efficiencies between 60% and 75% when $(T_m\text{-}T_a)/G$ is between 0.05 and 0. When $(T_m\text{-}T_a)/G$ is low, such as 0.05 to 0.1, the collector efficiency reduces to 45%. In addition, at steady state the TZ58-1800 series collector follows the second order efficiency equation. Zero loss efficiency (η_o) of the collector based on aperture area is 73.4% and convection heat loss coefficients shown in equation (2.12) are C_1= 1.529 W/K m^2 and C_2= 0.0166 W/K m^2.

2.12 Tests for Unsteady State Performance Evaluation

The literature on performance evaluation under unsteady state conditions is very limited, but Fischer et al. (2004) has given guidelines for unsteady state performance evaluation based on EN 12975. The general heat gain model under unsteady state is suggested for solar thermal collectors (equation (2.2)) and the procedure of selecting data for the calculation is given. Following are the steps for selecting data for the unsteady state performance evaluation of the solar thermal collectors.

1. Solar Availability on the day should be more than 300 W/m^2 and less than 1100 W/m^2
2. No limitation on wind speed

The lack of literature is evidence for the importance of developing a model for performance evaluation of heat pipe evacuated tube under unsteady conditions.

2.13 Previous Studies on Performance Evaluation of ETCs Using International Standards

Zinko, Holst, Perers, & Eriksson (1984) have investigated heat pipe evacuated tube collector and compared with other ETC collector types and concluded that heat pipe evacuated tube collectors has higher performances.

Collector performances were measured according to standards and ASHRAE 93-77, ISO 9806 and EN 12975. Zambolin & Del Col (2010) have used EN 12975 for steady state and unsteady state analysis of direct flow trough evacuated tube collector for an outdoor experiment was conducted in Italy. Performance was measured by using collector efficiency vs. $(T_m\text{-}T_a)/G$ graph. Nkwetta & Smyth (2012) have tested two types of concentrated heat pipe evacuated tube collectors using ANSI/ASHRAE Standard 93-2003 and linear steady state equation was used for

efficiency calculation and collector efficiency vs. (collector inlet temperature-ambient temperature/ global insolation) graph was used to conclude results. Zambolin & Del Col (2010) have tested two types of U type evacuated tube collectors according to EN 12975. Steady state and quasi-dynamic state efficiencies were calculated using data obtain from outdoor test.

Harrison, Rogers, Soltau, Wood (1993) argued that testing standards have limitations and "They often produce a 'snap shot" of performance derived under standard test conditions rather than a characterization of how the collector will perform under range of metrological conditions".

Jackman (2009) stated that heat pipe evacuated tube collector is the best solar thermal collector for Alberta and Heat pipe evacuated tube collector can perform better in cold climate up to -40°C in Alberta. But there are no literatures available for heat pipe evacuated tube collector performance in Alberta and Jackman's (2009) statement has not been validated.

Southland Leisure Centre solar thermal project produces hot water by using heat pipe evacuated tube collectors and their performances were tested by Fraunhofer institute in 2007. Testing standard EN 12975 has been used and showed that it has zero loss efficiency 0.734 under steady state conditions.

The heat pipe evacuated tubes are working in outdoor uncontrolled environment and in Calgary metrological conditions. It is necessary to estimate the steady state and unsteady state efficiencies of HP ETC under Calgary metrological conditions and assess the deviations from steady state efficiency results supplied by the manufacture. This will provide a good picture of the suitability of heat pipe evacuated tube collectors for Calgary and accurate estimation of performance of the heat pipe evacuated tube collector. In addition, this study will also provide a background to estimate the performance of entire solar thermal system.

2.14 Previous Literatures on Large Scale Solar Thermal Systems

Ayompe & Duffy (2013) have conducted a study similar to the present SLC solar thermal project in Dublin, Ireland. Thermal performance of a solar water heating system with heat pipe evacuated tube collector (HP ETC) was evaluated using data obtained from a field trial over one year. The annual efficiency of HP ETCs was 63.2% and the energy absorbed from the collectors was further reduced due to piping losses before reaching the hot water tank. Ayompe & Duffy (2013) also suggested that better pump control strategy for heavily overcast and intermittent cloud covered days could result in system improvement. Major limitation of this study to our case is that only steady state analysis of the collector efficiency was performed. Another incompatibility is the results derived from this experiment can not apply for Calgary where weather conditions are different from Dublin, Ireland. But Ayompe & Duffy (2013) have compared the HP ETC performance with flat plate collector using data obtained from another study and concluded HP ETC are more efficient than a flat plate counterparts when operating as a component of a solar water heating system.

Chow, Chan, Fong, Tan, & Dong (2012) conducted a more relevant outdoor study for this experiment. They compared and analyzed daily efficiencies and transient efficiencies of water in glass (WG ETC) and heat pipe evacuated tube collectors (HP ETC) in Hong Kong. This study concludes that in the early morning, the transient efficiency of the WG type is higher than the HP type. At noon, the difference in transient efficiency of the two systems is not significant. In the late afternoon, the transient efficiency of the HP type is higher than the WG type. It appears that longer time duration is required for the HP type to transmit the absorbed solar heat to the water. As a consequence of the time delay, the transient efficiency of the HP type can be exceptionally

high after 4pm (even more than 100 per cent in one case). Under zero loss condition, the daily system efficiency of the HP type is slightly higher than the WG type.

The daily system efficiency was calculated according to Taiwan Testing Standard CNS B7277 and transient efficiency was estimated according to Chinese National Standards GB/T 12915-91. But in our case we use European standard EN 12975 which is different from the standards used in this study.

2.15 Previous Literature on Potential for Solar Thermal System in Canada

Jackman (2009) conducted a feasibility study of using solar thermal system for water heating for houses in Alberta. Jackman (2009) and Jagoda, Lonseth, Lonseth, & Jackman (2011) have suggested that the use of solar thermal systems in Alberta will reduce greenhouse gas emission and best use of solar collector is heat pipe evacuated tube collectors which can operate in winter months with -40°C temperatures. Jackman's (2009) study compares the financial and environmental benefits and concluded solar thermal is the most cost effective renewable energy source when installation cost and saving of GHG emission included in the calculation. This study concluded that a solar thermal system in a new home has four years payback period. Jackman (2009) also suggested there is a potential for use of solar thermal systems in community swimming pools. Jagoda et al. (2011) have concluded solar thermal systems are the best renewable energy method for domestic water heating in Calgary, Alberta.

Islam, Fartaj, & Ting (2004) have stated that the studies in Canada showed that solar pool heaters could provide the performance that pool owners desire and have a simple payback ranging from 2 to 4 years. The studies indicate that solar heating could capture 40%–50% of the pool heating market in the long term. Test promotions during 2001 at three locations in Canada

confirmed this potential. This study showed the potential for solar thermal swimming pool heating in Canada in 2004.

Jackman (2009) provided a good background for importance of solar thermal systems in Alberta. But this study do not include any analysis of heat pipe evacuated tube collector performance in Alberta but include a statement that the heat pipe evacuated tube collector has the best performance for Alberta winter conditions. There is no evidence to support the statement and there are no literature quoted for heat pipe evacuated tube collector performance in Alberta.

Chapter Three: **RESEARCH METHODOLOGY & EQUIPMENT SETUP**

3.1 Background of Solar Thermal Project

The solar thermal system at the Southland Leisure Centre (SLC) preheats the swimming pool water and provides hot water for domestic hot water (DHW) system in the facility. This large swimming pool is used by several hundreds of Calgarians every day and is opened from 8 am to 6 pm, 7 days a week. DHW system provides hot water for other areas such as washrooms and showers in the sporting and office facilities.

The purpose of first stage of this research project was to set up sensors and data acquisition systems to collect data required to calculate steady state and unsteady state efficiencies. In addition, functionality of SLC solar thermal system and its automated control system was also studied.

3.2 Schematic Diagram of Solar Thermal System and Experimental Setup

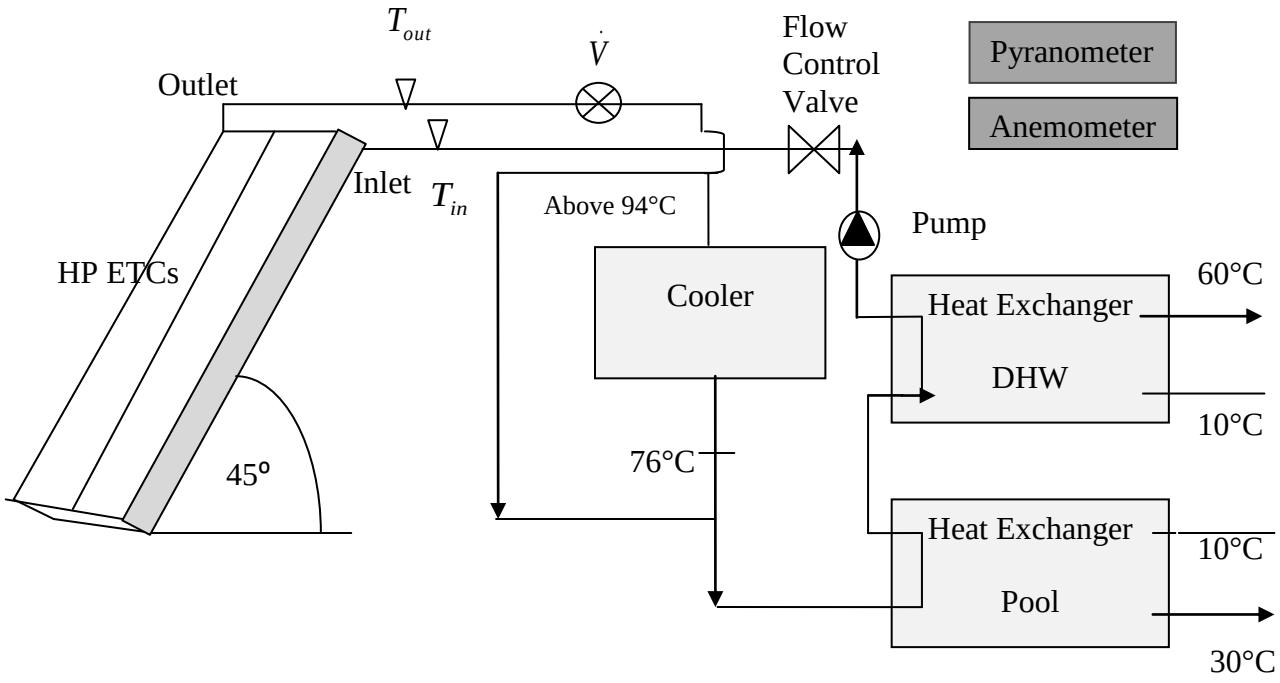

Figure 3.1: Schematic Diagram of Combination of Data Collection Setup and Solar Thermal System. Reproduced from (Williams Engineering, 2010a)

3.3 Functionality of Solar Thermal System

SLC solar thermal system is a fully automated system implemented using sensors and microcontrollers (BIM-Bus Interface Modules). It is also a pump operated forced circulation system. Water/glycol mixture (the working fluid) which circulates in a closed loop absorbs heat from collectors while the pump is OFF. When the pump is ON, the hot water/ glycol mixture starts to flow from collectors to two heat exchangers in pool and DHW system. If the average temperature in three locations of collector network is higher than 94°C a 3 way diverting valve

opens and supplies the working fluid to a fan operated heat exchanger which reduces temperature to 76°C (Williams Engineering, 2010c). This is where the excess heat is dumped.

If the temperature is lower than 94°C, then the water/glycol mixture is directly fed to the pool heat exchanger. When the hot water/glycol mixture reaches the pool heat exchanger, heat is transferred to the cold water in the heat exchanger, which goes to the swimming pool. Heat absorption continues until the swimming pool water reaches 30°C. When the pool water reaches 30°C, another 3-way diverting valve opens and starts to supply water/glycol mixture to the DHW system. In the DHW side, heat is absorbed by cold water that flows through the heat exchanger until it reaches to 60°C. After dissipating the heat, the cold water /glycol mixture goes back to collectors .The pumps in the system continue the circulation of water/glycol mixture until satisfies the pool and DHW system demands (Williams Engineering, 2010c).

Pump ON/OFF sequence is determined by the pool and DHW system demands. Automation system has configured to provide the pump ON/OFF signals after monitoring sensors in the system (Williams Engineering, 2010c). Chapter 3 discusses the experimental equipments mounted in this system.

3.4 Specifications of Solar Water Heating (SWH) System

Heat generated by the solar thermal system contributes 6% of heat required by the swimming pool (City of Calgary, 2013). The solar thermal system contains 150 heat pipe evacuated tube solar collectors (HP ETCs) manufactured and supplied by Jiangsu Sunrain Solar Energy Co. Ltd , China. The model of the collector is TZ58/1800-30R. Each collector has 30 all-glass evacuated tubes with a heat pipe (Jiangsu Sunrain Solar Energy, n.d). Figure 3.2 shows the

two HP ETC panels those were instrumented for the study. All these collectors were inclined at 45° to maximize heat absorption in Calgary.

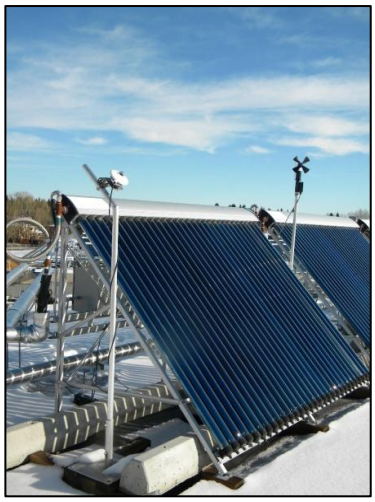

Figure 3.2: Heat Pipe Evacuated Tube Collector: Photographed by Athaudage Dona, (2012)

The location of SLC is latitude 51° North, Longitude 104º West. All panels face due south and there is no significant shading from trees or from other panels (Figure 3.3).

Figure 3.3: Spacing and Orientation of SLC ETC Panels. Photographed by Athaudage Dona, (2012)

The panels are arranged in rows as shown in Figure 3.3. The spaces between two rows are 5.1 m (Williams Engineering, 2010b). This is enough to prevent significant shading by other panels. The instrumented panels are shown in Figure 3.2 experienced no shading. All 150 HP ETCs are arranged as three panel sets that are connected in series and shown in Figure 3.3. This panel arrangement reduces the load on pump as well as increases the heat absorption.

Heat transfer media of the system is 50% water and 50% Glycol by volume. 50/50 water and polypropylene glycol has following physical properties. The boiling point at atmospheric pressure 760mmHg is 105°C, freezing point is -34°C, specific heat is 3.56 kJ/ kg. K , density 1054 kg/m^3(Dusseldorf, 1991). The Propylene Glycol prevents freezing during winter and anticorrosive material added reduces corrosion of piping system. This water/glycol mixture passes through the collector manifold and absorbs heat from the heat pipes.

The flow rate of constant flow pump is 5.36 l/s and it circulates the water/glycol mixture in the piping network. Two heat exchangers that absorb heat from the water/glycol mixture and supply heat to swimming pool and DHW system can be find in Appendix A: A1: Plumbing and Control Schematics. The fan operated heat exchanger which dumps excess heat, prevents over heating of the system (Appendix A: A1: Plumbing and Control Schematics).

3.5 Selection of Measurement Locations

A set of three panels were selected for instrumentation. They were selected based on ease of access to power supply, ease of installation of sensors and isolation from other panels. Fig 3.4 shows the location of the selected three panels and the flow direction of water/glycol mixture.

This section contains two flow control valves (Appendix A.1). One is an air vent located in the east side. The other valve is a flow control valve located in the west side. It limits the flow

rate through instrumented panels to 0.107 l/s (Williams Engineering, 2010a). Though this control valve limits the working fluid's flow rate, the actual flow rate through a collector is an unknown. Therefore, a flow meter is considered as an essential component of the instrumentation.

In Figure 3.4, 3 testing panels are connected in series and the temperature rises across collectors from west to east. The water/glycol mixture that reaches the east end has highest temperature and west end has lowest temperature. However, the West end and the Center panels were selected for the efficiency estimation considering ease of sensor mounting.

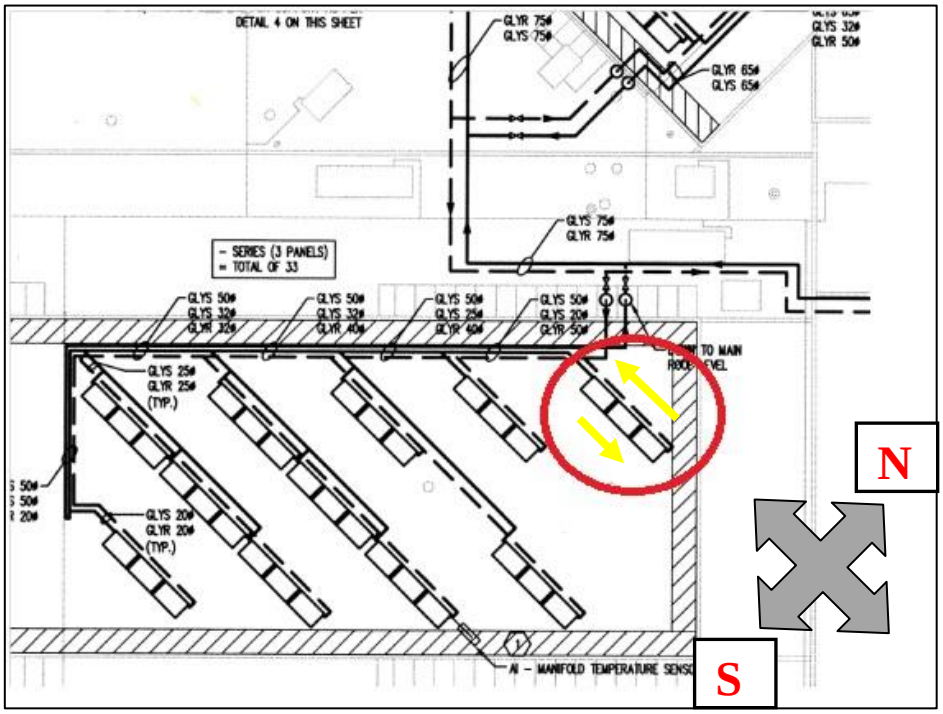

Figure 3.4: Schematic of the Part of SLC Layout with Instrumented Panels (Williams Engineering, 2010b),

3.6 Selection of Data to be Acquired

Parameters to be measured were selected based on the collector efficiency equation (2.9).

3.6.1 *Input Energy & Heat Losses*

Energy received by an HP ETC in this setup, depends on global solar radiation (*I* or *G*) at the 45° angle of the collectors. Heat losses can be higher due to wind blowing through the collector. Wind speed (u), and wind direction ($\emptyset$) were measured to assess the impact of wind. Two sensors used to measure solar radiation and wind characteristics. A CMP3-L pyranometer used to measure global solar radiation (direct, diffuse and ground reflected radiation). R.M Yong anemometer used to measure the wind speed and wind direction.

3.6.2 *Output Energy*

The useful energy gain of HP ETC can be estimated using the heat absorbed by the water/glycol mixture that enters the collector manifold (equation (2.9)). For steady state operation, the amount of heat absorbed by the working fluid can be written as $\dot{m}C_p(T_{out} - T_{in})$ (equation (2.4)). $\dot{m}$ can be estimated by measuring volume flow rate $\dot{v}$ of water/glycol mixture. C_p can be assumed as 3.56 $kJ/(kg.K)$ (Dusseldorf ,1991). T_{in}, T_{out} are inlet and outlet temperatures of the manifold and they need to measure using temperature sensors. The flow meter and two temperature sensors were attached to testing panels to measure the flow rate and temperatures. The ambient temperature T_a was also measured using an additional temperature sensor.

3.7 Equipment Setup and Testing Procedure

The Locations of Pyranometer, anemometer, flow meter and temperature sensors those mounted in testing panels are shown in Figure 3.5 a) and b).

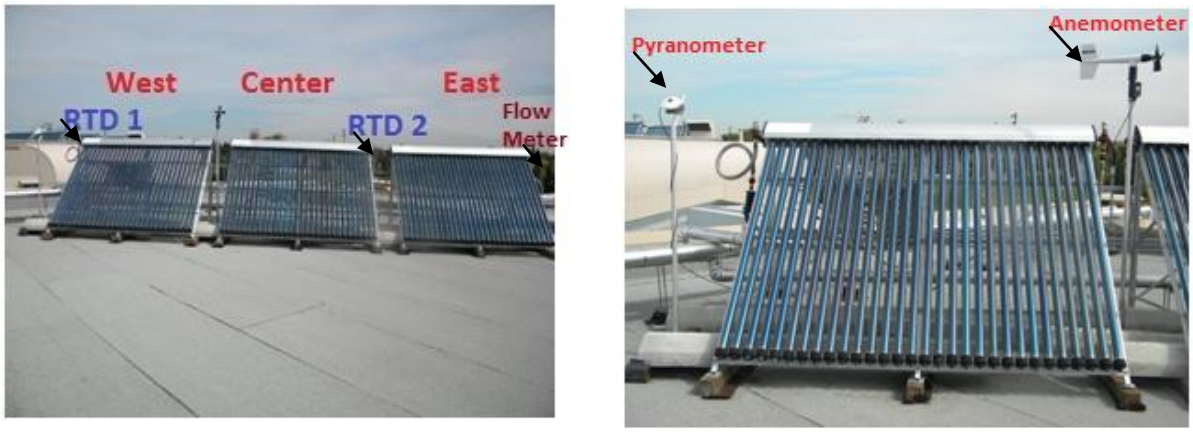

Figure 3.5: a) Testing Panels (Left), b) Wind(Anemometer) and Solar Radiation Sensor (Pyranometer) (Right). Photographed by Athaudage Dona ,(2012)

The two temperature sensors were Platinum 1000Ω Resistance Temperature Detectors (RTDs). They were attached to the west and east ends of two collectors as shown in Figure 3.5 a). Flow meter was attached to the east end of the collector array and it is used to measure the volume flow rate of water/glycol mixture. Flow direction of water/glycol mixture is from west end to east end. Figure 3.5 a) shows the location of flow meter and two temperature sensors.

The pyranometer was mounted on a structure, which sits close to collectors in west end and tilted to 45° angle to make it parallel with collector face, Figure 3.5 b). It measures global solar radiation (I or G) in W/m^2 and was sampled to provide 1 minute averages. The RM Young propeller anemometer was mounted close to west collector (Figure 3.6 a)). It measures wind direction (°) and speed (m/s) in 1 minute intervals.

A data logger was placed at the rear of the west panel (Figure 3.6 b)). It collects data from pyranometer and anemometer (Figure 3.6 a)). This data logger cannot take direct current (milli Ampere - mA) input to log flow rate. So the flow meter output was acquired through the building management system (BMS).

The City of Calgary monitors the solar thermal system through the building management system. Considering the ease of accessing and collecting data, a bus interface module was integrated with the BMS. Three temperature sensors and the flow meter (Figure 3.7) were attached to the BMS. This system collects instantaneous flow rate data in every 5 minutes and instantaneous temperatures in every 1 minute.

3.7.1 *Data Monitoring System: Data Logger, Pyranometer and Anemometer*

Figure 3.6: a) Front View West Side Collector (Left) b)Back View of West Side Collector(Right). Photographed by Athaudage Dona ,(2012).

3.7.1.1 Data Logger

Figure 3.6 b) shows the CR800 data logger from Campbell Scientific Canada. This collects the solar radiation, wind speed, wind direction data in every 10 seconds, and averages them over 1 minute. The storage capacity is 6MB and a program written in C++ runs the system. Accuracy of the data logger is (±0.12% of a reading + the offset) in temperature range -25°C to 50°C (Appendix B: Pyranometer). An inbuilt processor converts voltage signals from the pyranometer and anemometer and saves them as solar radiation data (W/m^2) and wind speed and direction data (m/s, °). A computer was used to download and analyze data and customize the data logger functions. A RS 232 connection was used to connect the data logger and computer. The clock of the data logger was synchronized with the clock of the computer to prevent data logging errors.

Logger net is the custom software that comes with the data logger. This allows sending a new program to the data logger; to write a program using SHORTCUT (small program that comes with data logger) and to write a complex program using C++. The program that supported the SLC sensor system is a SHORTCUT program (Appendix C: SHORTCUT Program) written in *Logger net*. The SHORTCUT program was included all features required for this application.

The SHORTCUT program also automatically generated the wiring diagram required to connect sensors to data logger. A computer can be used to send this program to the data logger. This SHORTCUT program that runs two sensors is capable of store data in 1 minute interval up to 243 continuous days.

3.7.1.2 Pyranometer

CMP3-L pyranometer was also supplied by Campbell Scientific Canada. Since same supplier provided the both equipment, pyranometer was compatible to integrate with CR800 data logger. CMP3-L pyranometer is sensitive to full solar spectrum changes and measures global radiation. The operating temperature range of pyranometer is -40°C to 80°C and accuracy is daily total ± 10%. Directional error (at 80° with 1000 W/m^2 beam radiation) is < ± 20 W/m^2. The maximum radiation measured from this pyranometer is 2000 W/m^2 (Appendix B: Pyranometer).

3.7.1.3 Anemometer

Anemometer is a R.M. Young propeller anemometer (Model 05106-10) measures the wind with an accuracy ±0.3 m/s (±0.6 mph) and in the range 0-100 m/s (0-224 mph). It also measures wind direction with accuracy ±3° and in range 0-360° Mechanical, 0-355° Electrical (5° Open) (Appendix B: Anemometer).

The anemometer is a four bladed propeller, which was fixed to a six-pole magnet and a stationary coil. The Rotation of the blades generates a sine wave in the stationary coil with frequency proportional to wind speed.

Wind direction is measured by the anemometer body, which is free to rotate. Body of anemometer contains a 10KΩ precision conductive plastic potentiometer, which requires a regulated excitation voltage. With a constant voltage applied to the potentiometer, the output signal is an analog voltage directly proportional to wind direction angle.

3.7.1.4 Data Collection Procedure

The same laptop with RS 232 connection was used to download the data from data logger every 30 to 45 days during site visits, which allowed equipment inspection and maintenance.

3.7.2 ***Data Monitoring System: Bus Controller, Temperature Sensors, Flow Meter***

Reason for a Second Data Logging System

The pyranometer and anemometer were connected to the data logger and manual data collection procedure was carried out. Outdoor equipment mounting will reduce its life time and manual data collection through site visit is difficult in winter. However, data collection through the BMS will provide more safety.

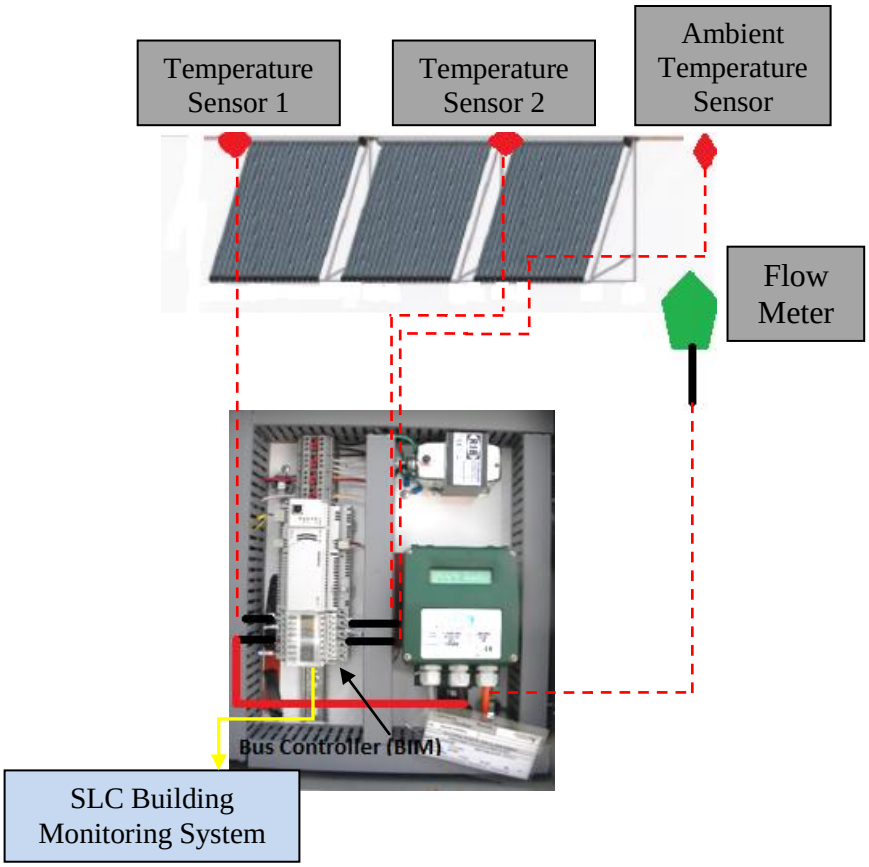

Figure 3.7: Bus Interface Module and Sensors. Athaudage Dona, (2013).

3.7.2.1 System Functionality

The City of Calgary information system collects data from three temperature sensors (Figure 3.7) and the flow meter. Flow meter has an in-built data display and it was attached to the weatherproof box shown in Figure 3.7 . Two temperature sensors installed at the west end and center panels were connected to the BIM. Ambient temperature sensor was already included in the SLC solar thermal system.

3.7.2.2 Bus Controller

P1 Bus Interface Module (P1 BIM) (Fig 3.8) collects the data from sensors and save data in main SLC information system. Time interval for temperature data collection was 15 minutes. Flow rate data was collected every 5 minutes.

3.7.2.3 Ambient Temperature Sensor

SLC solar thermal system is controlled by an automation system configured by Siemens Canada, which includes an ambient temperature sensor located close to panels and to the roof top. The building monitoring system collects ambient temperature data in every 15 minutes.

3.7.2.4 Temperature Sensors

Two Immersion Well Temperature Sensors (Platinum RTDs) were used to monitor temperature changes at inlet of west panel and at outlet of the center panel. They were threaded into the pipe and monitor water/glycol mixture temperature. Outputs were attached to BIM. Temperature Sensor specifications are PT 1000 Ohm (385 α), 2.5 inches long (Figure 3.8 a)). Accuracy of RTD is ±0.4° C (Appendix A).

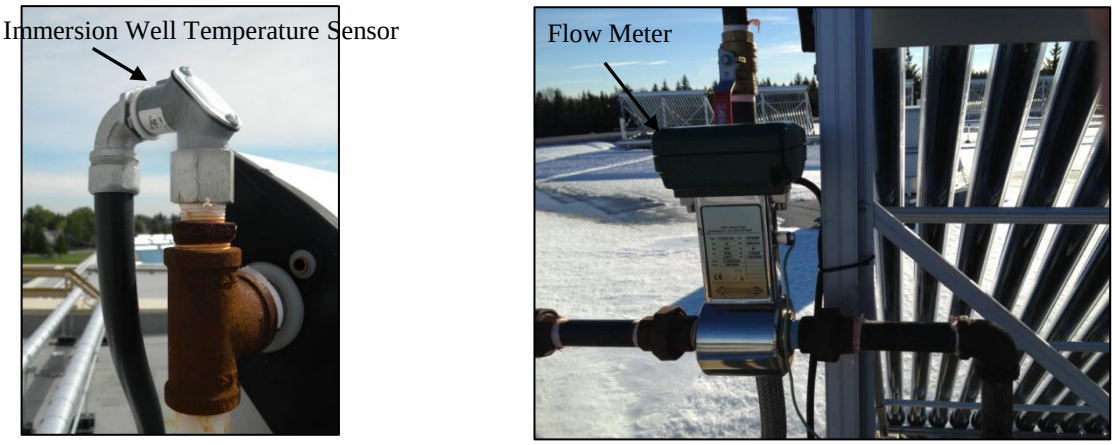

Figure 3.8: a) Immersion Well Temperature Sensor (Left) b) Onicon Flow Meter (Right). Photographed by Athaudage Dona , (2013).

3.7.2.5 Flow Meter

ONICON F-3100 Series In-line Magnetic Flow Meter (Figure 3.8 b)) was used to measure flow rate of water glycol mixture in liters/sec. This flow meter can measure at temperatures up to 140°C. Also it can operate in outdoor conditions up to -30°C and measures flow rate as low as 0.01 l/s. This flow meter was one of very few selections available to estimate the flow rate under the special conditions posed by Calgary winters. Accuracy of flow meter is ± 0.0023 m/s at flows less than 0.3 m/s. (Appendix B: Flow Meter).

3.7.3 ***Unexpected Behaviour of Flow Rate Data***

Flow rate data was first recorded on 2012/10/27 and data showed an unexpected reverse flow value -0.124 l/s throughout the day. The expected positive flow direction is from west to east or the inlet to outlet of collector. Negative flow rate indicates the water/glycol mixture flows from east to west or outlet to inlet of collector during testing period. Flow rate data for 3 weeks during Feb 2012 are shown in Figure 3.9.

Siemens Canada technical staff identified the reason for negative flow rate data: bidirectional flow meters show negative values when the flow rate is close to zero which is -0.124 l/s (1 l/s was the recorded maximum flow rate). Since this solar thermal system is a forced circulation system driven by a constant flow pump, the expected flow rate during daytime was positive. Their suggestion was that negative flow rate data should be set to zero during data analysis.

The second issue was sudden positive flow rates data such as 1 liters/sec during the day. 2013/02/08 is an example, which shows sudden positive values (Figure 3.9). Data were recorded with these negative and sudden positive flow rates for 7 months. In May 2013, steady state efficiencies of the collectors were calculated according to equation (2.9) for the period of 2012/10/27 to 2013/5/31. Results showed negative efficiencies and sometimes efficiencies higher than 100%. Due to inconsistent nature of flow rate data and unexpected values of efficiencies, the flow meter was checked for accuracy at the beginning of June 2013. As the first step, the flow meter and its electrical groundings were assessed.

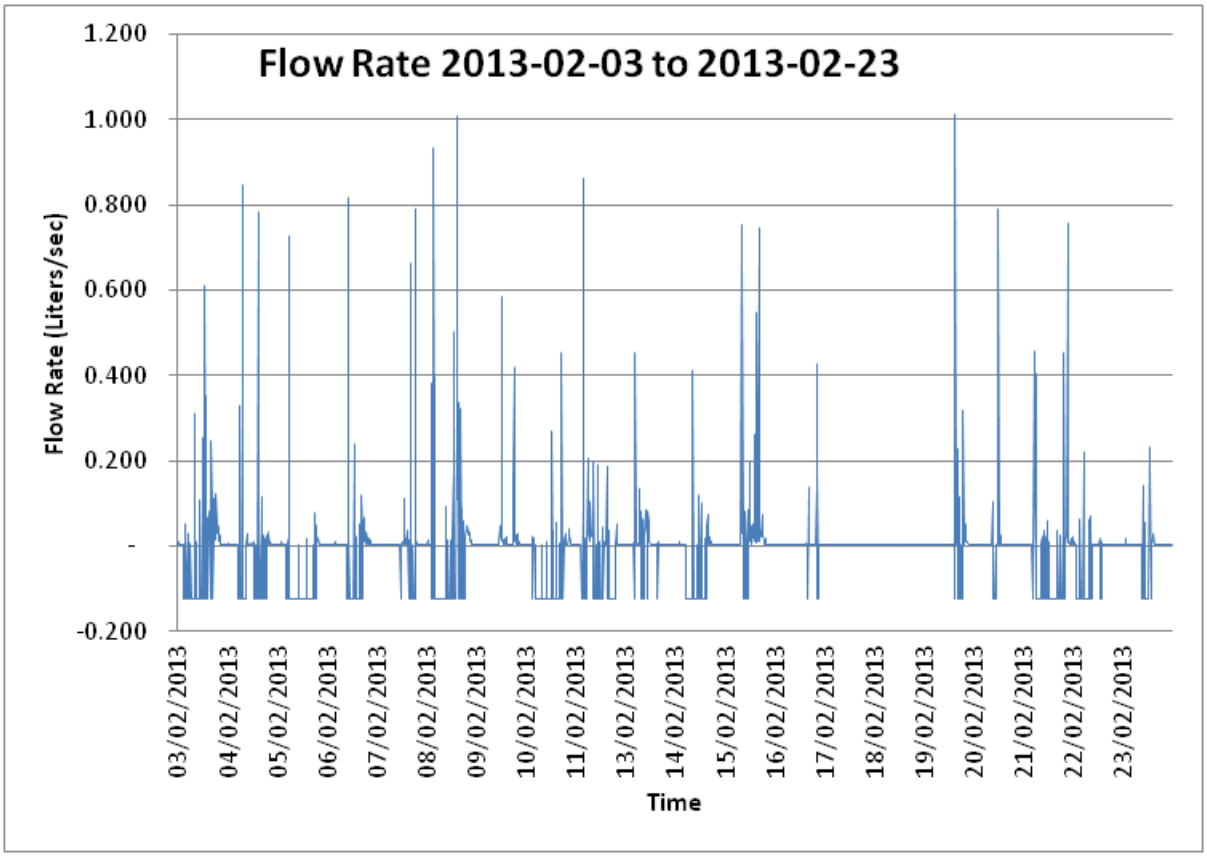

Figure 3.9: Flow Rate Variation of water/Glycol Mixture from 2013/02/03 to 2013/02/23

Flow Meter and Installation Position

One mandatory installation requirement of flow meter was to set the positive flow indication arrow to the expected positive flow direction of water/glycol mixture. In June 2013 an agent of flow meter supplier checked the flow meter installation position and confirmed it was installed to the right direction of flow. Flow data was then logged for one week and graphed. This one week data contained negative flow rates. In July 2013 the flow meter was disconnected from system and sent to the manufacture ONICON Incorporated where the flow meter was tested in a standard test facility (in USA) and confirmed the flow meter is accurate.

The flow meter was installed for a second time and data logged for another week. Again, the flow rate data showed negative flow rates and sudden positive values. In August 2013, the flow meter installation requirements were checked and it was found out most accurate flow rates occur when the meter is horizontal. Because the horizontal position minimizes problems associated with partial filling of the pipes and the presence of bubbles. In September 2013, the flow meter orientation was changed to horizontal. After changing the position, in October 2013, the flow meter started to show highest positive value as 0.15 liters/sec. Still it showed negative flow rates. This positive flow rate is also higher than 0.107 l/s, which is the designed maximum flow rate through the control valve in the circuit.

3.7.3.1 Flow Rate Data from October 2012 to May 2013

Flow meter was installed in the vertical position as shown in Figure 3.10 from October 2012 to May 2013. Then the flow meter positioned horizontally as shown in Figure 3.12. Flow rate from October 2012 to May 2013 period was graphed and it is shown in Figure 3.11. Flow rates for the horizontal position are shown in Figure 3.13.

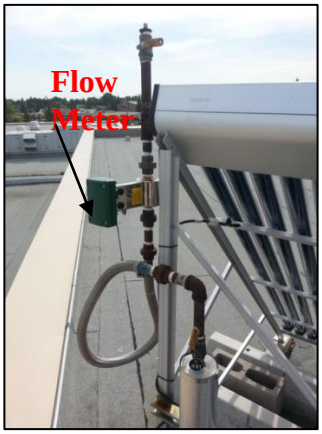

Figure 3.10: Flow Meter Vertical Installation Position from October 2012 to May 2013. Photographed by Athaudage Dona ,(2013).

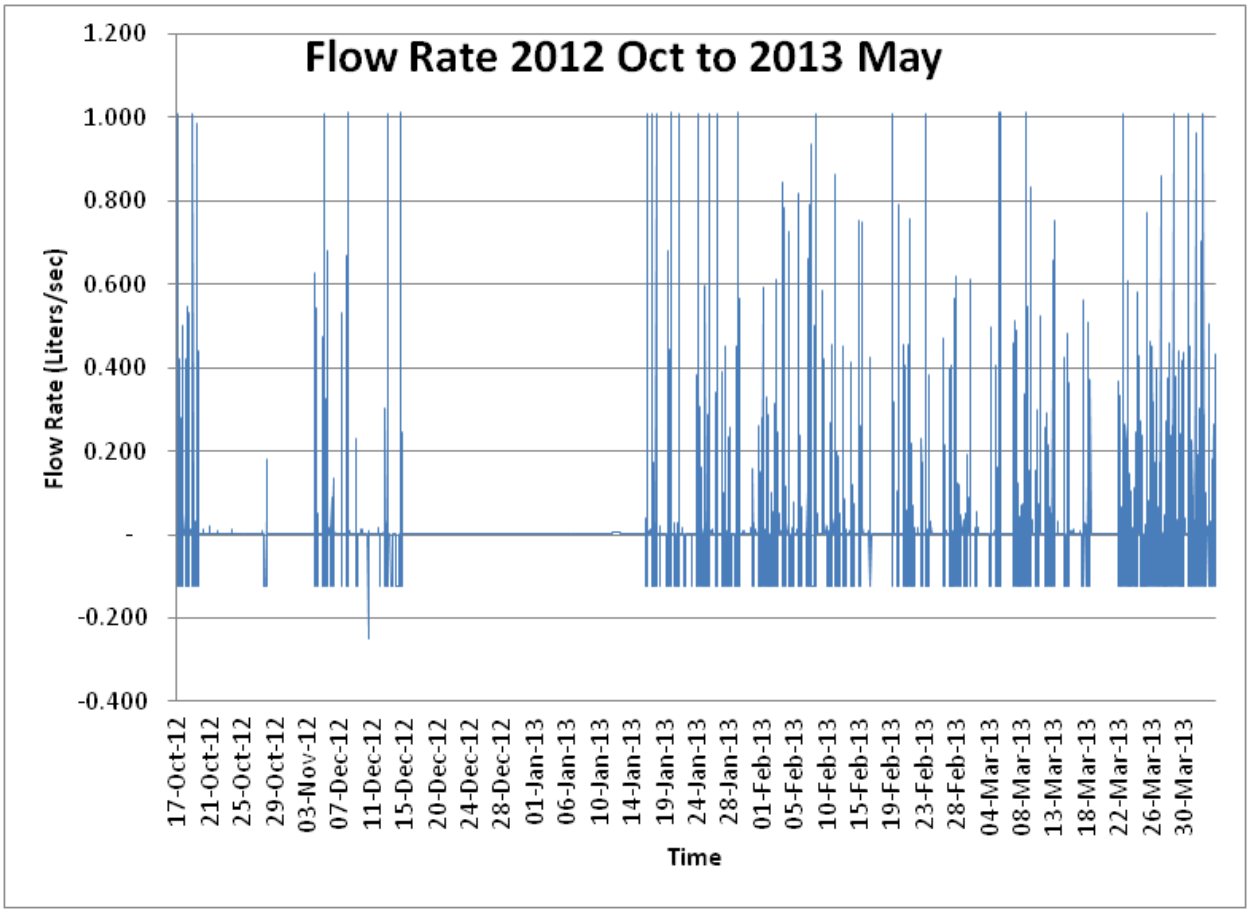

Figure 3.11: Flow Rate Variation from October 2012 to May 2013

3.7.3.2 Flow Rate Data from November 2013

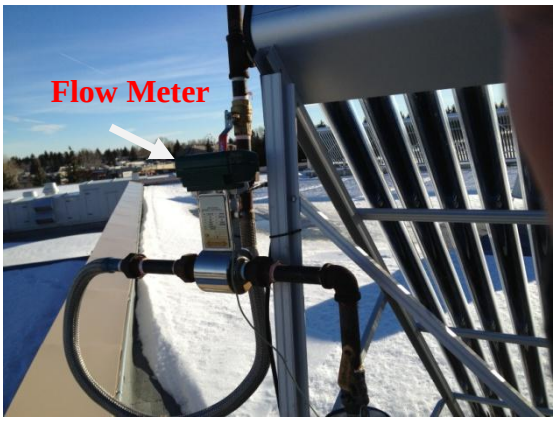

Figure 3.12: Flow Meter Horizontal Installation Position from November 2013 to Present. Photographed by Athaudage Dona ,(2013).

Figure 3.13 shows the flow rate from November 2013 to January 2014 where the flow meter was installed in horizontal position. New flow meter setup shows negative values during daytime and flow rate does not exceed 0.15 l/s.

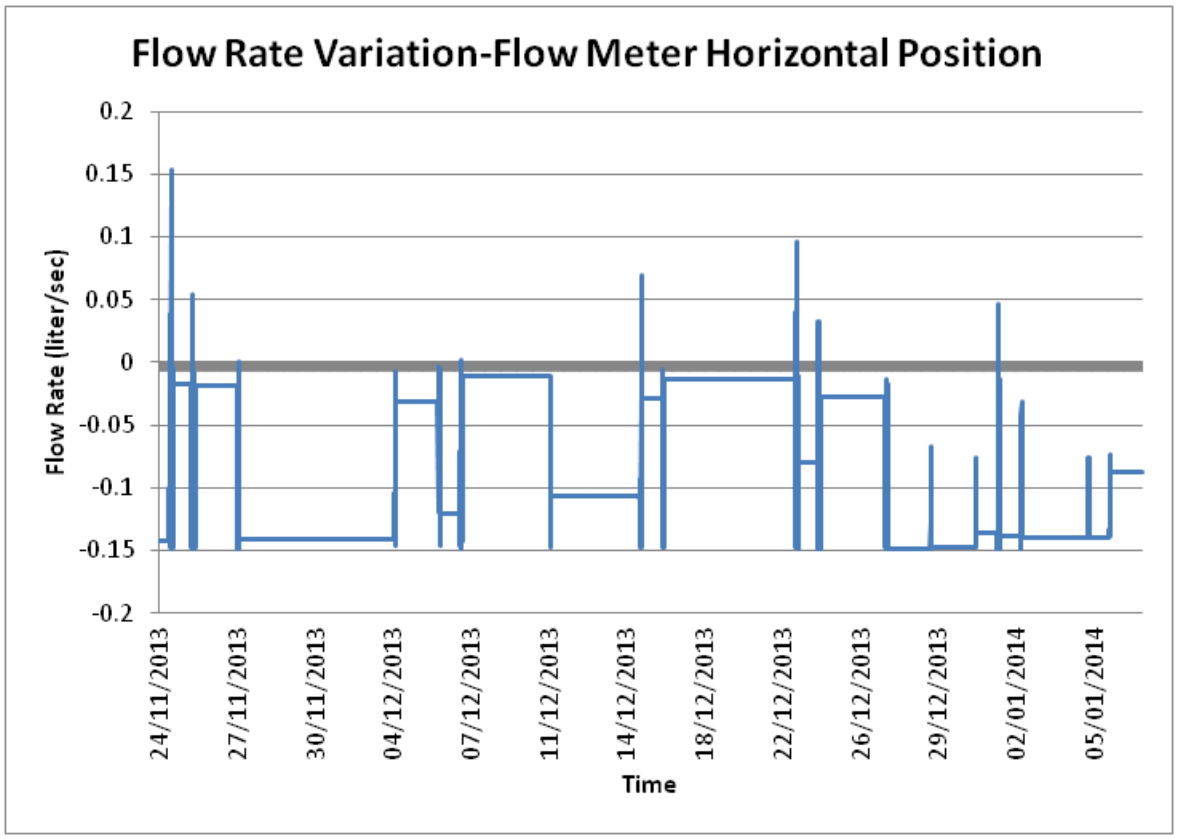

Figure 3.13: Flow Rate Variation from November 2013 to January 2014

After comparing flow rate data in vertical and horizontal position of flow meter, it was concluded that negative flow rate behaviour and the sudden flow rate changes were not caused by a fault in flow meter. Further the accuracy of the flow meter could not be improved once it was installed in the horizontal position. By considering the most consistent data, the data analysis was based on October 2012 to May 2013 data.

3.8 Experiment on Heat Capacity of HP ETC

Equation (2.5) contains the term $(MC)_e$ which is the effective thermal capacity of the HP ETC collector. In other words, it is the summation of heat capacities of each component of collector. The component with highest heat capacity bears the largest internal energy if the whole collector at same rate of change of temperature. The collector temperature can be approximated with mean temperature T_m of working fluid (Duffie & Beckman, 2013). Therefore, the magnitude of heat capacity is a good indicator for internal energy, which generated in each component.

An experiment was conducted to estimate the heat capacity of a heat pipe evacuated tube in the absence of the manifold to allow determination of the heat capacity of 30 heat pipe evacuated tubes. The total heat capacity of the collector is given by the international testing institute Fraunhofer (Jiangsu Sunrain Solar Energy, n.d) as 15.6 kJ/m^2K. The difference of two values will provide the heat capacity of manifold.

A clear day was selected based on environmental Canada weather network weather forecast. The forecast. The criterion for defining a clear day is discussed in section 4.2. A single tube was placed on the roof close to the testing panels and tilted to 45^0 in a structure as shown in Figure 3.14. A type K thermocouple was used to measure the temperature of condensation bulb and its sensing junction was attached to the heat pipe's condensation bulb as shown in

Figure 3.15 a). This thermocouple can measure up to 200°C.

Figure 3.15 a) and b) shows the attachment of temperature sensor to data logger and to the condensation bulb. The black cloth covering the heat pipe was then removed and the

temperature of heat pipe, solar radiation and wind speed logged in every 10 seconds on 2013/09/29 from 3.38pm to 5.45pm. Figure 3.16 shows the results.

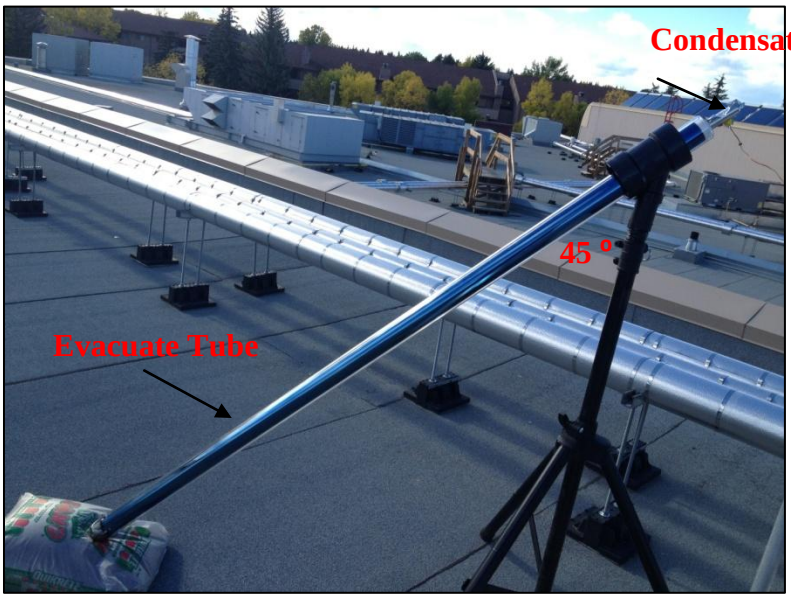

Figure 3.14: Experimental Setup to Determine Heat Capacity of Evacuated Tube. Photographed by Athaudage Dona, (2013)

The tripod holds the tube and sand bag on floor protect the glass end of tube.

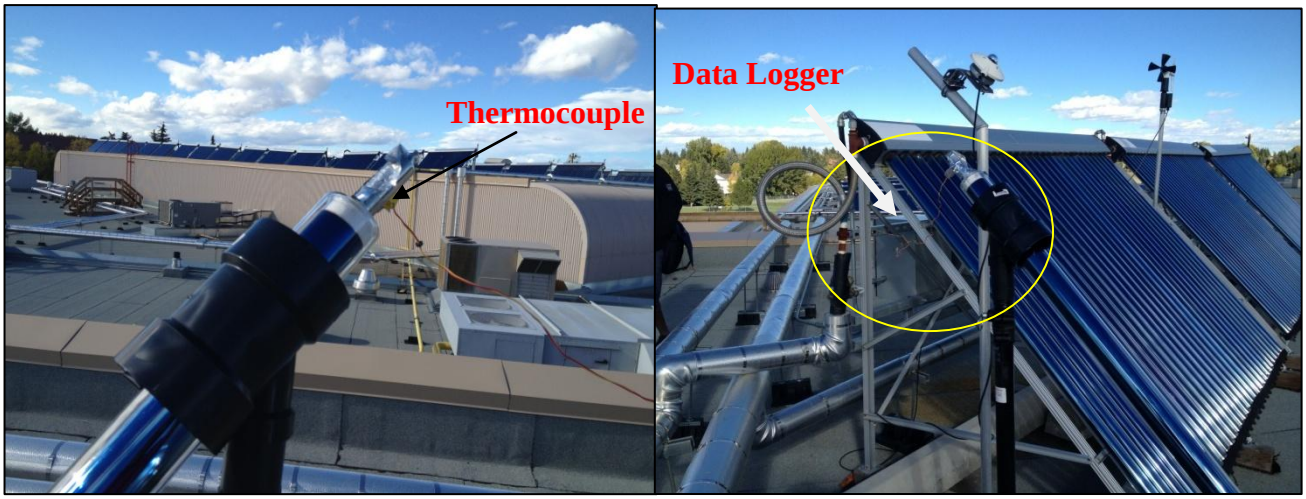

Figure 3.15: a) Temperature Sensor b) Data Logger Locations. Photographed by Athaudage Dona, (2013)

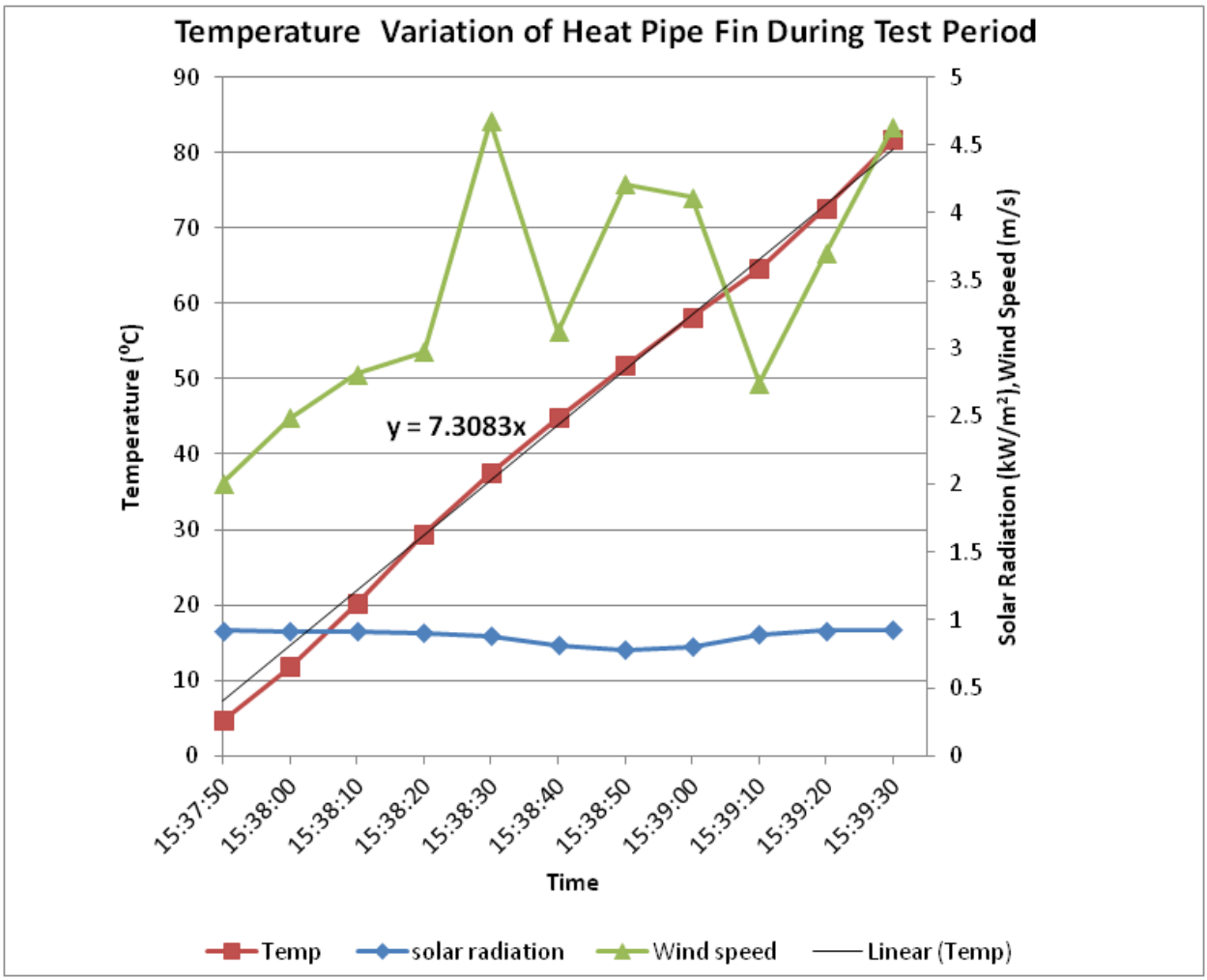

Figure 3.16: Experiment on Heat Capacity: Temperature of Heat Pipe Condensation Bulb and Wind Speed, Solar Radiation Variations During Test.

The heat absorbed by the evacuated tube transfers to the condensation bulb as explained in Section 1.3. The energy received by the condensation bulb is the useful heat gain of HP evacuated tube. The relationship of useful heat gain and the unsteady state heat generation of the

system are explained in Equation (2.5). The same equation can be applied to one heat pipe evacuated tube. If the wind speed is between 2 m/s to 4 m/s convection losses can be neglected according EN 12975 test standards (Fischer et al. (2004).

The solar radiation variation during experiment was almost constant and the wind speed was between 2 m/s to 4 m/s. Figure 3.16 shows the data logged during 3.37.50 pm to 3.39.30 pm. The temperature rise of the condensation bulb (also called as fin of heat pipe) vs. time was almost linear and is given by,

$$T_{bulb} = 7.083\ t.$$

T_{bulb} is the temperature measured at the end of condensation bulb, and t is the time. Time derivative both sides give,

$$\frac{dT_{bulb}}{dt} = 7.083$$

After neglecting convection and irradiance losses through tube, the Equation (2.11) reduces to the simple heat balance:

$$IA_{tube} = (MC)_e\ \frac{dT_{bulb}}{dt}$$

A_{tube} is the absorber area of a single tube. Solar radiation variation was almost constant during tested period at 880.4 W/m^2. Absorber area of the collector is 0.808 m^2 (Jiangsu Sunrain Solar Energy, n.d.).Then the $(MC)_e$ can be estimated as follows,

(3.1)

$$880.4\ \left(\frac{W}{m^2}\right) \times \frac{0.808\ m^2}{30} = 7.083\ \left(\frac{K}{s}\right)(MC)_e$$

so that

$$(\mathrm{MC})_\mathrm{e} = 3.35\ \mathrm{J/m^2K}$$

Since there are 30 tubes in a collector, the heat capacity of the collector is

$$3.35\frac{\mathrm{J}}{\mathrm{m^2K}} \times 30 = 0.10047\ \mathrm{kJ/m^2K}$$

This compares to

$$(\mathrm{MC})_{\mathrm{e,collector}} = 15.6\frac{\mathrm{kJ}}{\mathrm{m^2K}}\ [\text{Given in (Jiangsu Sunrain Solar Energy, n. d)}]$$

$$(\mathrm{MC})_{\mathrm{e,manifold+other}} = (15.6 - 0.1) = 15.5\ \mathrm{kJ/m^2K}$$

It can be concluded that the internal energy generation within the system is largely due to the manifold and can be estimated from the inlet and outlet temperatures and the MC value given above. Further, it is not necessary to monitor the ETC temperatures in order to determine their contribution to the internal energy.

Chapter Four: **RESULTS AND DISCUSSION**

4.1 Introduction

This chapter presents the analysis of data collected from September 2011 to May 2013. Solar radiation data indicated good solar availability at Calgary Southland Leisure Centre (SLC). Temperatures of water/glycol mixture at inlet and outlet of two ETC panels showed high temperature readings. Flow rate of water/glycol mixture showed high flow rate variations including negative flow and sudden high positive values. The unsteady nature of environmental conditions assessed to identify reason for rapid changes in variables of the solar thermal system. These data was used to estimate the efficiencies of heat pipe ETC under steady and unsteady state conditions.

4.2 Solar Radiation

Solar radiation data collected at SLC (Sections 3.6, 0) was graphed using Microsoft Excel to see the radiation variation over time. Pyranometer data provided 1-minute average of solar radiation (as discussed in Section 0). Figure 4.1 shows the solar radiation vs. time (on daily basis) for May 2012. The shape of the radiation curve becomes smoother when the sky gets clear. Due to daily weather condition, the shape of the radiation curve differs from day to day, hence has a significant impact of the efficiency calculation. In order to handle that issue in the efficiency calculation, days during the observed period was separated into three different categories, clear day, partly cloudy day and cloudy day. These categories indicate different levels of solar availability. It also allows estimating the performance of collectors under different levels of solar energy availability. The mathematical model describe in next section was developed to process the daily total radiation (DTR) to separate days in to above three categories.

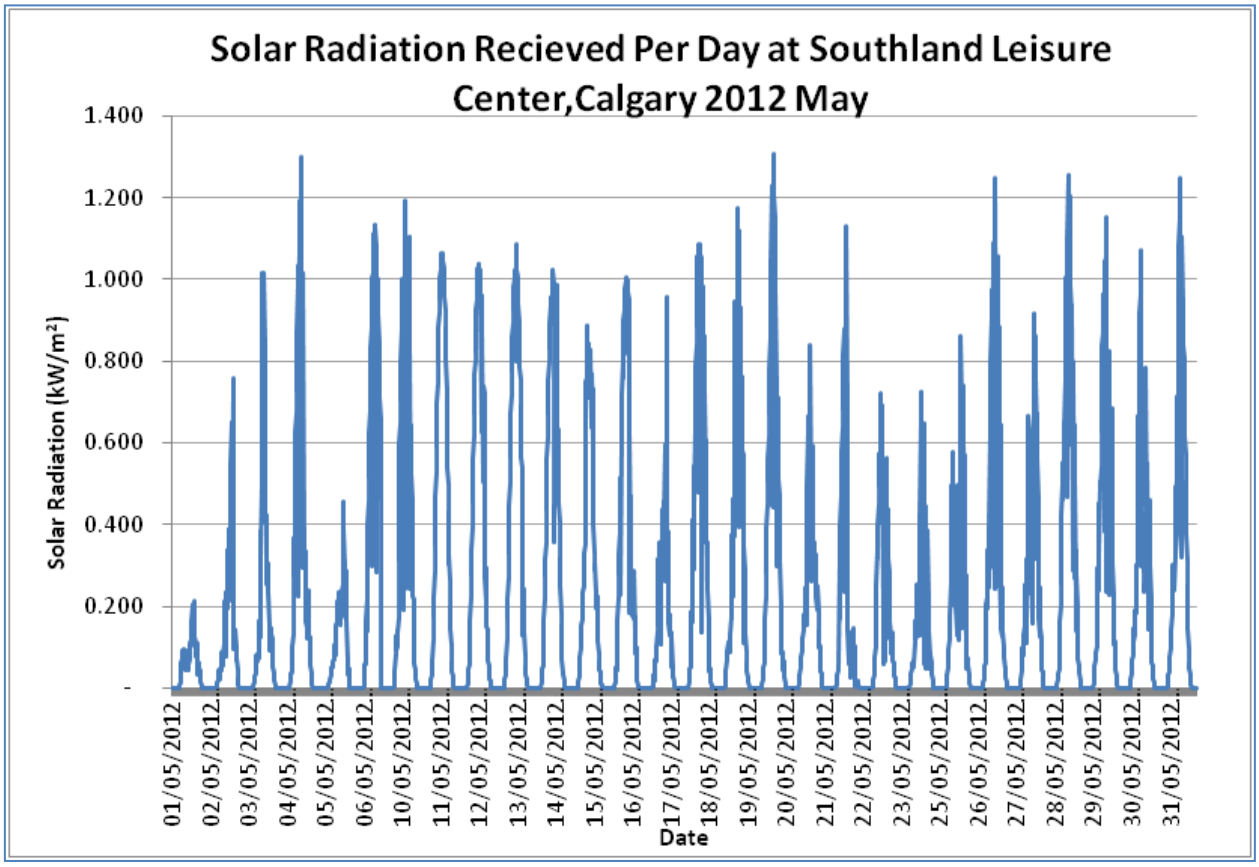

Figure 4.1: Solar Radiation Variation in May 2012 at SLC

4.2.1 *Methodology Selecting Clear, Cloudy, Partly Cloudy Days*

The Figure 4.1 represents the radiation variation for the month of May 2012.The area under the radiation curve for each day is the daily total radiation, DTR. DTR will indicate the density of cloud cover available during the daytime. Clear, cloudy and partly cloudy days were separated based on the DTR. The DTR is high for a clear day and very low for a cloudy day. However, the area under two clear days in summer and in winter can be different. Monthly average of daily total radiation (MAv-DTR) indicates the monthly variation (as shown in Figure

4.9). DTR compared with the monthly average of daily total radiation (MAv-DTR) to reduce the impact of seasonal variation. DTR data for a month is shown diagrammatically in Figure 4.2. Days to the right of the mean are likely to be sunny and those to the left likely to be cloudy. The days in right and left end can be separated by using factor defined as [(DTR)-(MAv-DTR)]/standard deviation (StdDev) of DTR for a month. In other words, this factor describes the amount of cloud cover during a day.

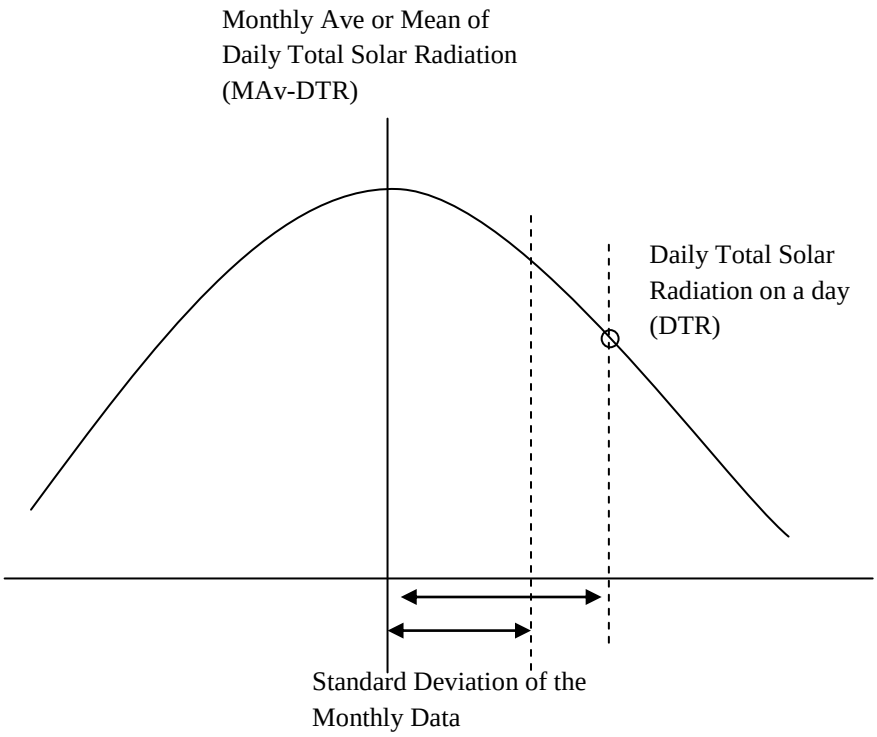

Figure 4.2: Distribution of Daily Total Solar Radiation in a Month

If the calculated factor is higher than +1 the day was considered as a clear day. If it is lower than -1 then it is a cloudy day. The days between -1 and +1 were taken as partly cloudy days.

As an example, the radiation for 2012/11/14 was taken. The mean DTR for the month was 2.51 kWh/m^2, and the standard deviation was 1.64 kWh/m^2. For 2012/11/14, the DTR was 4.99 kWh/m^2. Since (4.99-2.51)/1.64 > 1 the day was clear.

The lower limit for clear days, +1 was adjusted to +0.92 for the period Jan 2013 to May 2013 after comparing observed clear days. The upper limit for cloudy days <-1was changed to -0.6 for Feb 2013 to May 2013 as after comparing observed cloudy days.

Daylight Time

The number of daylight hours was used to select long days and short days from winter 2012 to spring 2013 to assess the seasonal performance of the HP ETC. The yearly average number of daylight hours is 12 hours. The procedure used here is based on the assumption that long days have more than 10 hours of daylight. 10 hours was taken considering half of the year that includes winter and spring. Winter and Spring have shorter daylight hours than summer. Figure 4.3 shows the short and long daylight days.

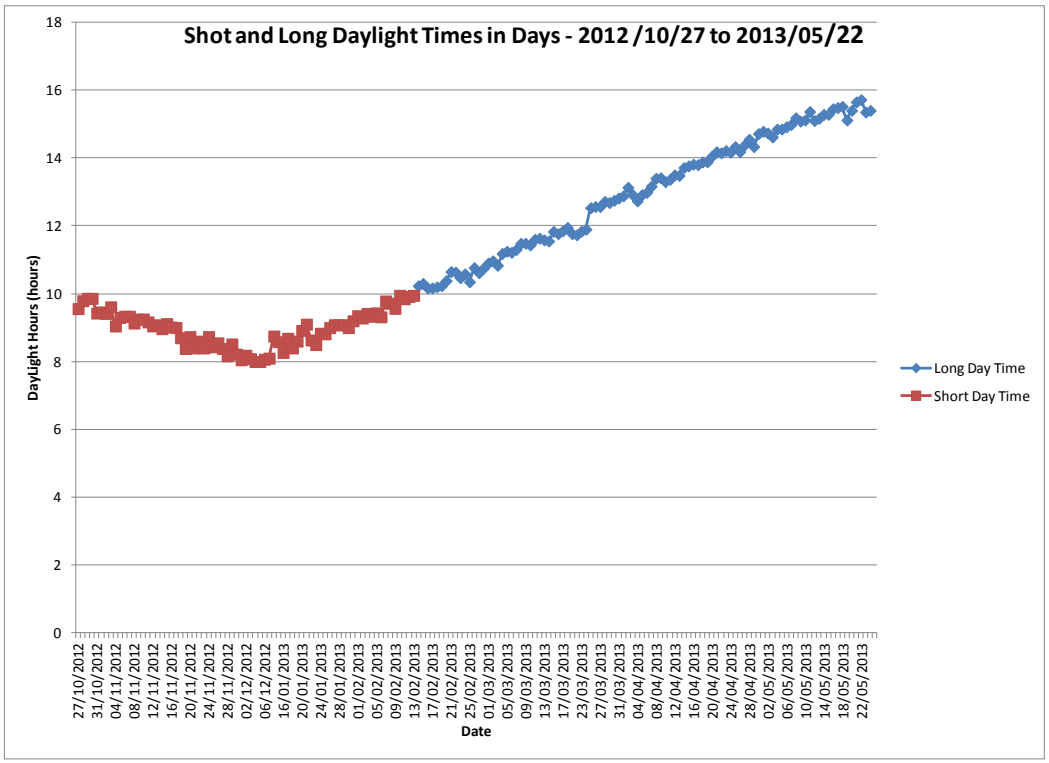

Figure 4.3: Short and Long Daytime Days in Testing Period

Figure 4.3 represents the time span of the solar radiation received and it was identified by the time when the radiation values greater than zero. (The reflected radiation monitored by pyranometer may have cause for the irregular pattern in the graph. The winter solstice was on 21st of December 2012[1] and it is not shown in this figure due to a power failure of pyranometer).

[1] Retrieved From: http://www.timeanddate.com/astronomy/canada/calgary

Days within the data analysis period (Oct 2012 to May 2013) were divided into three categories based on the technique discussed in Section 4.2.1. The shape of typical radiation curves for clear days, partly cloudy days and cloudy days are shown in Figure 4.4.

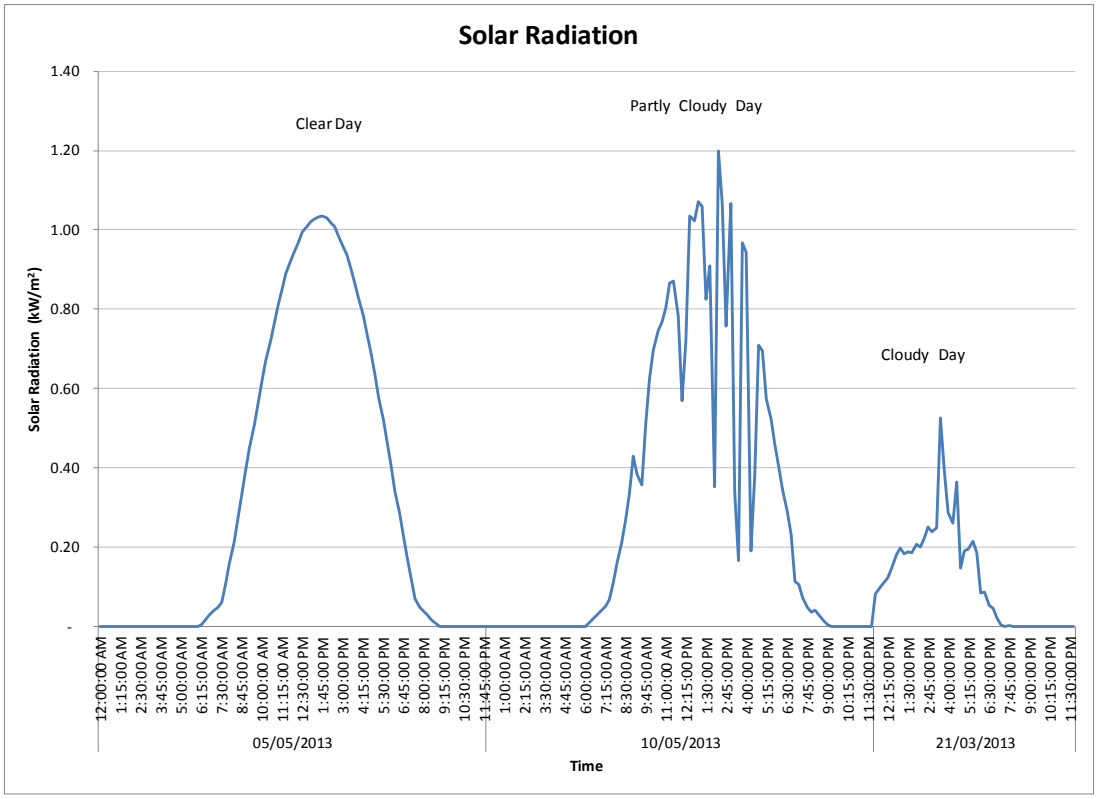

Figure 4.4: Solar Radiation Variation on a Clear Day, Partly Cloudy Day and Cloudy Day

2013/05/05 is classified as a clear day. It has maximum solar radiation around the noon and a smooth variation of solar radiation over the whole day, which is typical for a clear day. The maximum solar radiation received at solar noon on this day was about 1000kW/m^2 on the 45° angle surface.

2013/05/10 was selected as a partly cloudy day for the efficiency estimation and it is the second curve of Figure 4.4. It has significant variations in solar radiation during the day. Cloud cover during daytime has intermittently blocked the solar radiation. Sometimes the maximum solar radiation received on partly cloudy day exceeds the clear day's maximum solar radiation. The main reason is the reflected solar radiation from ground and clouds.

2013/03/31 is a cloudy day with lower solar gain. It has very low solar availability around noon. Cloud cover for a long period has blocked most of solar radiation.

Manual Selection of Days

The daily solar radiation variation curves from 9.00am to 6pm (as shown in Figure 4.4) were graphed for the whole data collected period from 2011/11/14 to 2013/5/25 (18 months) using Microsoft Excel. The manual selection of clear days and cloudy days were based on this graph and the criteria in Figure 4.4. Manually selected days, which were based on observation were compared with filtered data in section 4.2.1. Manually picked data were used to adjust the filtered data in section 4.2.1.

4.2.2 ***Solar Radiation at SLC***

Solar radiation data collected at SLC and Calgary International airport were compared. The radiation data at Calgary International Airport was obtained from RETScreen. The main objective of this comparison was to assess the accuracy of solar radiation data collected at SLC. Two parameters were calculated at both places. Those were the monthly average solar radiation (MAv-Rad) and daily total solar radiation (DTR). In addition, the daily maximum solar radiation received (DMax-Rad) at SLC was estimated.

Pyranometer at SLC measured the global solar radiation received at 45° angle that is direct, diffuse and ground reflected radiation. First daily maximum radiation, daily total radiation and monthly average radiation were calculated using these data. Figure 4.5 shows the daily maximum solar radiation (DMax –Rad) variation over 18 months at SLC.

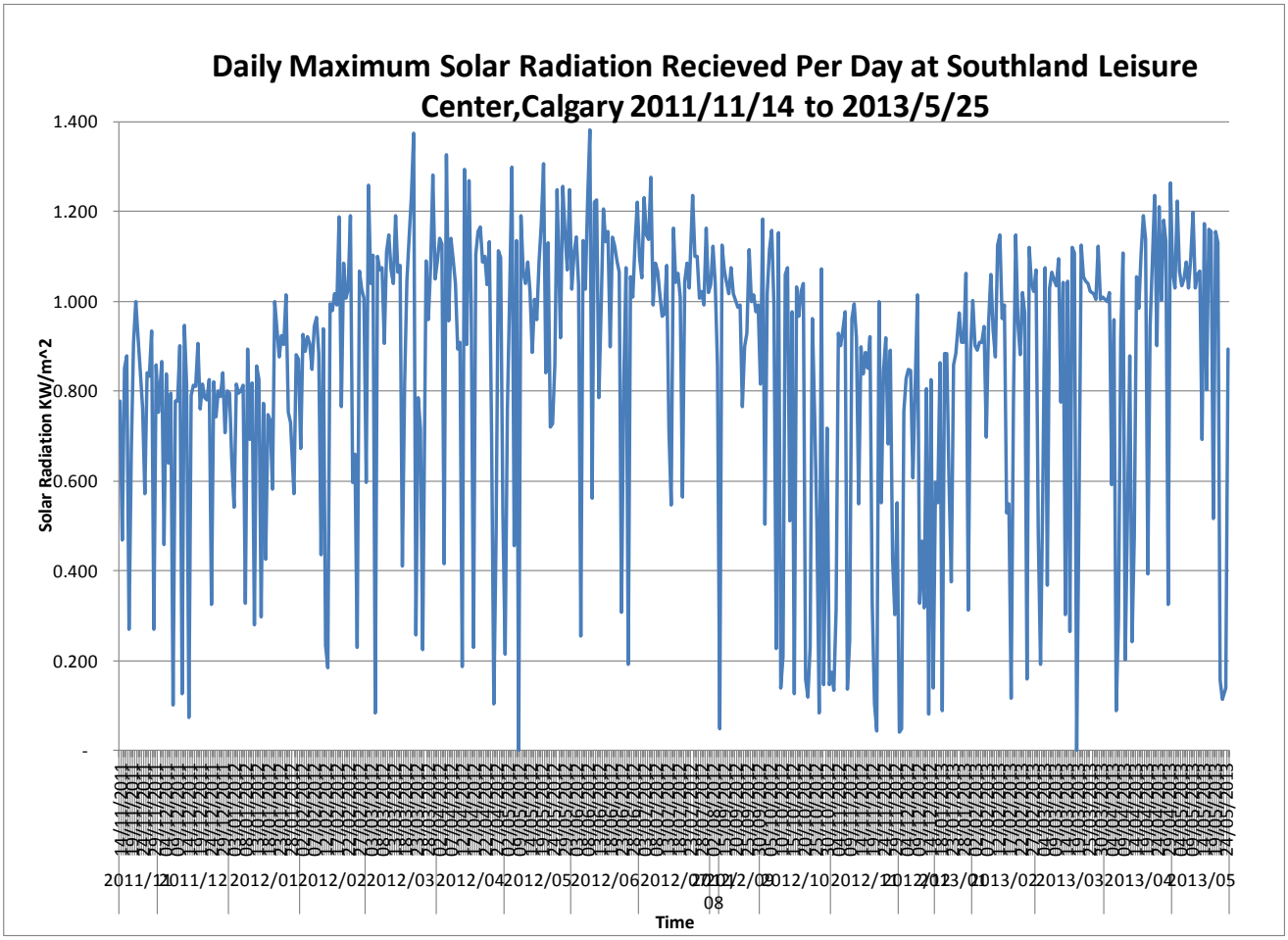

Figure 4.5: Daily Maximum Solar Radiation on 45° at Southland Leisure Centre, Calgary

Ghosh & Prelas (2011) have shown that in the absence of cloud cover (that is a clear day) the maximum possible solar radiation that can be received in a time instant on a horizontal surface of earth is 1000 W/m^2. It can be further calculated that for a 45° angle the maximum possible solar radiation is about 1100 W/m^2. Sometimes clouds can cause reflected radiation

over short periods, which increase the solar radiation received by a collector. Based on Figure 4.5 solar radiation data, SLC has received 1000 W/m^2 to 1200W/m^2 daily maximum solar radiation in summer. In winter (Nov 2011 to Feb 2012 and Nov 2012 to Feb 2013) the maximum can be roughly estimated as 800 W/m^2.But there are few days where daily maximum radiation was higher than 1100 W/m^2. 2012/10/12 is an example, which received maximum radiation between 1100 W/m^2 -1200 W/m^2. In Figure 4.5 the period from 2012/02/25 to 2012/07/26 has few days that received maximum radiation even above 1200 W/m^2.

Daily maximum radiation 800 W/m^2 during winter indicates high solar intensity at SLC. The daily maximum solar radiation in 2011 and 2012 is approximately constant throughout the year. These two factors show a good solar source for solar thermal system implementations in Calgary. This good solar intensity in winter months will be further analyzed in Section 4.2.3 using daily total radiation (DTR) to estimate its effectiveness for an application.

Figure 4.6 shows the solar radiation vs. time for the period 2012/10/27 to 2013 /05/25. It also indicates the categorization of days according to Section 4.2.1. Different colors are used to indicate the type of the day.

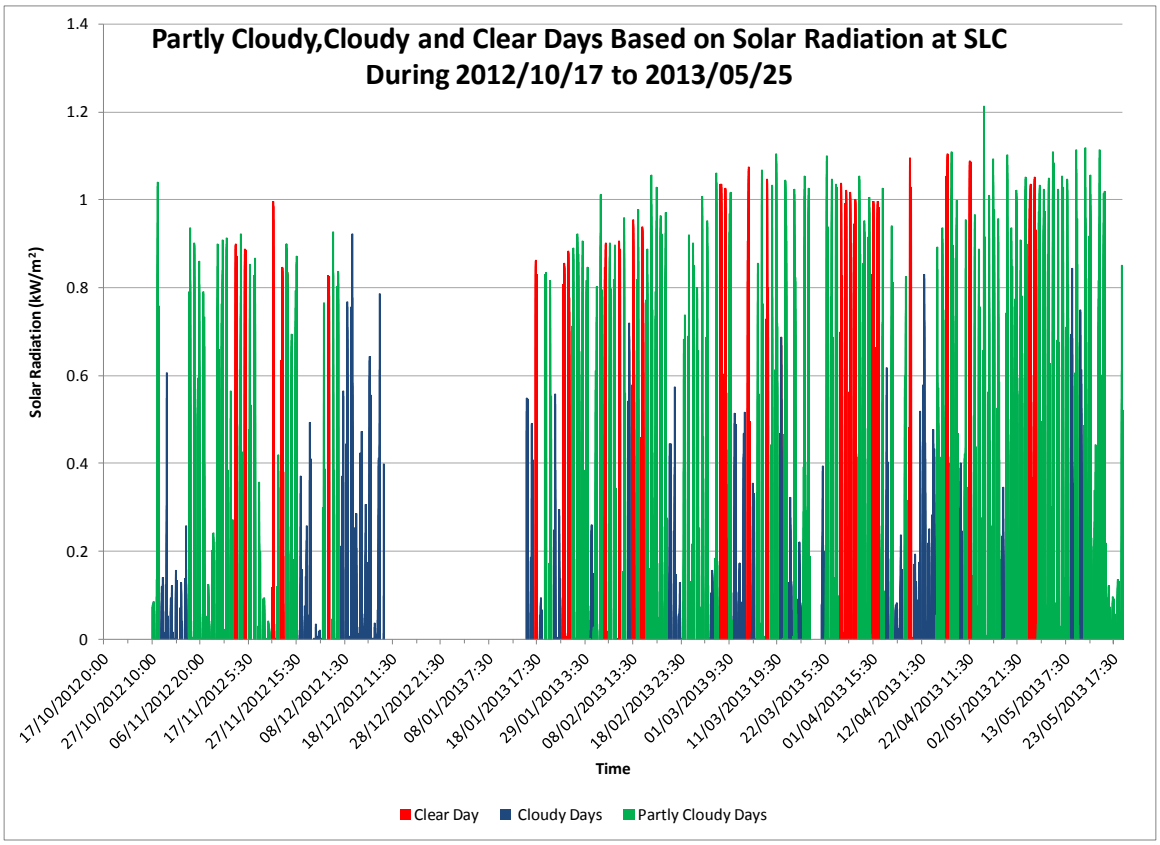

Figure 4.6: Solar Radiation at SLC During 2012/10/17 to 2013/05/25 (From Dec 2012 to Jan 2013, no data was collected due to a power failure). Individual days are marked as clear, partly and cloudy according to the scheme described in Section 4.2.1.

Figure 4.6 shows significant day-to-day solar radiation variations, which indicate the intermittency of the solar resource at SLC. It also shows numbers of partly cloudy, cloudy and clear days during the measurement period. Partly cloudy days are more frequent than clear days. Partly cloudy days and cloudy days are likely to require unsteady analysis due to high intermittency. Steady analysis of system performance according the procedure in ref (ISO, 2010) was intended to be done for the clear days.

Daily Total Solar Radiation (DTR) Received by Calgary

Daily total radiation (DTR) received at SLC and Calgary international airport from 2011/11/14 to 2013/5/25 were compared to check the accuracy of pyranometer data. Daily total solar radiation (DTR) received at SLC on a 45° surface was calculated by summing recorded solar radiation data in 1 minute intervals from 12 midnight to 12 midnight for each day. Results were compared with the horizontal solar radiation at Calgary International Airport corrected to 45°. Solar radiation at Calgary International Airport was obtained from NASA Satellite data (NASA Near Real-time Global Radiation and Meteorology database) available in RETScreen Plus Software. It is also corrected to 45° using RETScreen tools[2]. The daily total solar radiation (DTR) at Southland Leisure Center and Calgary International Airport over 18 months period is shown in Figure 4.7 and

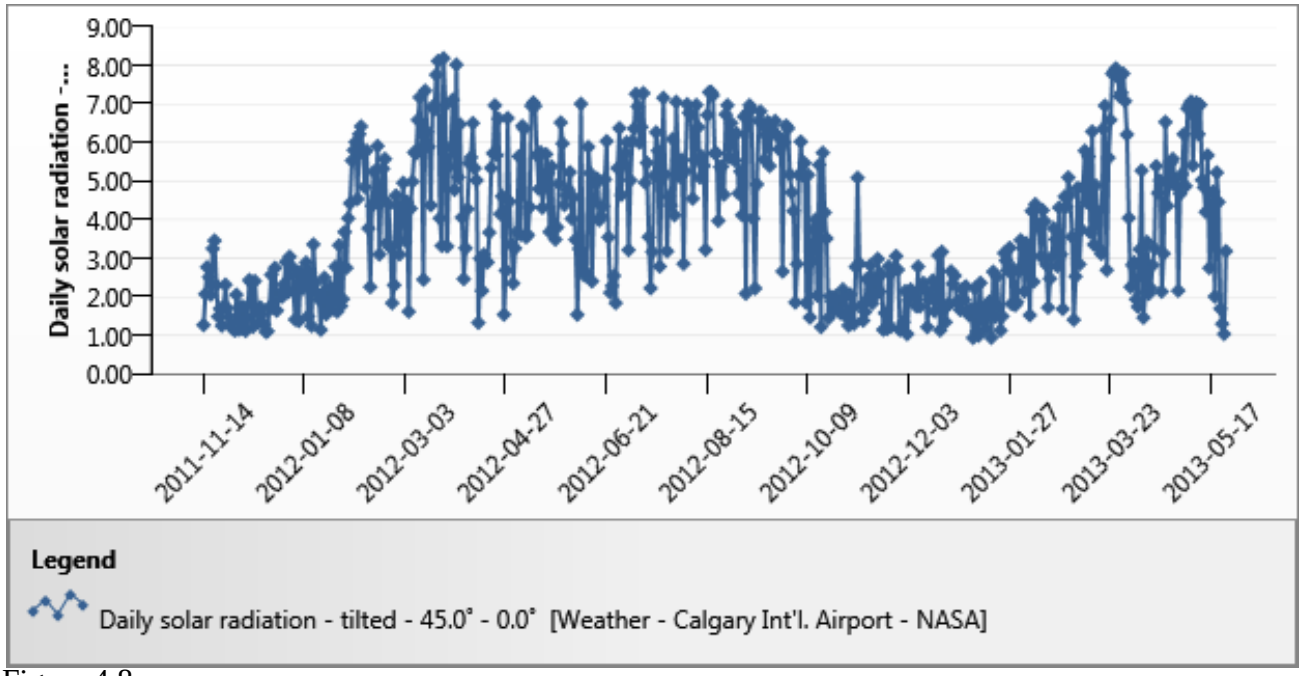

Figure 4.8.

[2] Retrieved from http://www.retscreen.net/ang/home.php, accessed: 2011

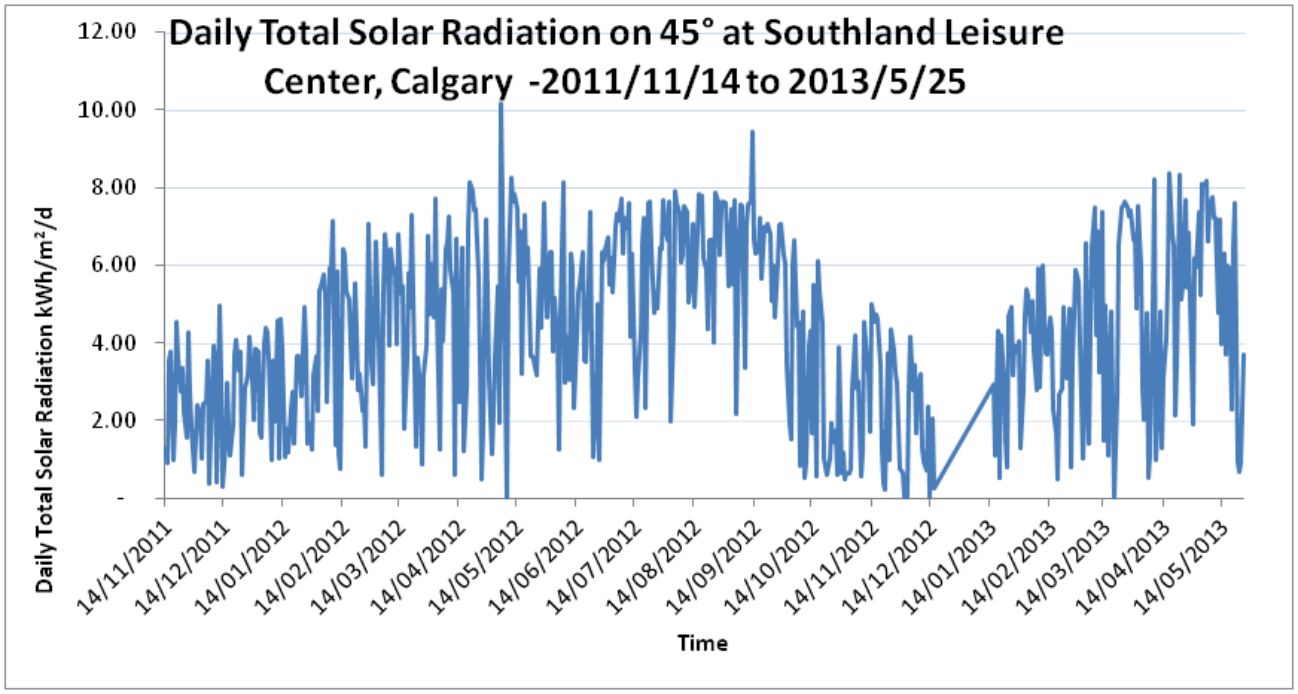

Figure 4.7 : Daily Total Solar Radiation (kWh/m^2/d) on 45° Surface at SLC, Calgary

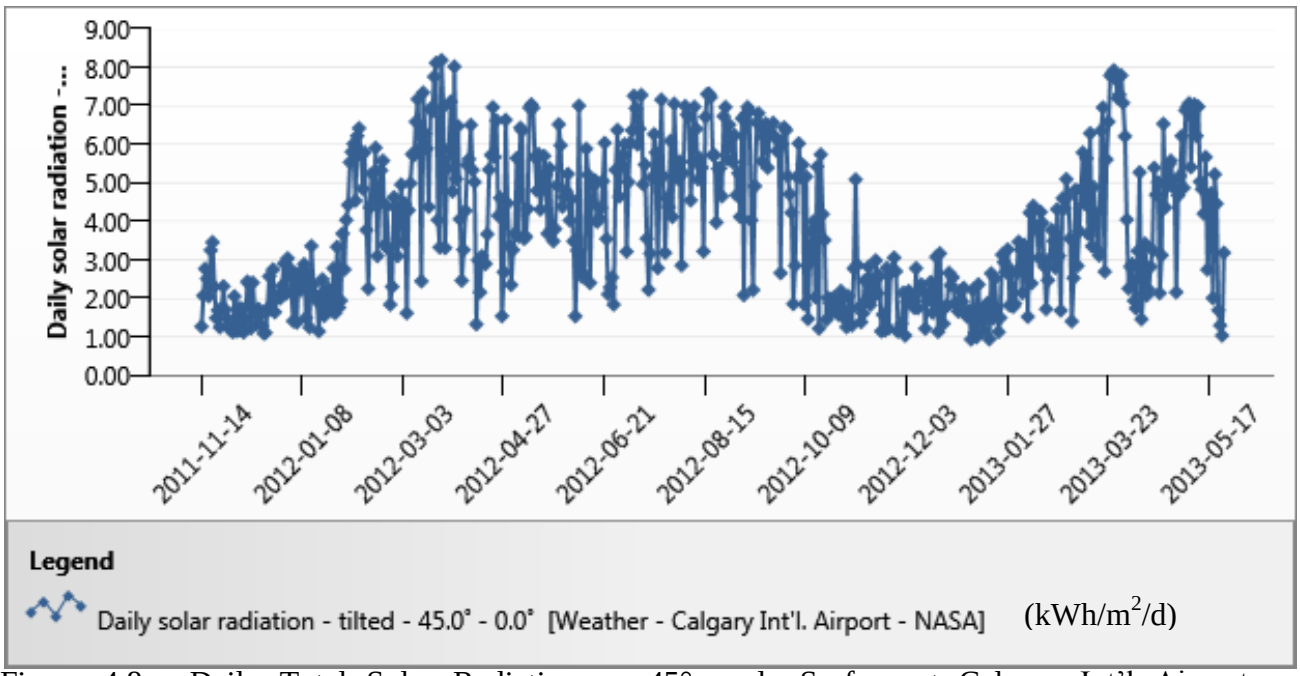

Figure 4.8: Daily Total Solar Radiation on 45° angle Surface at Calgary Int'l Airport

(kW/h/m^2/d).(Both figures have the same X axis range, but due to system limitation in RETScreen and Excel tick marks shows different values)

Figure 4.7 shows the variation of daily total daily radiation (DTR) over the measurement period at SLC. There is a significant difference between total solar radiation (DTR) received on winter and summer even though the maximum daily radiation in Figure 4.5 did not show a significant variation in winter.

According to Figure 4.7 , the daily total solar radiation (DTR) received in 2012 and 2013 winters was between 1kWh/m^2/d to 3 kWh/m^2/d. Daily total solar radiation (DTR) received in 2012 summer was 5 kWh/m^2/d to 7 kWh/m^2/d . Daily total solar gain during winter is almost of half of summer gain. Total solar radiation (DTR) received by Calgary Int'l airport in 2012 and 2013 winters was 2 kWh/m^2/d to 4 kWh/m^2/d. Summer time daily total(DTR) was 5 kWh/m^2/d to 8 kWh/m^2/d. When compares the SLC and Calgary Int'l airport data, SLC has slightly higher solar gain throughout 2012/2013.

Monthly averages of daily total solar radiation (MAv-DTR) received at SLC and Calgary Int'l Airport were evaluated to verify the pattern identified in DTR. Figure 4.9 shows the monthly averages of daily total solar radiation (MAv-DTR) at SLC. MAv-DTR at Calgary Int'l airport which was retrieved from RETScreen. RETScreen MAv-DTR data was on a horizontal surface and it was corrected to 45°. Calculated MAv-DTR at SLC for 18 months and MAv-DTR at Calgary Int'l airport data that was retrieved for the same period were compared and results are shown in Figure 4.9. According to Figure 4.9 total solar radiation (DTR) received by SLC is higher than Calgary Int'l Airport.

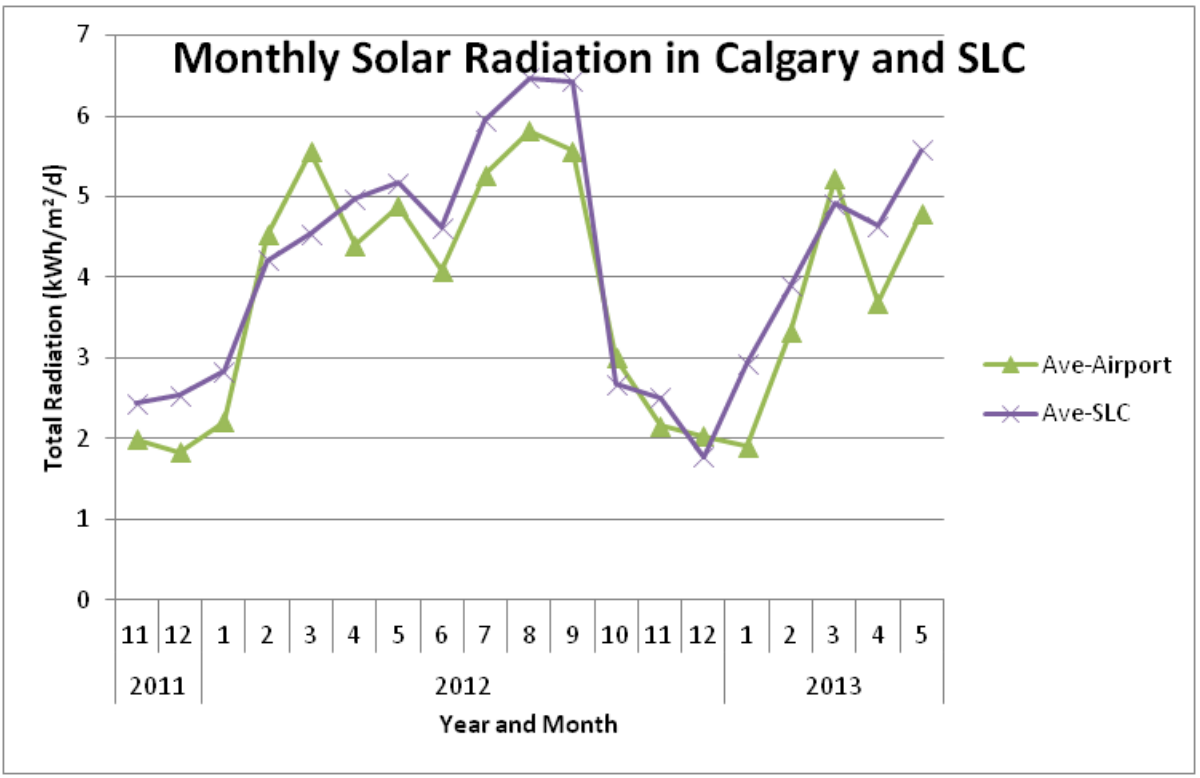

Figure 4.9: Monthly Average Solar Radiation on 45° Angle Surface, Calgary

4.2.3 *Conclusion on Solar Availability at SLC, Calgary*

According to Figure 4.5, Figure 4.7 and Figure 4.9 SLC has high solar intensity throughout the year but much lower daily totals in the winter. Combination of both factors indicates that Calgary has a useful solar source even in the winter months and much stronger solar source in rest of the year. Because of shorter day in winter, solar thermal system implementations may need some backup system or energy storing mechanisms.

According to Figure 4.9 monthly average radiation at SLC and Calgary airport are similar, but SLC has a slightly higher solar gain. This indicates that the SLC Pyranometer data are accurate. The difference of solar radiation at two locations may be due to different amount of ground reflected radiation. The Pyranometer at SLC receives ground reflected radiation that

comes from large rooftop area which is not the case for airport. The ground reflected radiation can be up to 10% of global radiation and it can be higher in winter months (snow reflects almost 80% of radiation receives) (Ineichen, Guisan & Perez, 1990).

4.3 Wind Speed

The wind speed data collected from the anemometer are plotted in Figure 4.10.

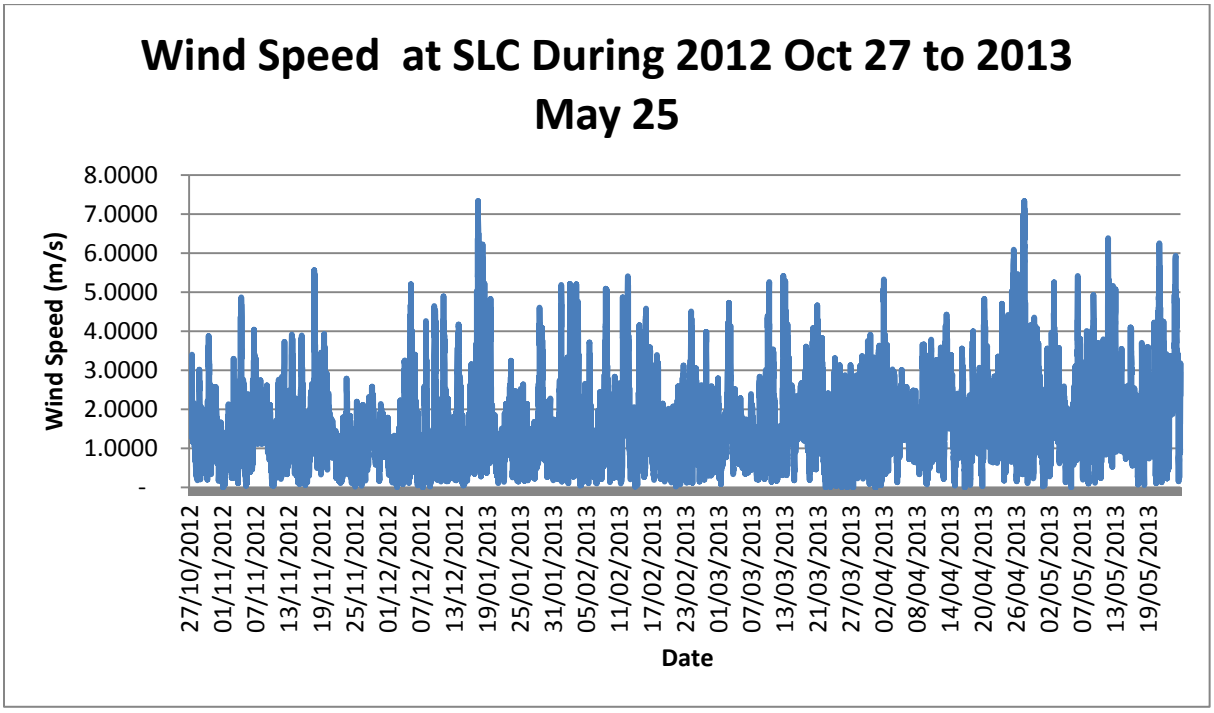

Figure 4.10: Wind Speed During 2012 Oct 27 to 2013 May 25

According to steady state efficiency analysis requirements discussed in section 2.11.2 the wind speed must be in the range of 2 m/s to 4 m/s. Figure 4.10 satisfies this condition most of the time. This indicates that the solar collectors mounted on SLC roof have low convection losses.

4.4 Panel Inlet and Outlet Temperatures

Temperatures variation of the inlet and outlet of two ETC panels (as shown in Figure 2.1) were graphed in Microsoft Excel. 2013/02/03 is a selected day for the illustration of daily temperature variation and it is shown in Figure 4.11. During midday, the inlet and outlet temperatures were between 100°C and 130°C. It also shows that the temperature has risen from inlet to outlet of collector around the solar noon.

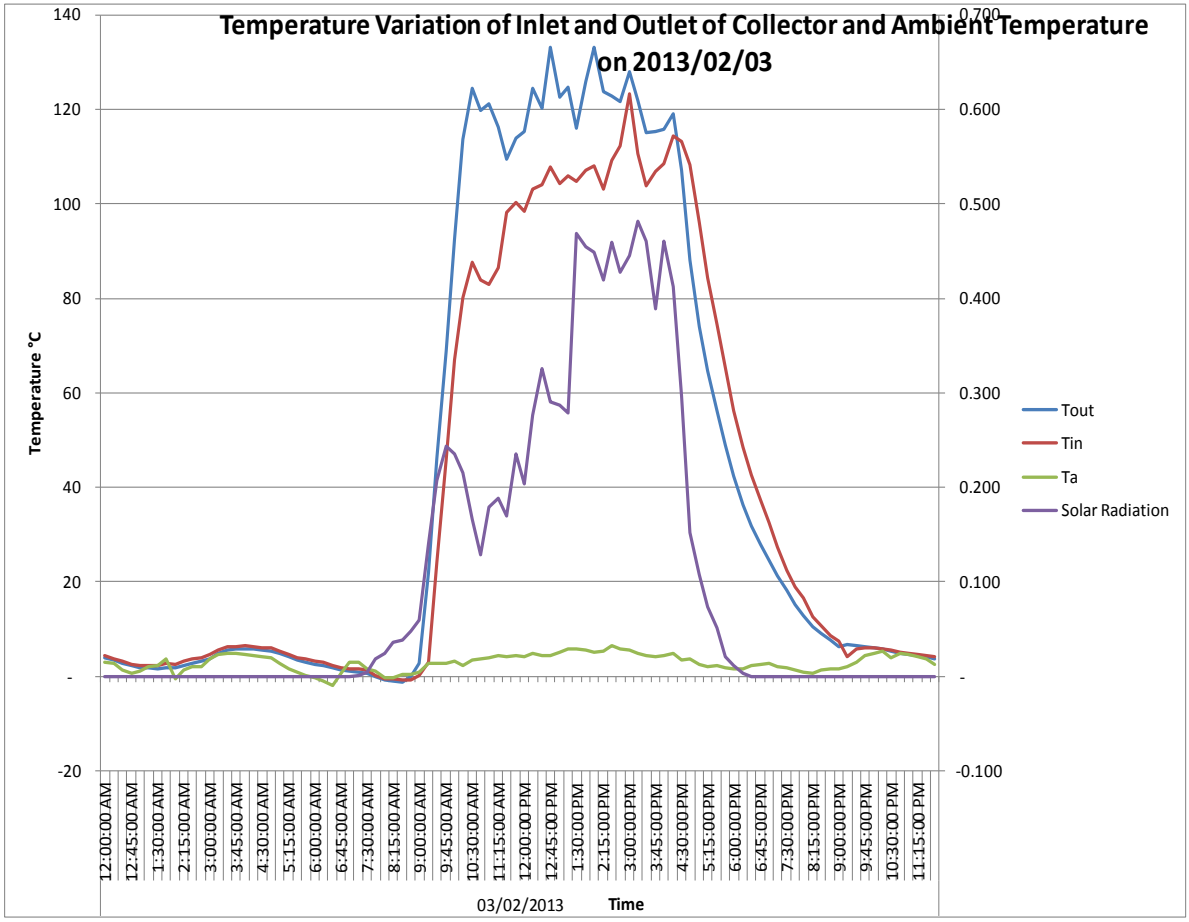

Figure 4.11: Inlet and Outlet Temperatures of Two Collectors and Ambient Temperature on 2013/02/03

2013/05/13 had positive and negative temperature differences between inlet and outlet of manifold during solar noon and it is shown in Figure 4.12. During this day the temperature rose to 120°C in inlet and 130°C in outlet at noon. Then, the temperature has risen in inlet and it has decreased in outlet.

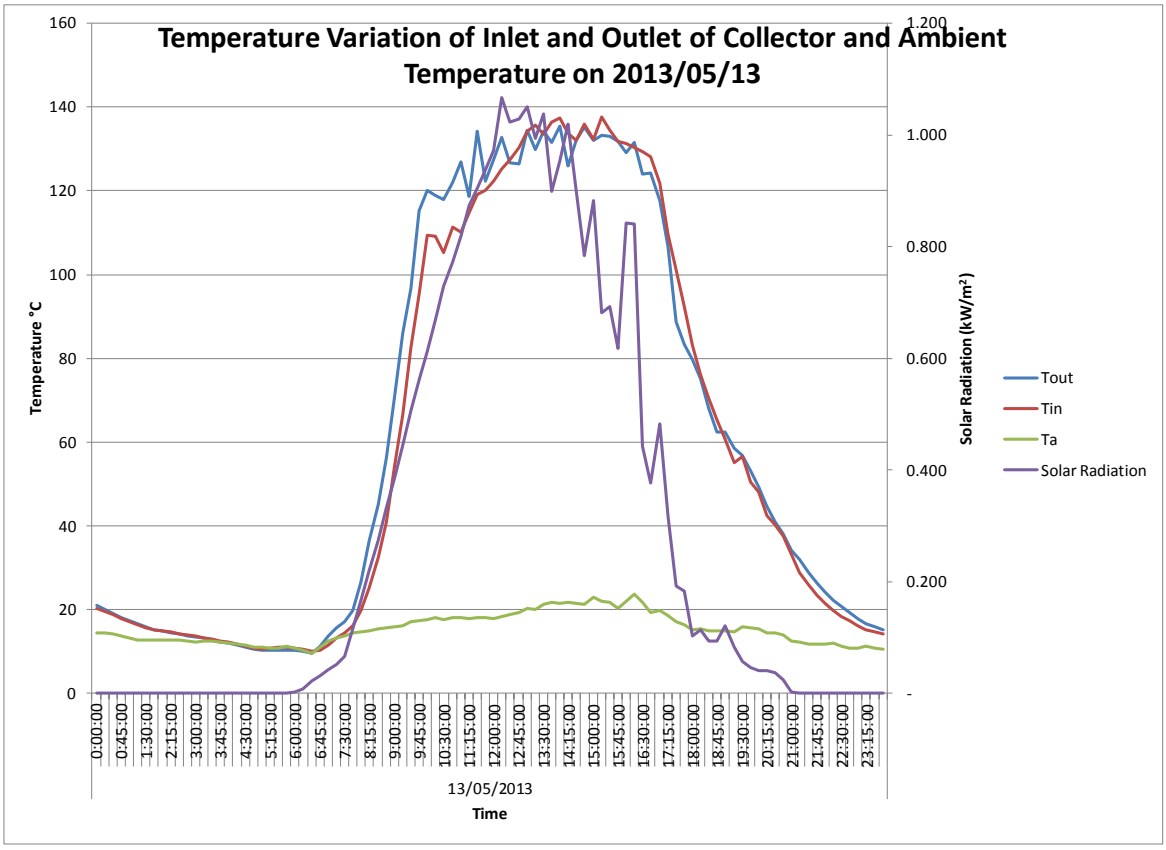

Figure 4.12: Inlet and Outlet Temperatures of Two Collectors and Ambient Temperature on 2013/05/13

Efficiencies of the collector were calculated for both positive and negative temperature rise (inlet to outlet and outlet to inlet). Efficiency results were grouped into two categories as efficiency during positive temperature rise (T_{out}-T_{in} positive) and efficiency during negative temperature rise (T_{out}-T_{in} negative) to clearly see collector behaviors in both directions.

Estimation of Errors in Thermocouples

Accuracy of Platinum RTD is +/- 0.4 °C (Siemens Industry Inc, 2013b). The negative temperature difference on 2013/05/13 varies from -1°C to -12°C. This difference is higher than manufacture's stated experimental error. Further T_{out}-T_{in} was graphed for selected clear day (2012/11/25) and compare with possible experimental error. The maximum possible experimental error in RTD is 0.8 °C. But on 2012/11/25 the temperature difference reaches to -20° C. Figure 4.13 show the temperature difference and the experimental error.

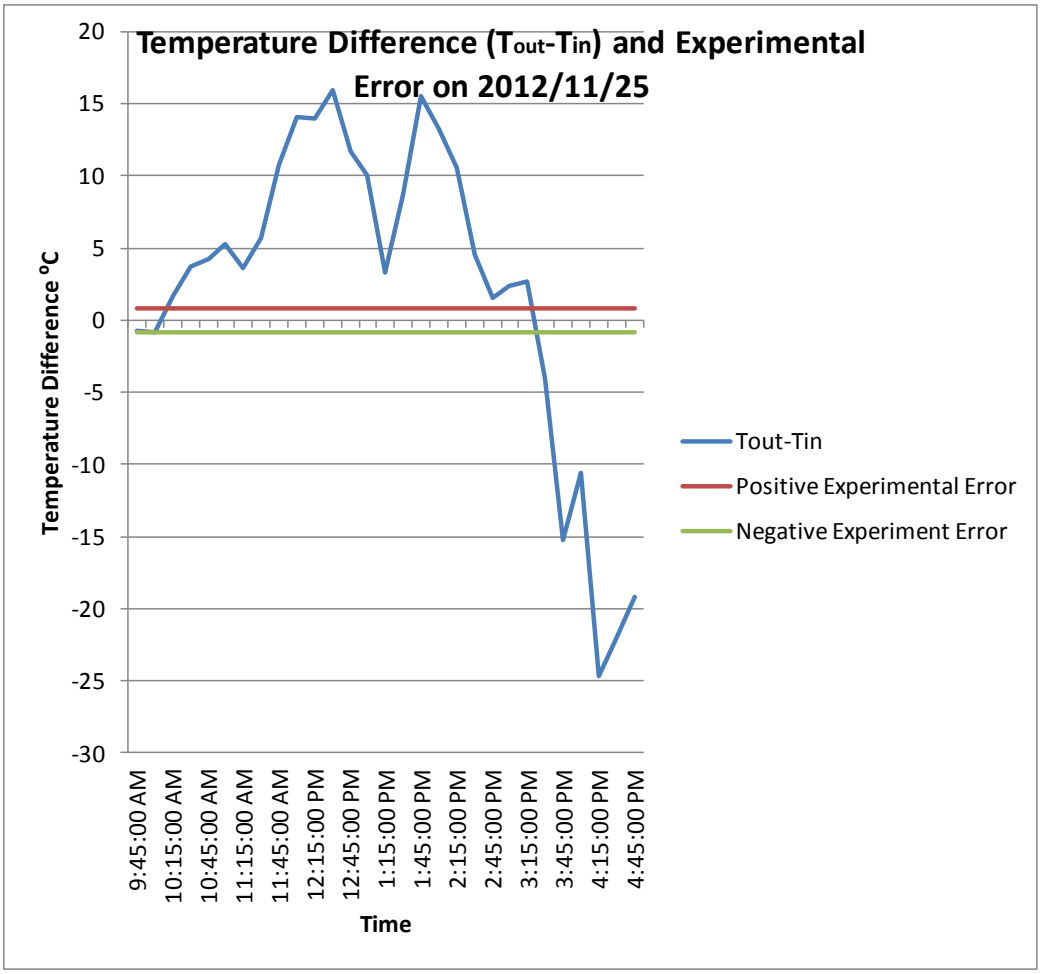

Figure 4.13: Temperature Difference on 2012/11/25 and Error According to manufacture Specifications

The accuracy of temperature sensors and data acquisition system was re-evaluated using a site test. The system consists of three Platinum RTDs and data collected using online monitoring system synchronized with BMS. For this test, the temperature sensors were disassembled from the pipe. Then a thermocouple inserted to the water/glycol mixture from the open point (where RTD was fixed). Platinum RTDs and thermocouple were used to measure the temperatures simultaneously. The thermocouple reading was 118°C and the RTD reading was a very close values such as 118.2°C. The next step was to check thermocouple measurements and data stored in the computer system. Both measurements should be exactly same. Thermocouple temperatures were read by two technicians, one stayed at the panels and the other one at the computer station. They were connected through a phone. In this procedure, no difference was found between temperature sensor and the computer station. These tests verified that negative temperature rise was unlikely to be caused by sensor errors.

4.5 Flow Rate

The instantaneous flow rate of water/glycol mixture that was recorded in every 5 minutes were graphed. Figure 4.14 shows the variation of flow rate on 2012/10/20.

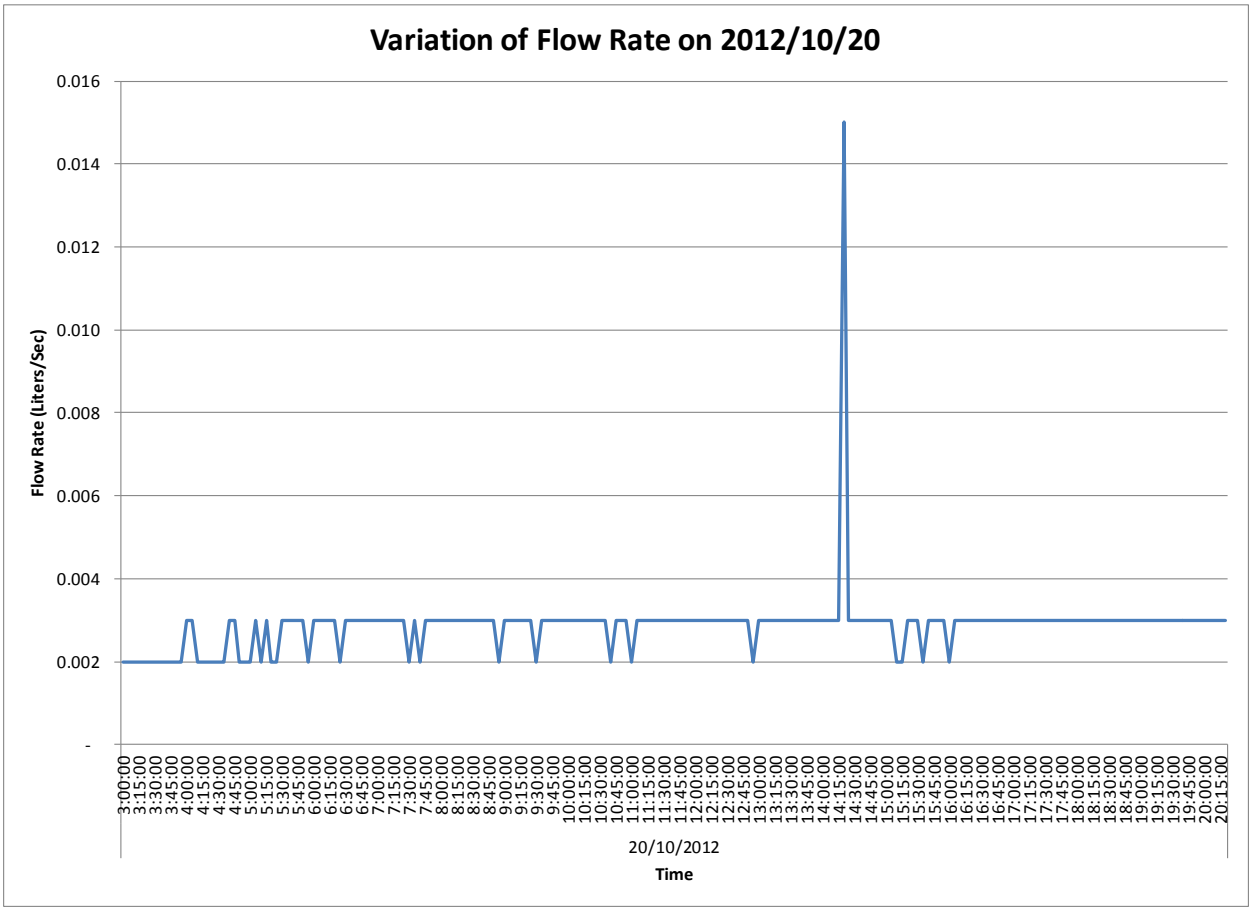

Figure 4.14: Flow Rate Variation of water/glycol Mixture on 2012/10/20

According to manufacturer's data sheet accuracy of the flow meter is +/- 0.4% of a reading . The flow rate after subtracting manufacture stated instrument error is shown in Figure 4.15. The difference between recorded flow rate and the flow rate after subtracting error is very small. Experimental error in flow rate data should be very small. Even the addition of error should follow the same behavior.

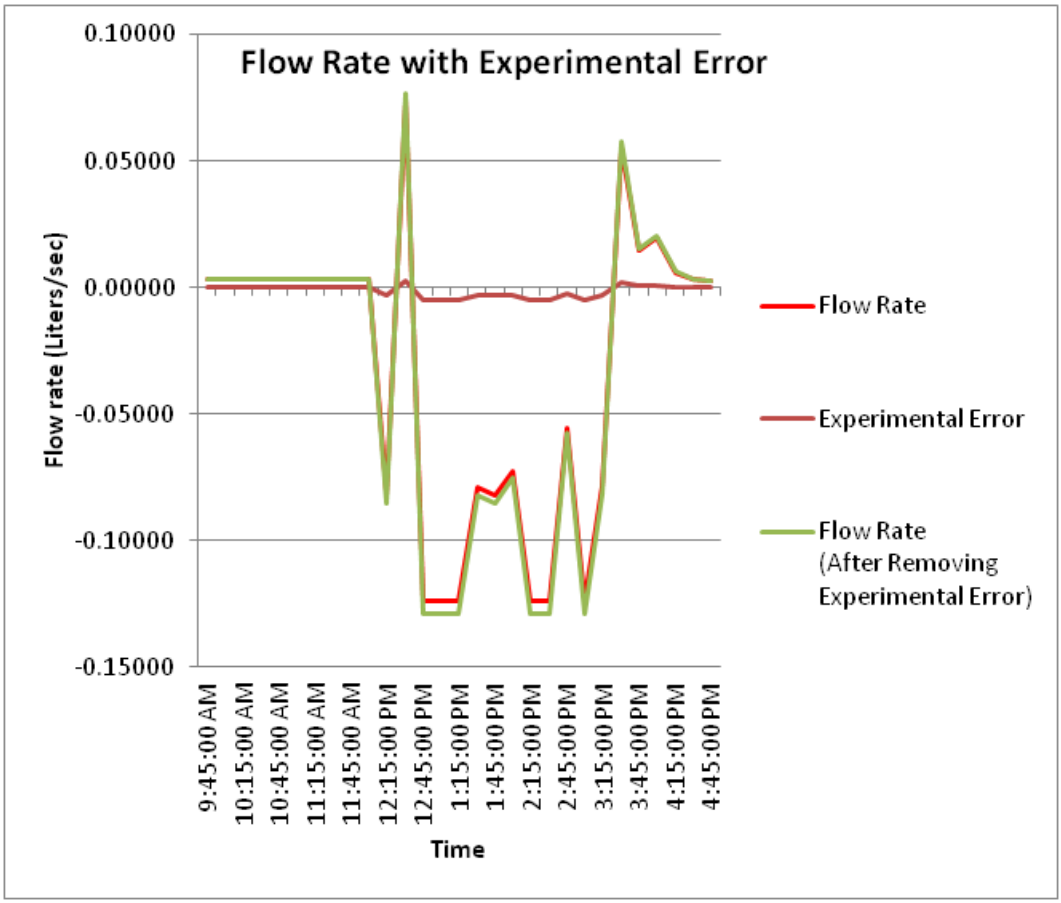

Figure 4.15: Flow Rate with Experimental Error

4.6 Unsteady Behaviour of the System

Steady state efficiency calculations (equation (2.9)) was based on clear days as these days have smooth and nearly constant solar gain around noon and the steady state performance criteria given in Section 2.7 were satisfied. During this calculation, it was identified that negative flow rate and the negative temperature variations of the water/glycol mixture are present even during clear days. Figure 4.16 shows the flow rate with negative values on clear day 2013/03/09.

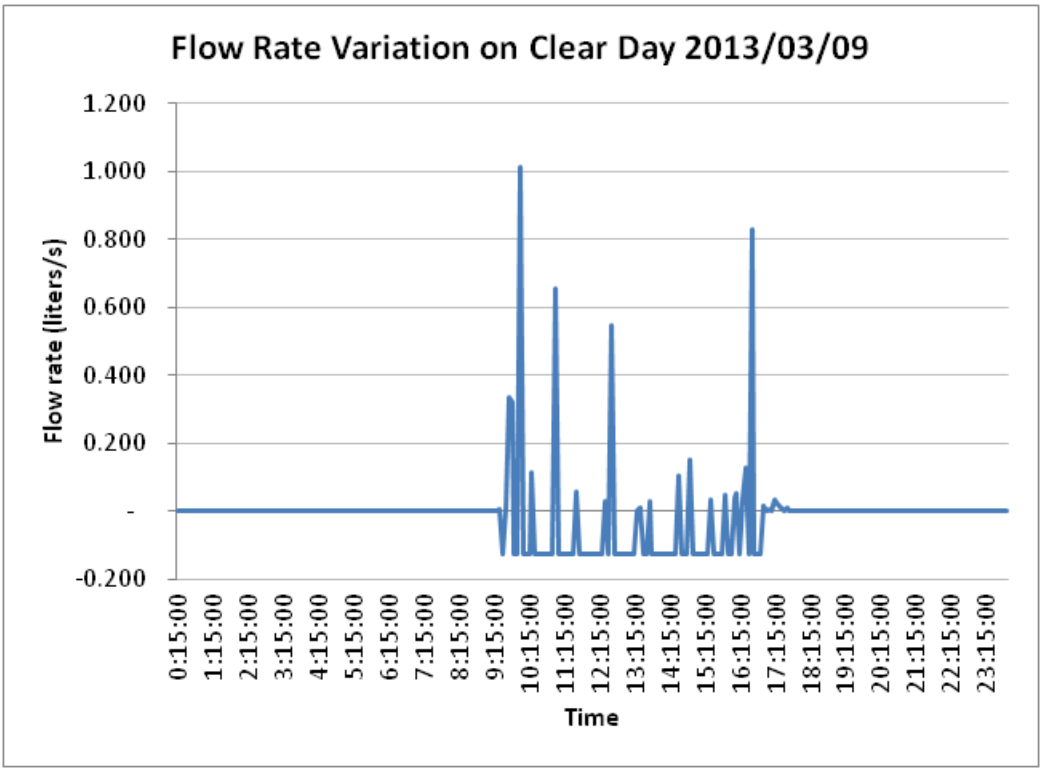

Figure 4.16: Flow Rate Variation on Clear Day 2013/03/09

As the variables of the system change with time, unsteady heat generation within the system was investigated. The ratio of the unsteady to steady terms in the numerator of Equation (2.6) was used to estimate the dominance of unsteady behavior in system performance. The ratio was defined as $(MC)_e \frac{dT_m}{dt} \Big/ \dot{m}C_p(T_{out} - T_{in})$. The ratio was graphed with respect to $(T_m - T_a)/G$.

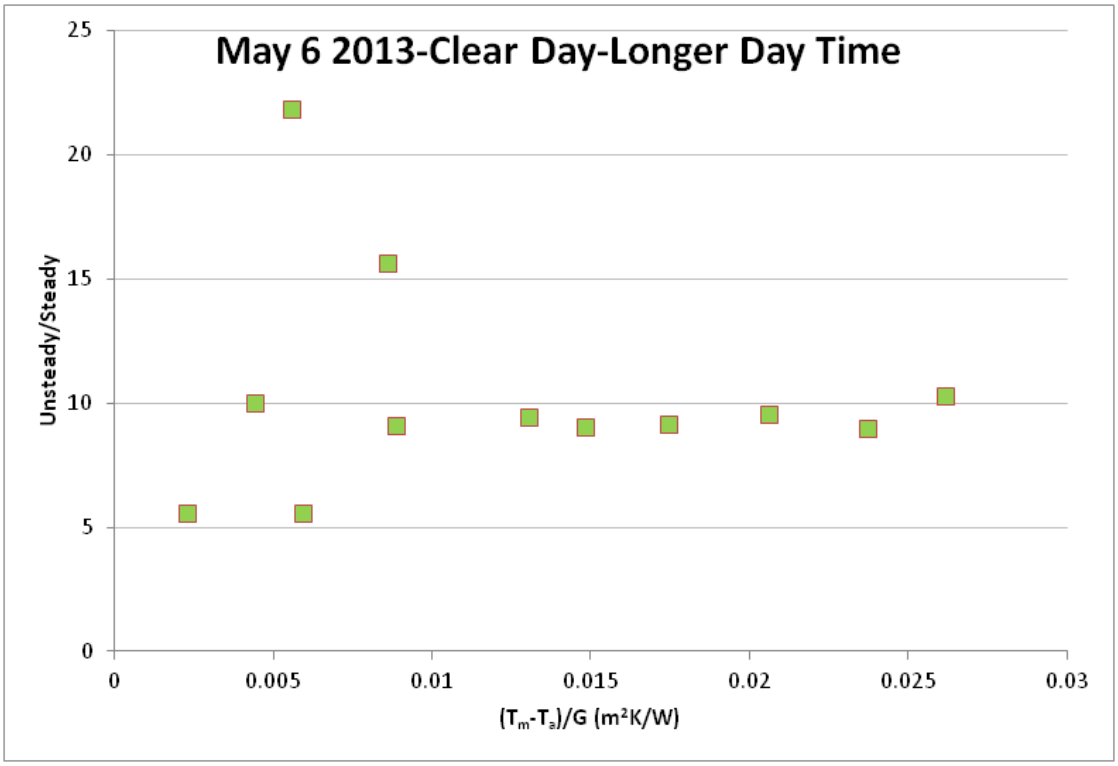

Figure 4.17: Unsteady vs. Steady Variation on a Clear Day

Figure 4.17 shows the ratio of Unsteady/Steady variation on clear day 2013/05/06. It exceeds unity for all the data points in Figure 4.17. This indicates that the heat generation within the system is higher than useful heat gain of working fluid.

4.7 Efficiency Estimation

Steady state and unsteady state efficiency of the collector were calculated to find performances based on equation (2.9) and (2.10) respectively. Solar radiation data, flow rate data and temperatures data collected during 7 months were separated into three categories for the efficiency calculation using the method described in Section 4.2.1. These are clear days, partly

cloudy days and cloudy days. Steady state and unsteady state efficiencies were calculated for clear days. Only unsteady state efficiency was calculated for cloudy and partly cloudy days.

4.7.1 *Steady State Efficiency Estimation of HP ETC*

Steady state efficiencies were calculated for 5 out of 41 clear days. The steady state efficiency values for clear day 2012/11/14 are shown Figure 4.18.

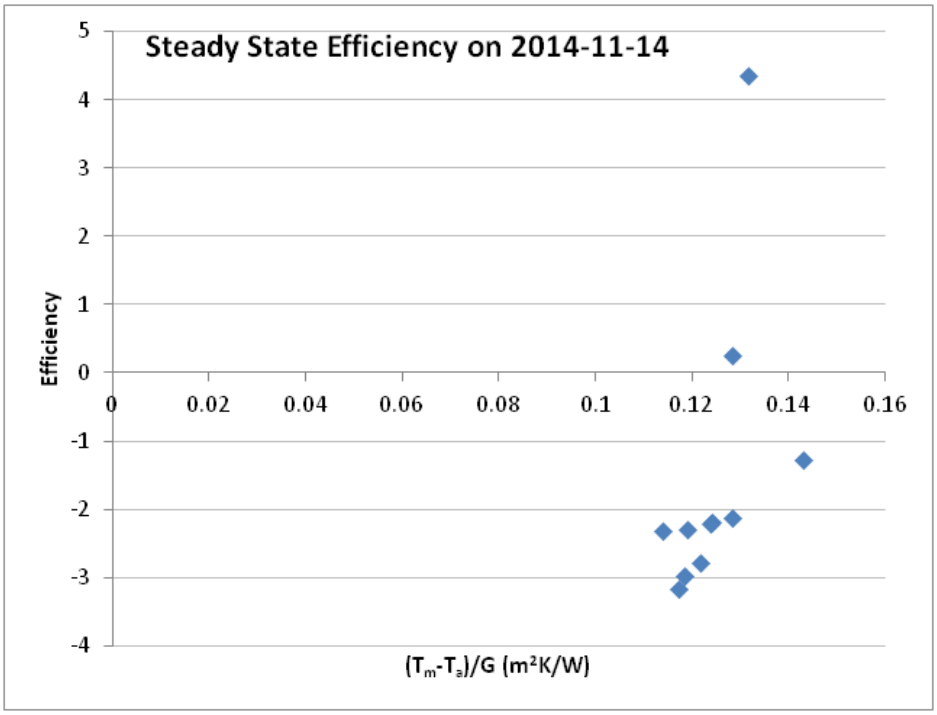

Figure 4.18: Steady State Efficiency on 2012/11/14

Figure 4.18 shows large negative values and one value exceeding 100% for steady state efficiencies. All 5 clear days do not have consistent efficiency results. Steady state efficiency results do not show reasonable values on any clear day at SLC. Unsteady state performance was investigated including clear days.

4.7.2 ***Unsteady State Efficiency Estimation of HP ETC***

Unsteady state efficiency was calculated based on equation (2.10). Main limitation to apply this equation was the data logging interval of water/glycol mixture temperatures. The data logging time interval was 15 minutes and it may be too long for an accurate numerical differentiation that required to estimate the internal energy term. Integration was introduced to avoid this limitation. Each term of the equation was integrated over the 15 minute period using the Trapezoidal rule. The following procedure describes the estimation of each term in equation (2.6).

Integration of both sides of equation (2.6) over a 15 minute interval:

$$\int_0^{15} IAdt = c_p \int_0^{15} \dot{m}(T_{out} - T_{in})dt + (MC)_e T_m\Big|_0^{15}$$

The components were estimated as follows;

Apply the trapezoidal Rule to the radiation data:

$$\int_0^{15} IAdt = \frac{(IA \text{ at } 15^{\text{th}} \text{ minute} + IA \text{ at } 1^{\text{st}} \text{ minute})}{2} \times 15 \times 60 \text{ seconds}$$

Apply the trapezoidal rule to the steady heat gain term:

$$\int_0^{15} \dot{m}(T_{out} - T_{in})dt = \frac{[\dot{m}(T_{out} - T_{in}) \text{ at } 15^{\text{th}} \text{ minute} + \dot{m}(T_{out} - T_{in}) \ 1^{\text{st}} \text{ minute}]}{2} \times 15 \times 60 \text{ seconds}$$

Estimate the change in internal energy:

$$MC \ T_m\Big|_0^{15} = MC \ (T_m \, at \ \ 15^{\text{th}} \text{ minute} - \ T_m \text{ at } \ 1^{\text{st}} \text{ minute})$$

4.7.2.1 Unsteady Efficiency Estimation for Clear Days

Clear days were divided into two categories based on shorter and longer days. Shorter days were from winter months (Oct 2012 to Feb 2013) and longer daytime days were from spring (Feb 2013 to May 2013). Unsteady efficiency and ratio of Unsteady to Steady were calculated for both categories. Efficiency results showed negative and positive efficiencies due to inconsistent behavior of flow rate and temperature rise. Unsteady State efficiency data were analyzed considering **only** the positive efficiencies. The efficiency results were compared with efficiency data provided by Fraunhofer Institute.

Negative Efficiency Results

Negative efficiency results were produced from negative flow rate and positive temperature difference plus positive flow rate and negative temperature difference. These negative efficiencies of the system were investigated separately to understand their cause. Figure 4.19 shows the negative and positive efficiencies for a clear day.

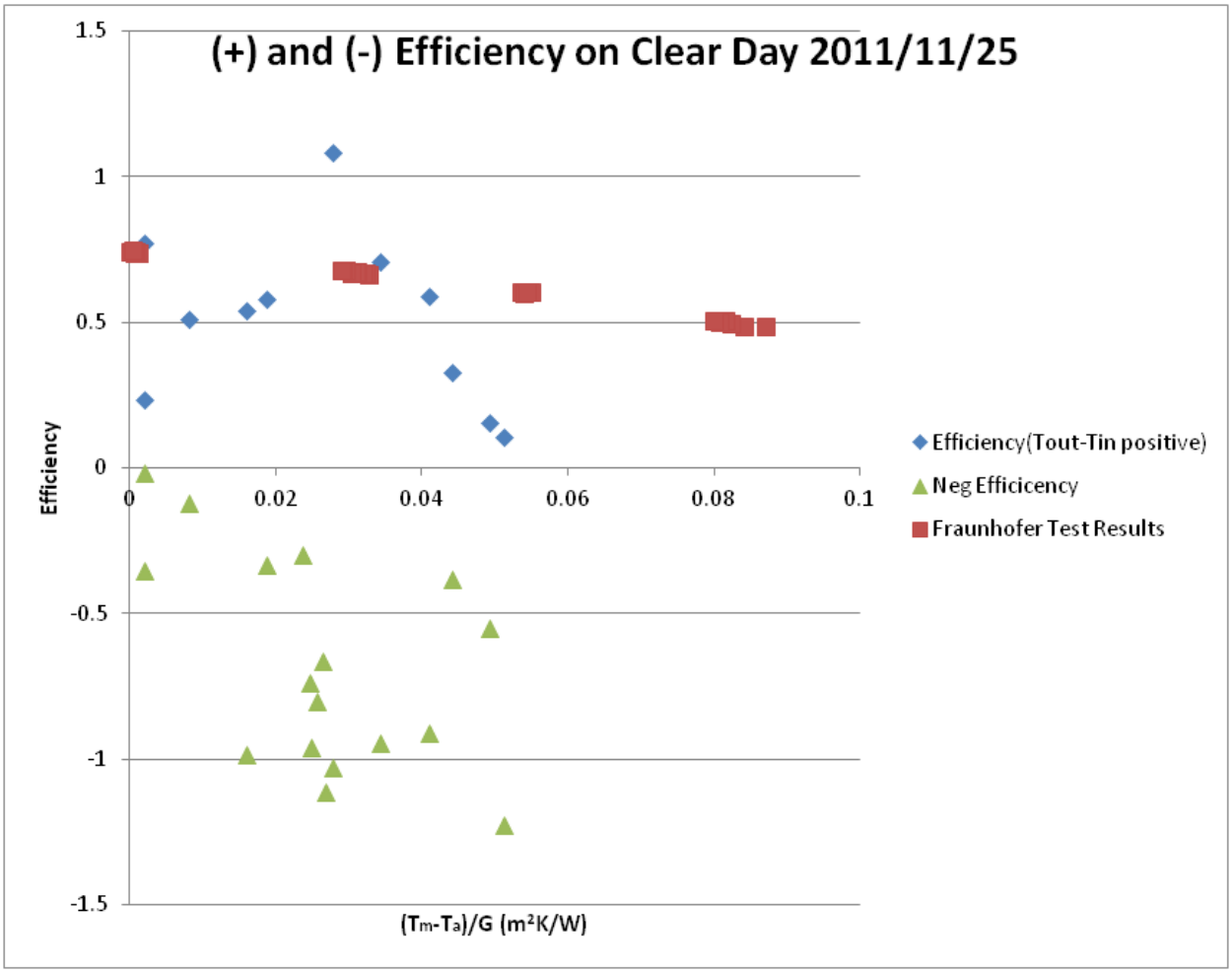

Figure 4.19: Unsteady State Efficiency Calculation for Clear Day 2012/11/25(Fraunhofer test results are from Figure 2.5)

Unsteady Behaviour

Figure 4.20 shows large positive Unsteady / Steady ratio for most positive efficiencies. An Unsteady/Steady higher than 1 indicates dominance of the unsteady term. 2012/11/22 and 2013/03/09 are two clear days selected from 41 clear days. The former is a short day and the latter is a long one (Figure 4.20 and Figure 4.21). The unsteady/steady term is shown in Figure 4.20 and the magnitude of Unsteady/Steady ratio is shown by secondary axis of graph. Both graphs show high positive values for Unsteady/Steady term.

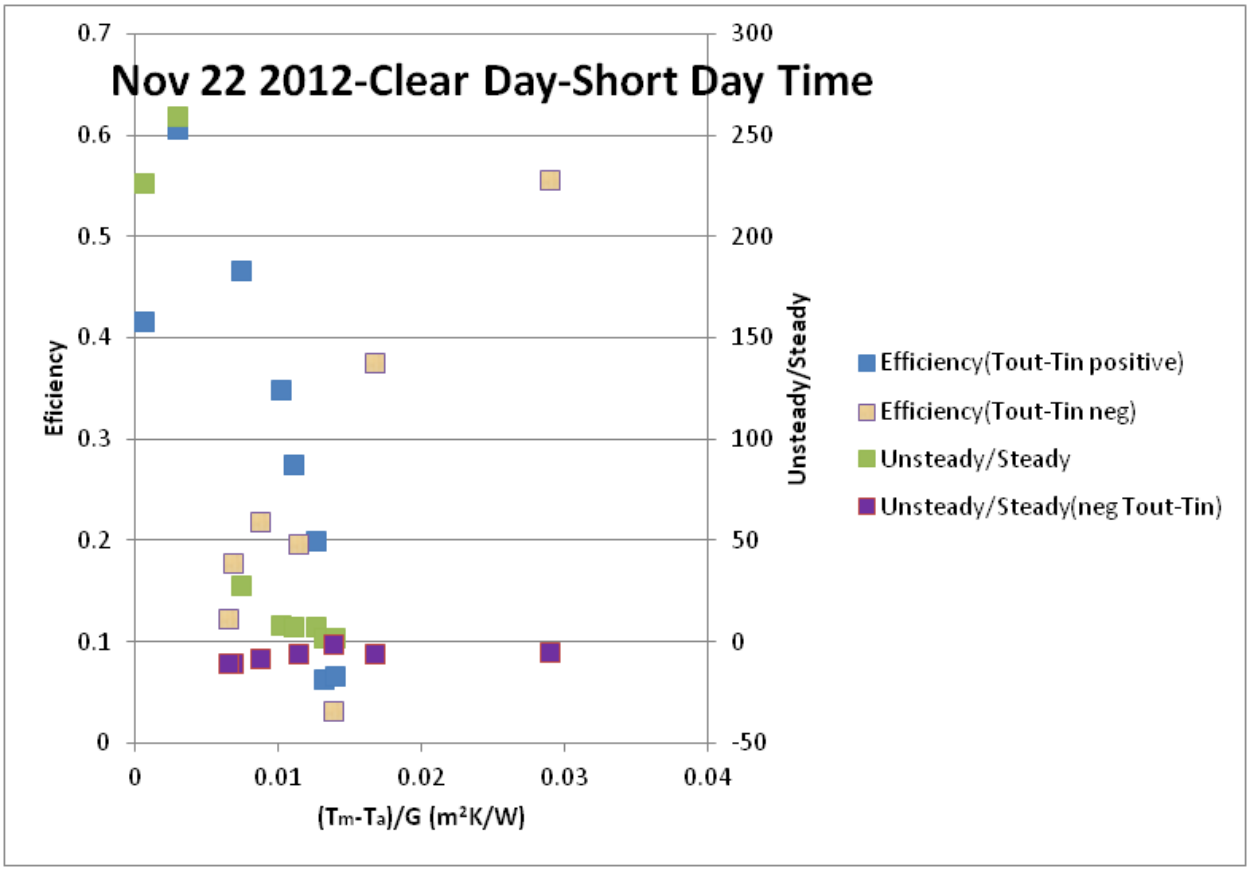

Figure 4.20: Ratio of Unsteady to Steady on Clear Day 2012/11/25

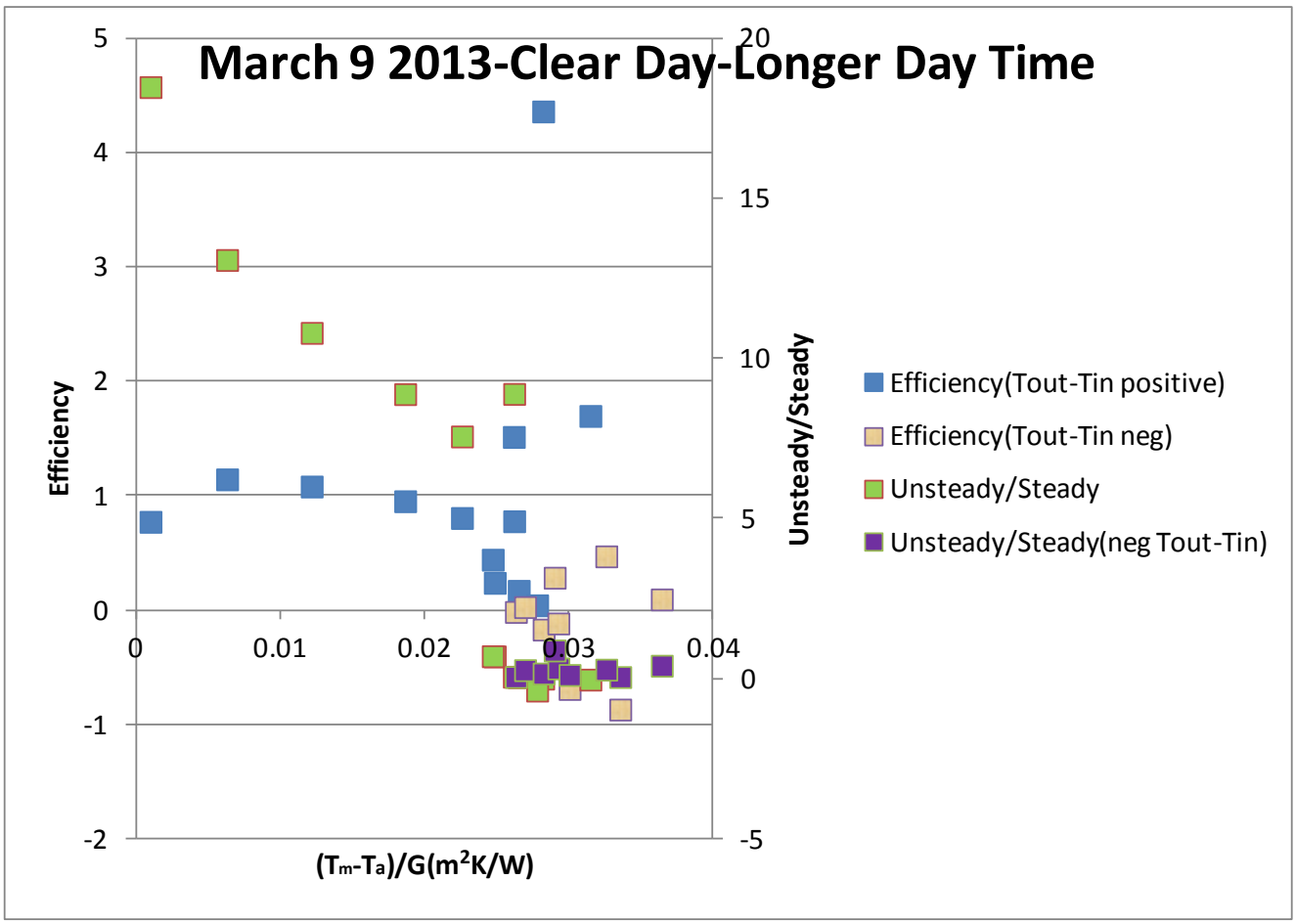

Figure 4.21: Ratio of Unsteady to Steady on Clear Day 2013/03/09

Efficiency of Collector

Unsteady state efficiencies for clear days are compared to the Fraunhofer test results (Jiangsu Sunrain Solar Energy, n.d) in Figure 4.22 and Figure 4.23 for two clear days 2012/11/25 and 2013/03/09.

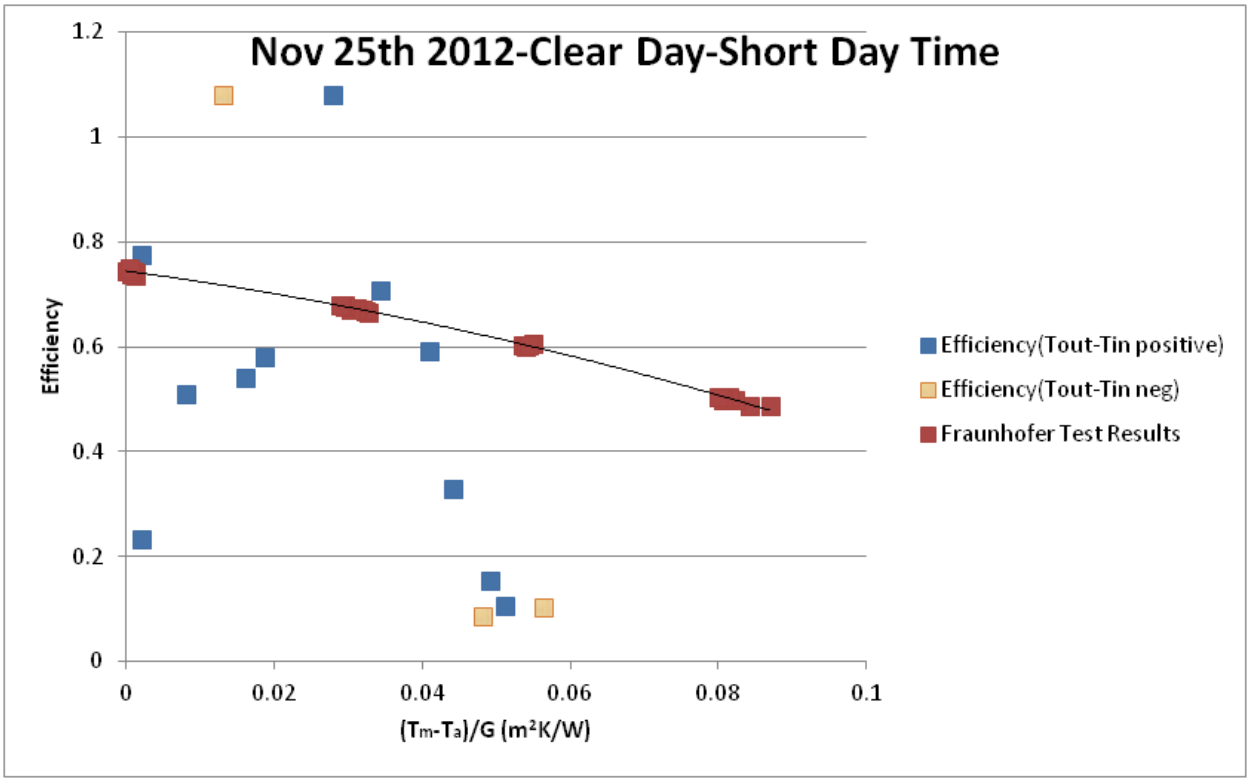

Figure 4.22: Efficiency vs. $(T_m\text{-}T_a)/G$ and Fraunhofer Test Results on 2012/11/25

Figure 4.22 shows that the collector has operated in the range of $(T_m\text{-}T_a)/G$ <0.06 on 2012/11/25 and this is a shorter day according to Figure 4.3. Several data points lie below η =0.2 and one has η >1. Most of the efficiencies lie between 0.4 <η< 0.8 and most of the current experimental data falls below the Fraunhofer test results.

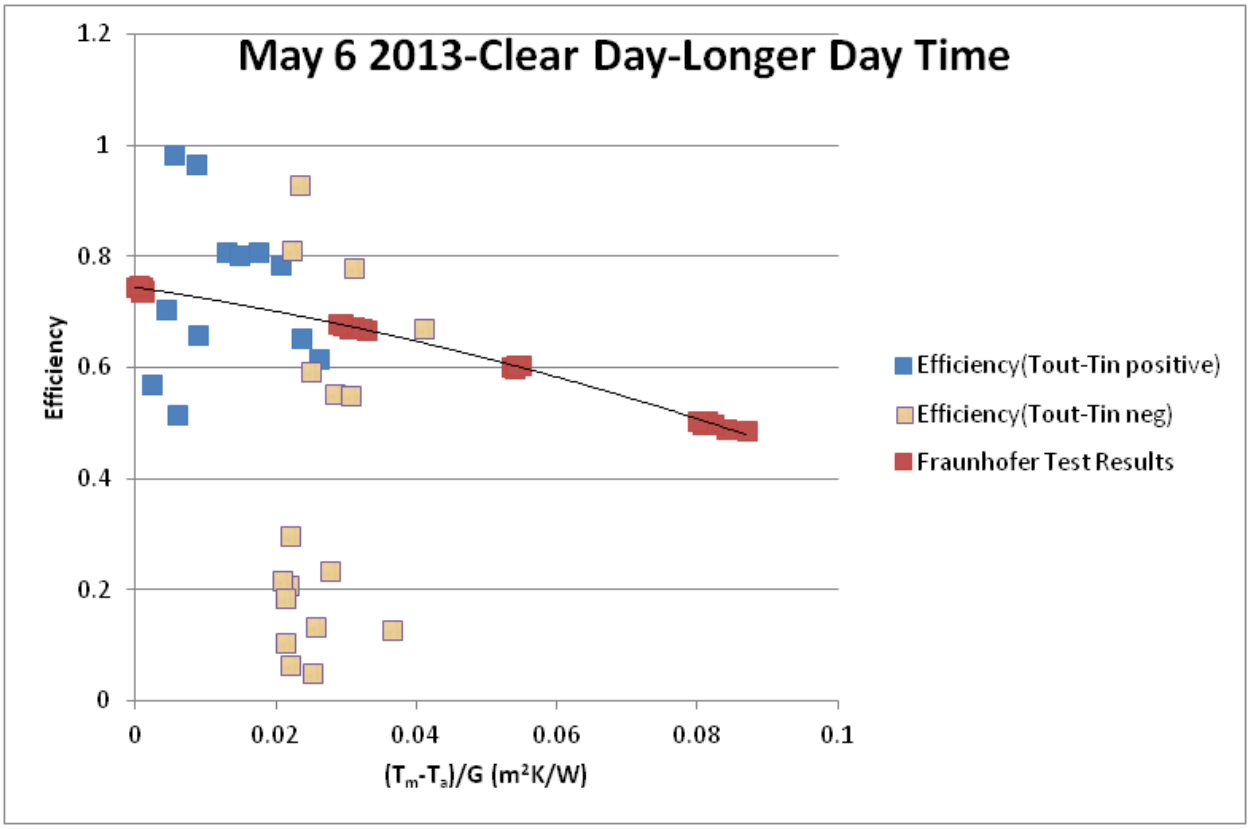

Figure 4.23: Efficiency vs. $(T_m\text{-}T_a)/G$ and Fraunhofer Test Results on 2013/05/06

Figure 4.23 shows that the collector operated in the range $0 < (T_m\text{-}T_a)/G < 0.03$ on a spring day which had 12 hours of daylight. The collector operated in the high efficiency range and low $(T_m\text{-}T_a)/G$ range. The trend of the current data is close to Fraunhofer test results but with is more scatter. This spring day has generally lower, but positive, efficiency for negative temperature rise.

4.7.2.2 Unsteady State Efficiency Estimation for Cloudy Days

Cloudy days were selected as described in Section 4.2.1 between 2012/10/27 to 2013/5/25 and efficiencies and the Unsteady/Steady ratio was calculated. Two cloudy days were selected from winter and spring. Collector efficiency and the ratio of the Unsteady to Steady terms on a winter day 2012/12/07 and a spring day 2013/05/16 are shown in Figure 4.24 and Figure 4.25.

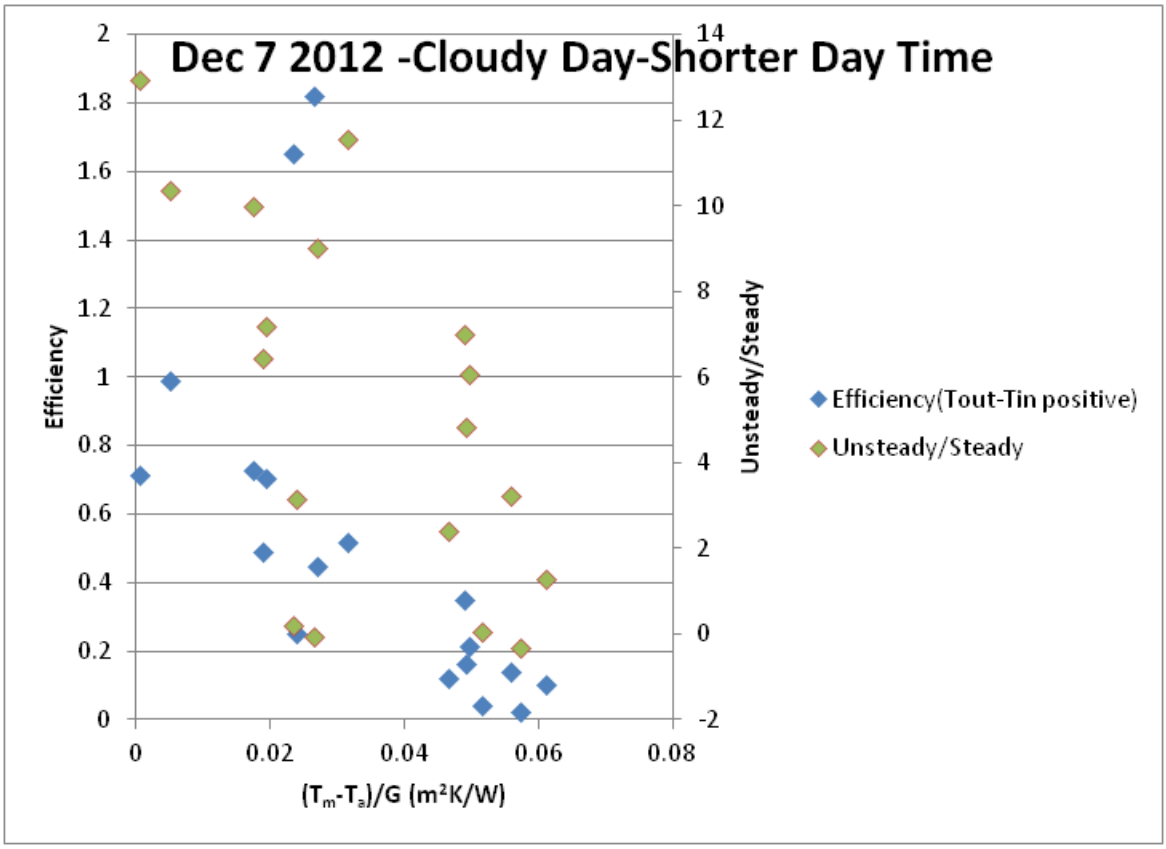

Figure 4.24: Ratio of Unsteady to Steady on Cloudy Day 2012/12/07

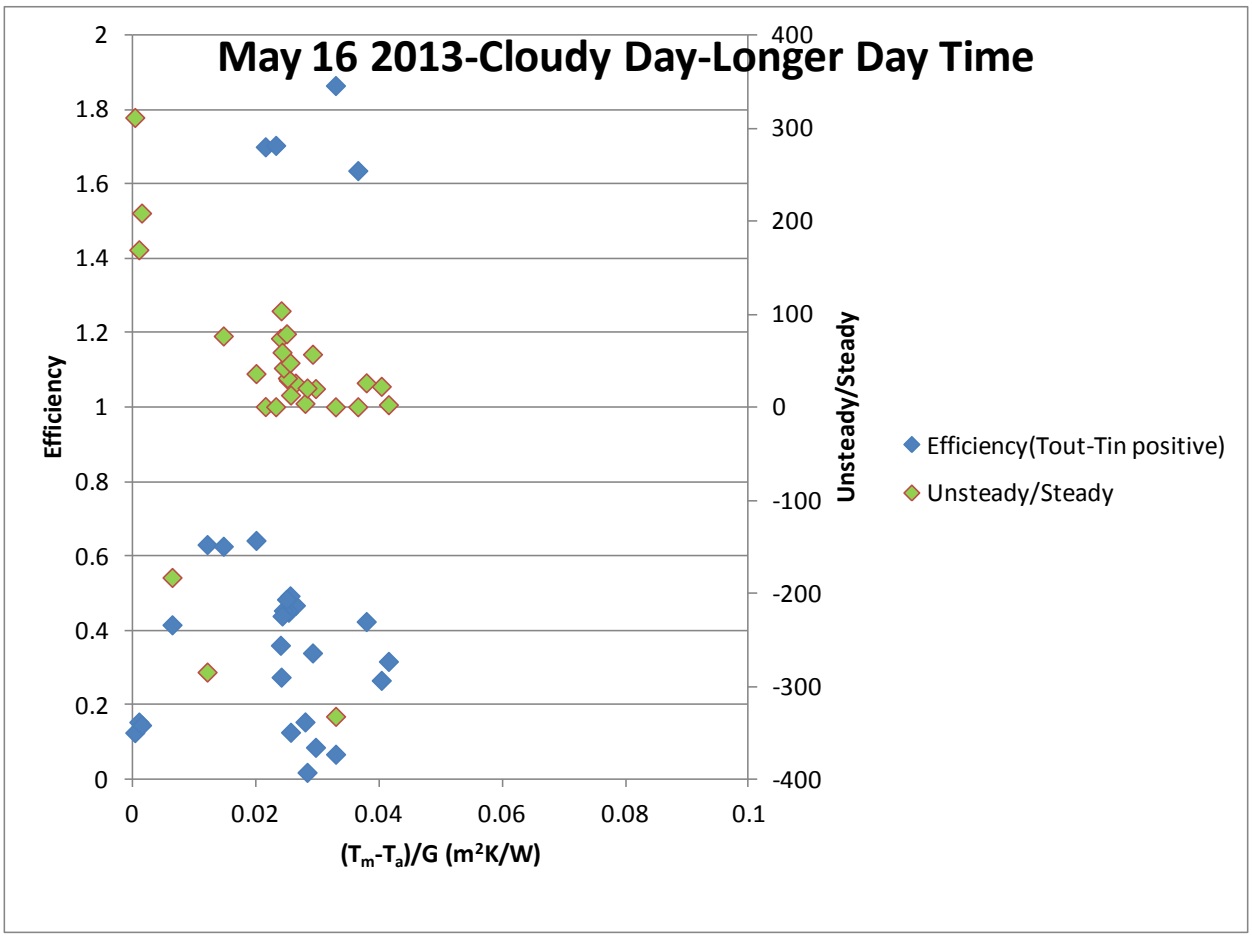

Figure 4.25: Ratio of Unsteady to Steady on Cloudy Day 2013/05/16

In Figure 4.24 and Figure 4.25, the unsteady /steady ratio has high positive values and ratios higher than 1 indicate the dominance of the unsteady term in the system. Efficiencies were calculated for cloudy days from 2012/10/27 to 2013/05/31 and plotted with Fraunhofer test results. Two days were selected from winter and spring and graphed in Figure 4.26 (2012/12/07) and Figure 4.27 (2013/05/16).

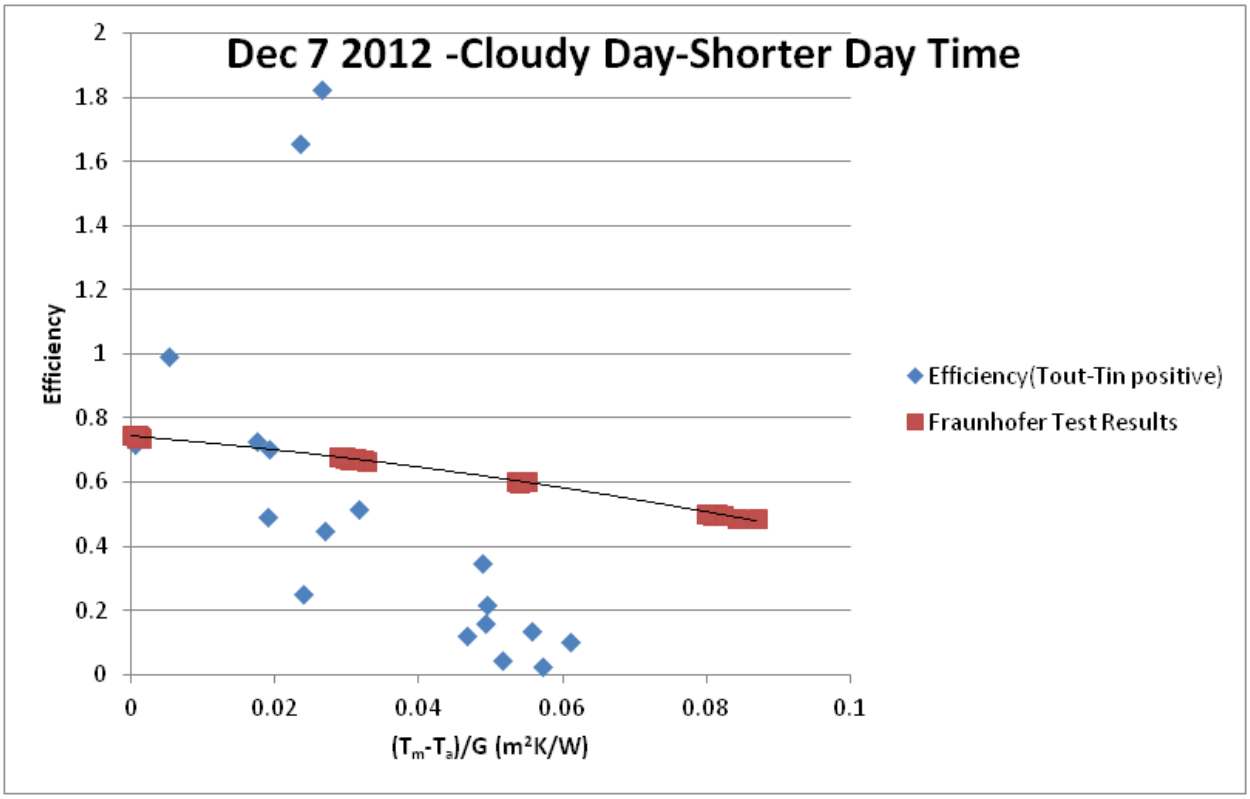

Figure 4.26: Efficiency vs. $(T_m\text{-}T_a)/G$ and Fraunhofer Test Results on 2012/12/07

On 2012/12/07, winter day collector efficiency has decreased when $(T_m\text{-}T_a)/G$ increases. In the figures showing collector efficiency, $(T_m\text{-}T_a)/G$ should be accurate as it contains data that are more accurate than flow rate. Thus it is reasonable to infer that the ETC operates inefficiently at high values of $(T_m\text{-}T_a)/G$ even if the efficiency cannot be accurately determined.

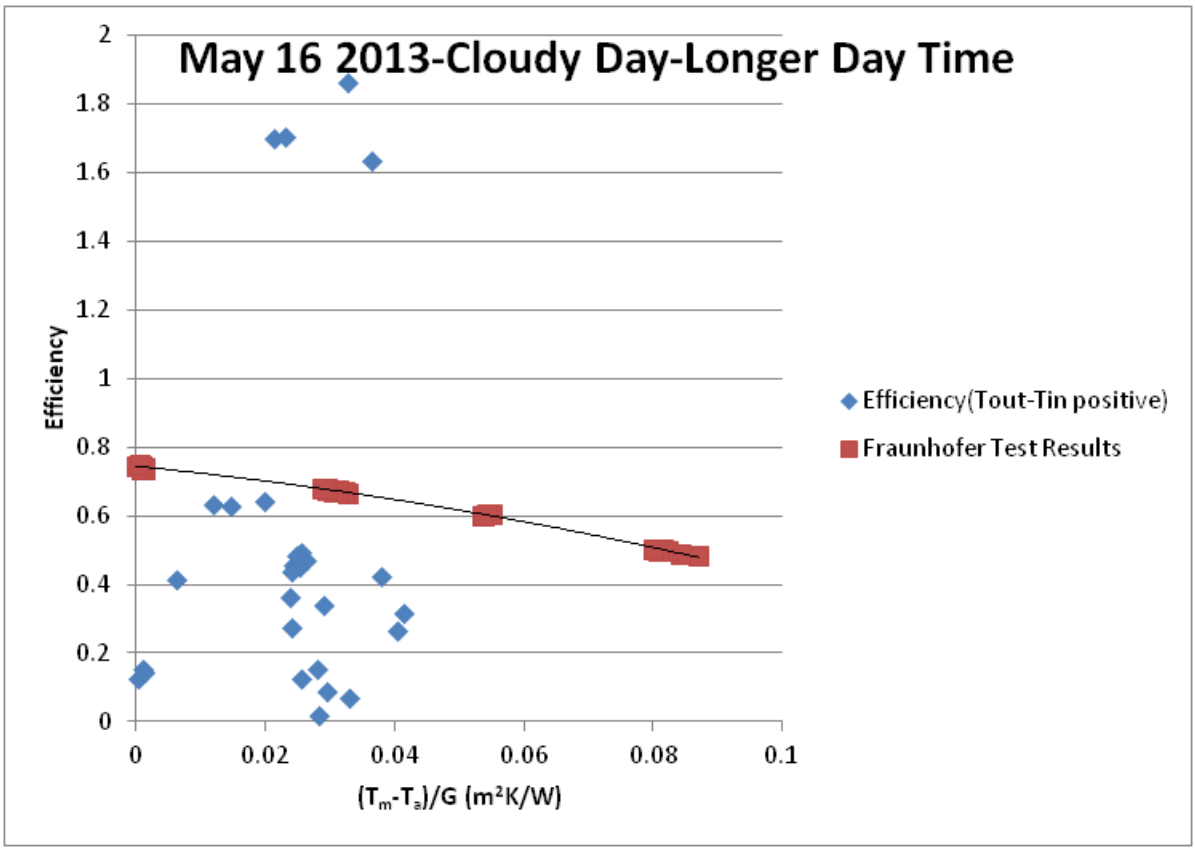

Figure 4.27: Efficiency vs. $(T_m\text{-}T_a)/G$ and Fraunhofer Test Results on 2013/05/16

On 2013/05/16 collector has operated in higher range of $(T_m\text{-}T_a)/G$ when compared to 2012/12/07 and efficiencies are lower than expected values from Fraunhofer test results.

On 2013/05/16 collector operated in higher range of $(T_m\text{-}T_a)/G$ when compared to 2012/12/07 and efficiencies are lower than the Fraunhofer test results.

There were 56 cloudy days between winter 2012 and spring 2013. Only six cloudy days had solar radiation higher than 300W/m^2. Figure 4.26 and Figure 4.27 show efficiencies for two of these six days. There were no positive efficiencies for $T_{out}\text{-}T_{in}<0$ so these results are not shown.

4.7.2.3 Unsteady State Efficiency Estimation for Partly Cloudy Days

Unsteady /Steady term variation on winter day 2012/11/19 is shown in Figure 4.28 and spring day 2013/05/12 is shown in Figure 4.29.

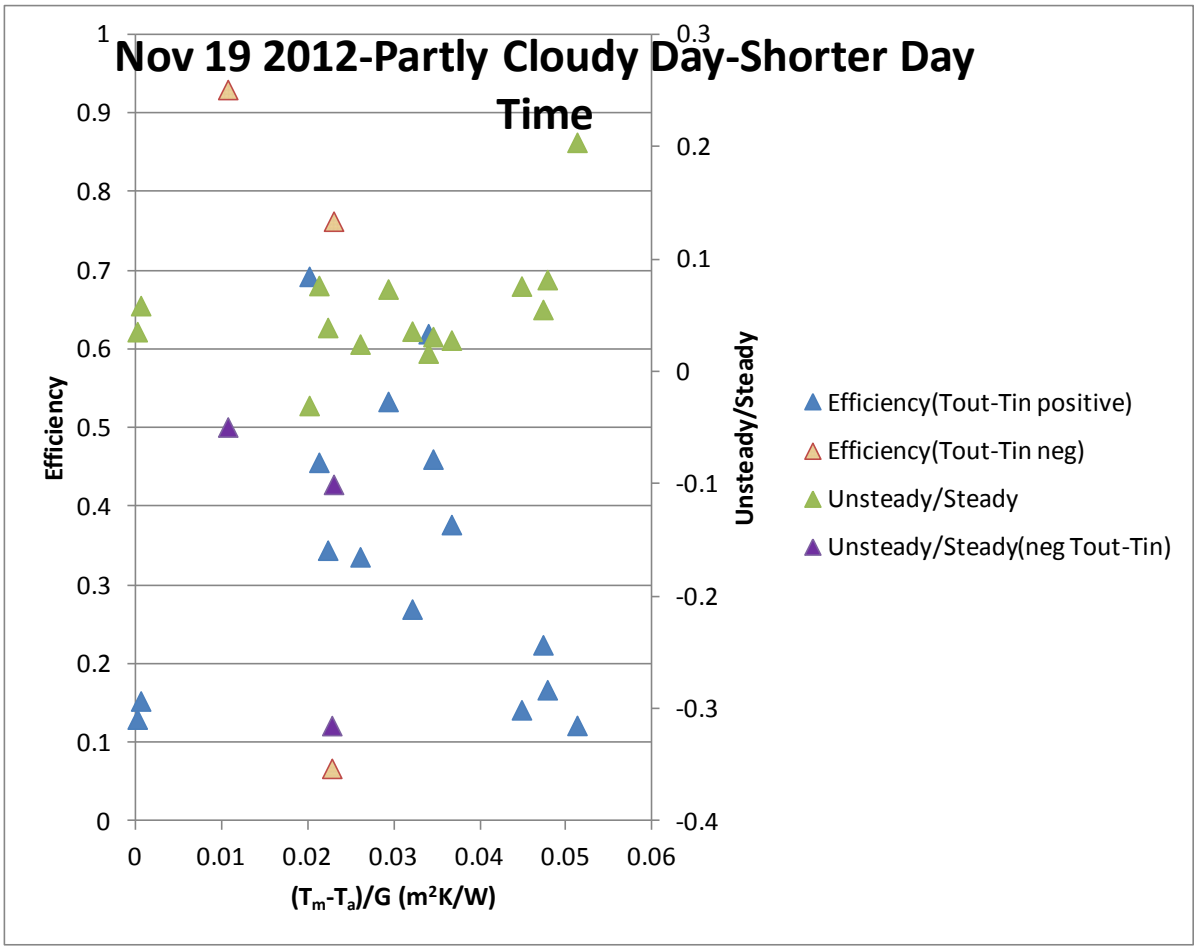

Figure 4.28: Ratio of Unsteady Steady on Cloudy Day 2013/05/16

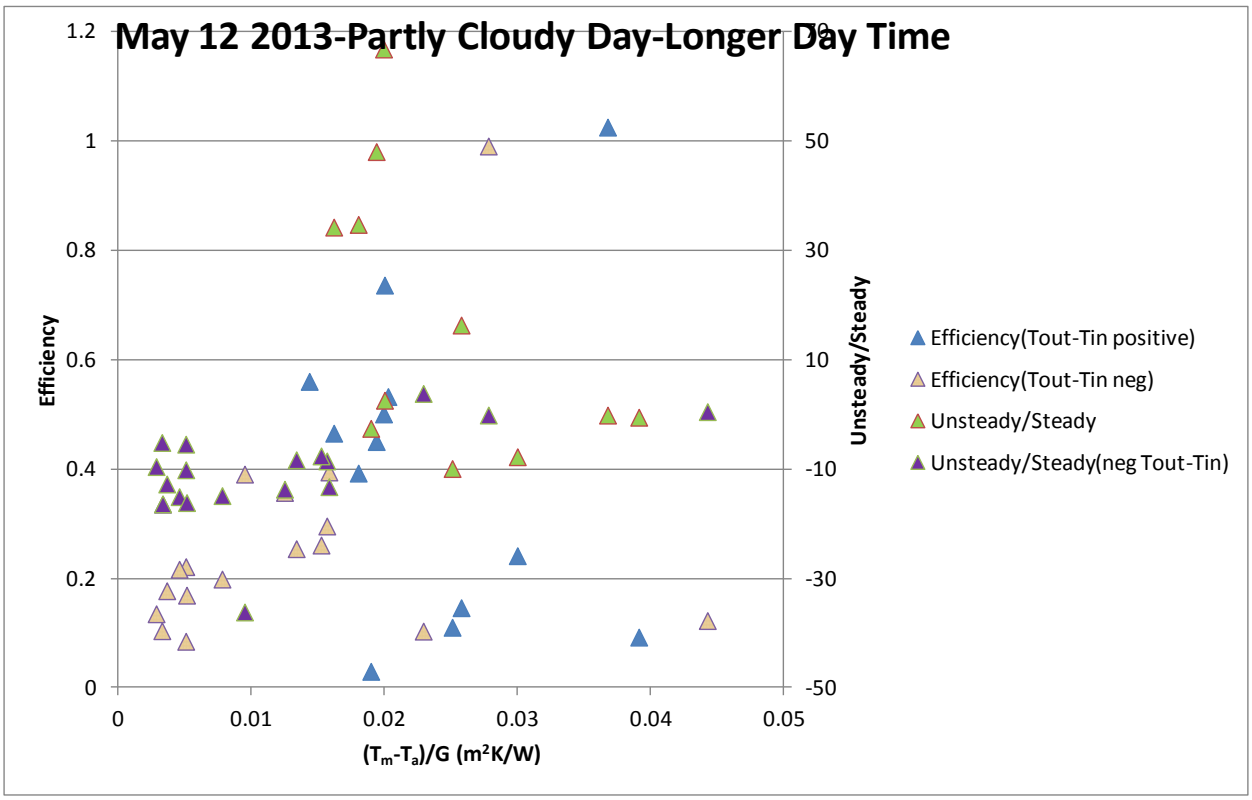

Figure 4.29: Ratio of Unsteady to Steady on Cloudy Day 2013/05/16

Partly cloudy day results also show that the unsteady/steady term has high positive values and unsteady term is dominant in the system.

Efficiencies were calculated for the partly cloudy days of 2012/11/19 and 2013/05/12. Figure 4.30 and Figure 4.31 shows the comparison of experiment results and Fraunhofer test results.

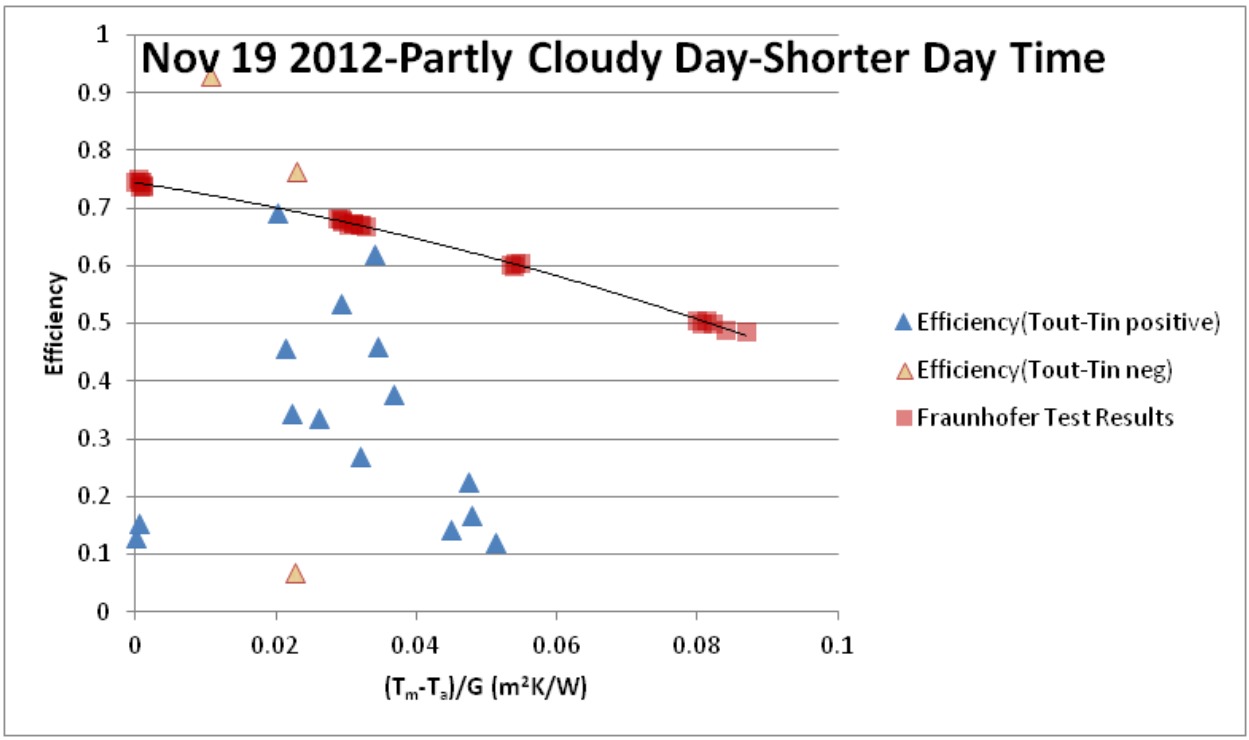

Figure 4.30: Efficiency vs. $(T_m\text{-}T_a)/G$ and Fraunhofer Test Results on 2013/05/16

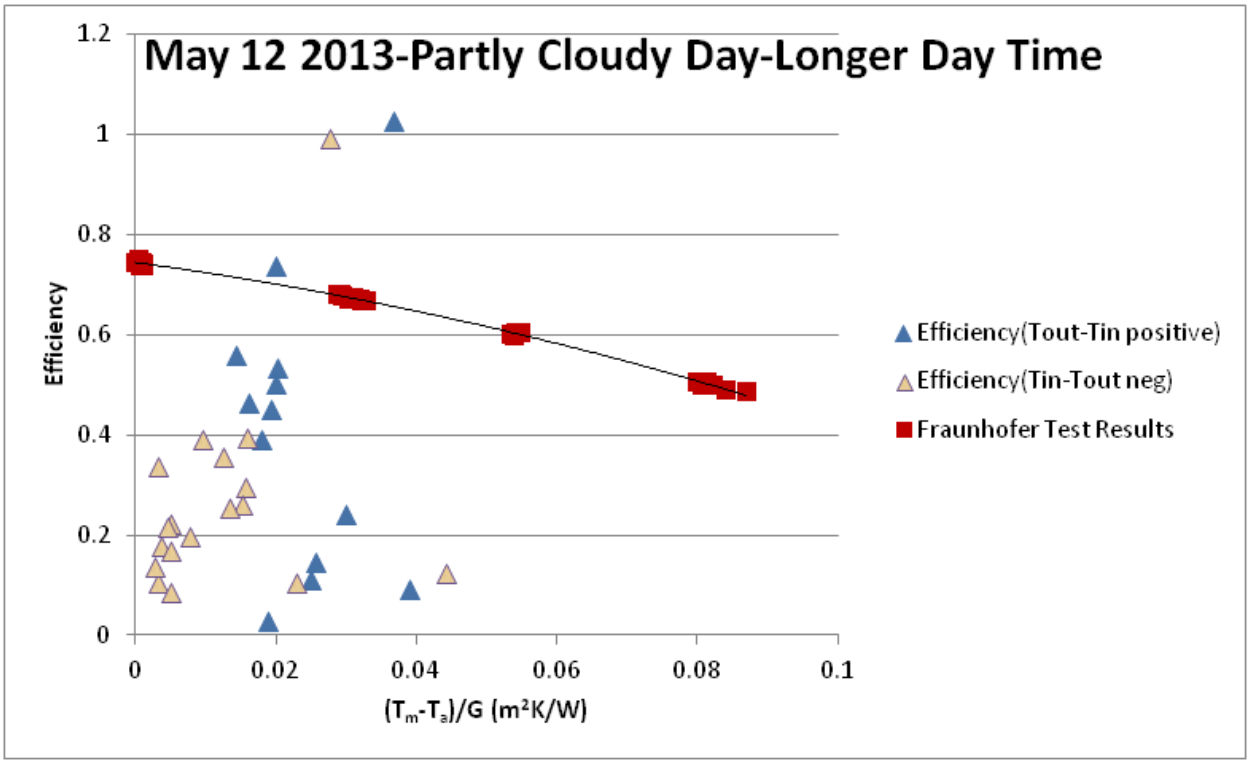

Figure 4.31: Efficiency vs. $(T_m-T_a)/G$ and Fraunhofer Test Results on 2013/05/16

The collector operated with $0 \leq (T_m-T_a)/G < 0.06$ on both partly cloudy days and efficiencies are very low compared to the Fraunhofer test results.

Figure 4.30 and Figure 4.31 contain positive efficiency points for negative temperature rise ($T_{out}-T_{in}<0$). The number of efficiency points for $T_{out}-T_{in}<0$ are fewer compared to number of efficiency points for $T_{out}-T_{in}>0$ on the same day.

4.7.2.4 Negative Efficiency Results

Collector efficiency for all three categories of days shows negative values. To investigate the possible cause of these results, changes in solar radiation, flow rate, temperature difference (T_{out}-T_{in}) and efficiency for 2013/02/08 are shown in Figure 4.32.

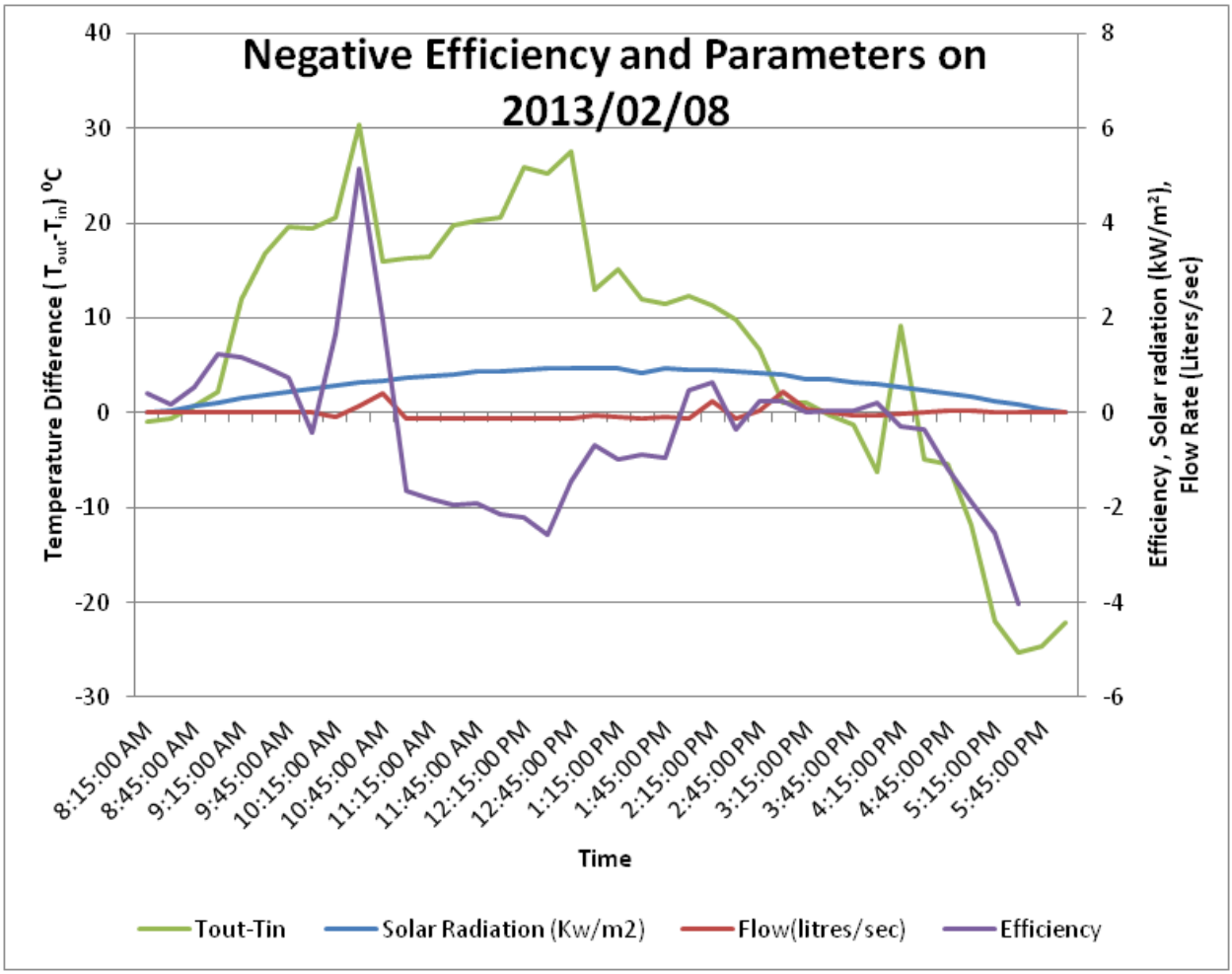

Figure 4.32: Negative Efficiency Results and Parameters on 2013/02/08

Figure 4.32 shows that the efficiency is positive early in the morning and it goes negative around 10.30 am. Then it becomes positive after 1.30pm. The temperature rise is positive in the morning (T_{out}-T_{in}>0) and it goes negative after 3.00pm. The flow rate changes direction (reverse the direction) around 10.30am and it changes to positive after 1.30pm. The Solar Radiation

varies smoothly over the day and it is not likely to cause significant unsteadiness in panel behavior.

This indicates changes of flow direction do not follow the direction of temperature rise in this system. That causes the negative efficiency of system.

4.7.2.5 Efficiency of Collector and Boiling Point of Working Fluid

The pressure of the working fluid at testing panels can be used to estimate the boiling point of the working fluid that passes through tested collectors. The pressure of working fluid at the testing panels was determined by the pressure losses through piping system, pressure loss due to division of flow to other branches and potential energy changes between pump location and the tested collectors (pump is in the basement and the panels are on the roof of 4^{th} floor). Pressure of working fluid could be accurately determined by a simulation of the system. But insufficient information on piping system restricted further analysis of the system.

The boiling point of the working fluid at the pump pressure (284kPa) was estimated and used to filter the efficiency data to increase the accuracy of performance data.

Boiling point of 50/50 Propylene Glycol/water at Pressure 284kPa

Appendix D shows the total pressure and boiling temperature of aqueous Propylene Glycol solution and it follows a linear relationship between $\log_{10}P$ and the boiling temperature. The boiling point of 50/50 water/Propylene Glycol by volume was estimated to be 136°C based on this data.

Filtering Data for boiling Point

On 2013/03/28 the outlet temperature of tested collector exceeded the boiling temperature 136°C. The figure 4.33 shows the variation of outlet temperature and the efficiency on this day.

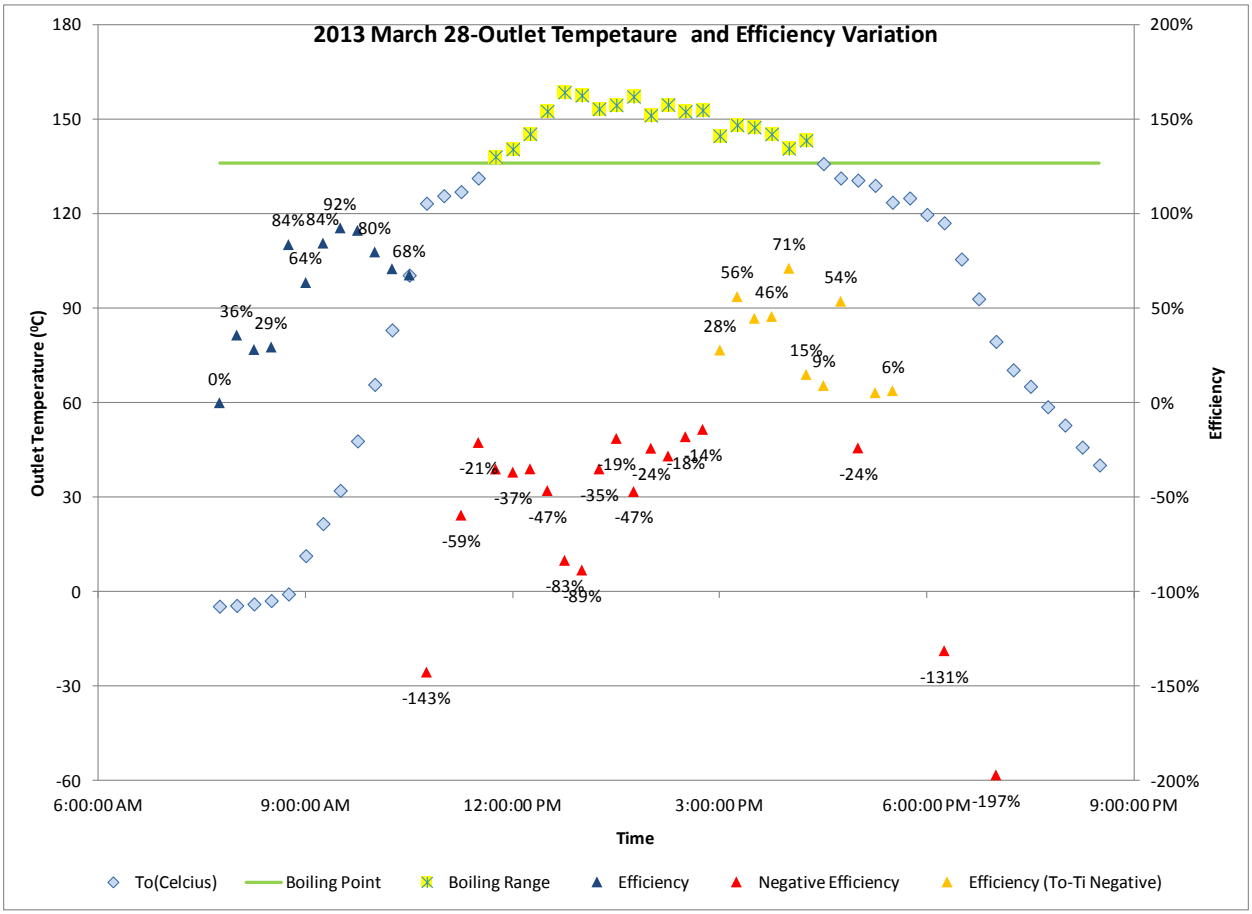

Figure 4.33: Outlet Temperature and Efficiency Variation on 2013/03/28

Figure 4.34 shows the efficiency of the collector vs. $(T_m\text{-}T_a)/G$ on 2013/03/28 and it shows the performance of the collector probably the water/glycol mixture is in liquid state.

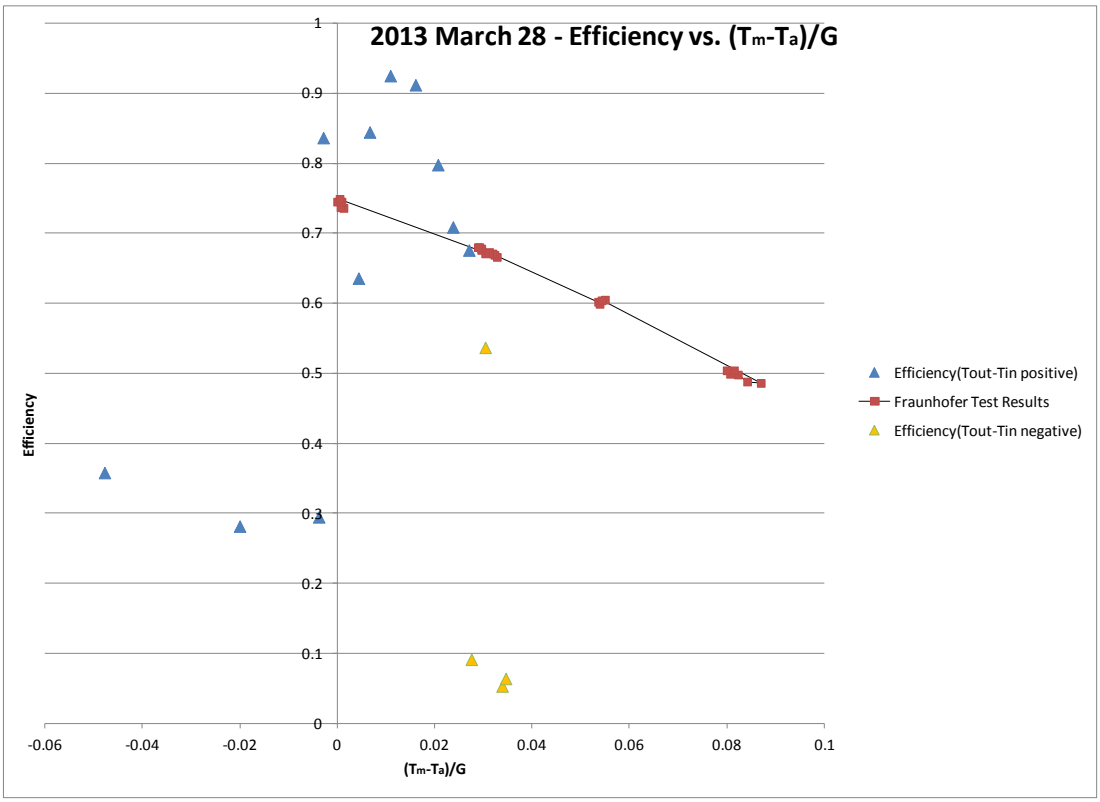

Figure 4.34: Efficiency vs. (T_m-T_a)/G and Fraunhofer Test Results on 2013/03/28

The section 4.7.2.1,4.7.2.2 and 4.7.2.3 were discussed the collector efficiency when the outlet temperature was below 136°C except for May 6 , 2013. The May 6 , 2013 efficiency data can be represent as in figure 4.35 after removing data in the boiling range.

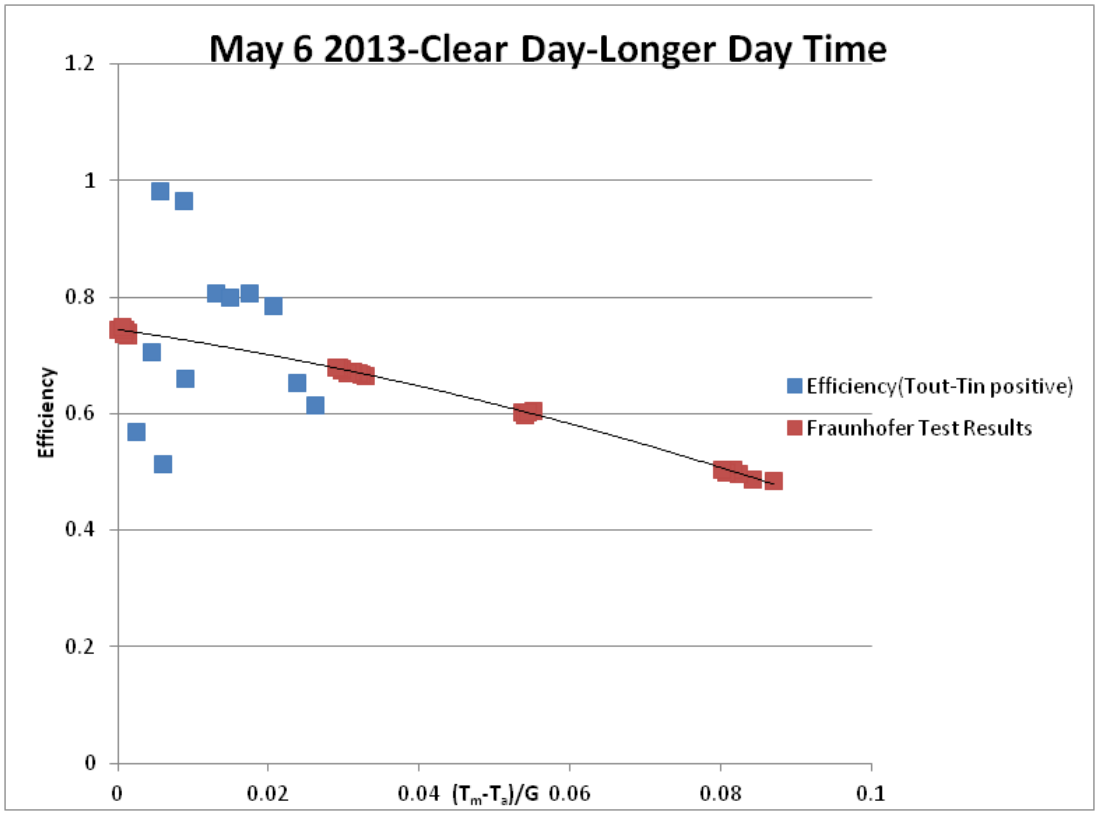

Figure 4.35: Efficiency vs. (T_m-T_a)/G and Fraunhofer Test Results on 2013/05/06 after Filtering

During the data filtering, efficiency <0 and efficiency data during (T_{out}-T_{in}) <0 were removed. When compare the collector efficiency in figure 4.35 and figure 4.23, figure 4.35 shows that the collector operates in high efficiency range (60% to 100%) while the working fluid is liquid state.

4.8 Discussion

4.8.1 *Flow Rate Behaviour*

On clear days, solar radiation received around noon is steady according to EN 12975 and flow rate of the system should be positive. But flow rate data shows negative flow rates around the noon on clear days. There can be two factors affecting for the flow rate:

After the main pump, the pipe network divides into two branches before it arrives to the tested panels. The first division supplies to the main group of 60 panels before the 33 panels, which includes the tested panels as shown in

Figure 3.4. There are no flow control valves before 60 panels group. Therefore, the flow rate in the tested panels can be altered by the behavior of the larger group.

The second possibility is boiling of the water/glycol mixture. The boiling point of 50/50 Polypropylene glycol and water at atmospheric pressure is 105°C (Dusseldorf, 1991) .This value change with the pressure. The pressure of water/glycol mixture at the panels decides the boiling point from place to place.

The main pump supplied the water/glycol with pressure 284kPa.The actual flow rate and the pressure of the working fluid at the tested panel will be lower due to pressure losses in the piping network. If the pressurized water/glycol mixture with 284kPa reaches the testing panels without losses then the boiling point of water/glycol mixture at testing panels is 136 °C. As the inlet and outlet temperatures of tested panels reaches 180° C (recorded maximum temperature at outlet of tested collectors during data collection period) during daytime the water/glycol mixture must have boiled. It must result in internal energy absorption for phase change of mixture (Latent

heat absorb by water/glycol mixture to change state from liquid to vapor) and alter the flow rate. The data analysis had to limit for liquid state of water/glycol mixture due to lack of information to estimate the pressure of water/glycol mixture at tested collector.

In addition, these two effects cannot be investigated further without doing a proper simulation of the system. A follow up project to this one is undertaking a detailed simulation of SLC solar thermal system using TRANSYS software.

4.8.2 *Unsteady Behaviour*

The ratio of the Unsteady to Steady term measures the importance of unsteady energy generation in determining the panel efficiency. According to experimental data unsteady term or the heat generated within the system is high for the periods analyzed (clear days, partly cloudy days and cloudy days). The internal energy generated within the working fluid is higher even in clear days such 2013/02/08 (Figure 4.32). This indicates that the unsteady factors are dominant in this system.

4.8.3 *Collector Efficiency*

Fraunhofer test results (Jiangsu Sunrain Solar Energy, n.d) show expected collector behavior: maximum efficiency at zero $(T_m\text{-}T_a)/G$ and lower efficiencies at high $(T_m\text{-}T_a)/G$. The presented clear day results showed following variations. On clear spring days collector operates in high efficiency, low $(T_m\text{-}T_a)/G$ range. In clear winter days collector operates with moderate efficiencies, middle range of $(T_m\text{-}T_a)/G$. However, during partly cloudy and cloudy days the collector efficiencies are lower than clear days. Figure 4.5 showed that SLC experiences cloudy and partly cloudy weather most of the time. High cloud covers result in lower solar energy

availability and the internal energy generation due to intermittency of sunshine. The collectors at SLC therefore operate with lower efficiencies than they could achieve under different operating conditions.

4.8.4 *Abnormal Behaviour of System*

Calculated efficiencies for all three categories of days have abnormalities such as efficiency higher than 100% and negative efficiencies. According to conservation of energy the efficiency higher than 100 % shows an energy gain due to an undefined factor in equation (2.11). However, most possibly cause is not an identified energy source. The sudden higher flow rate data is the main reason for high useful energy gain. The calculation had following limitations those lead to abnormal efficiency results. The data recording frequency was not high enough to capture the accurate flow rate behavior and temperatures. This limitation could not prevent due to BMS and data gathering limitations. In addition, when setting up the equipments sudden changes in flow rate and temperature data were not predicted. Negative efficiency also generated due to negative temperature rise and negative flow rate data. The negative efficiency is a result of low frequency data gathering.

4.8.5 *Suggested Improvements*

Heat absorbed by the working fluid inside manifold can be explained using the relationship $\dot{m}C_p(T_{out} - T_{in})$ as showed in equation (2.8). In solar thermal systems, when working fluid has high mass flow rate ($\dot{m}$), then temperature difference ($T_{out} - T_{in}$) becomes low at constant *IA*. This occurs when the pump capacity is high and it results in high thermal efficiency. When mass flow rate $\dot{m}$ is low, then temperature rise becomes high($T_{out} - T_{in}$). That

results in lower thermal efficiency and indicates a lower capacity pump. According to efficiency results and the flow rate data at SLC, the pumping system of solar thermal system was designed for low mass flow rate. With the effect of other group of panels as discussed in section 4.8.1 currently flow rate of the system can be greatly lower than designed flow rate.

Two ways can be proposed to increase the flow rate of water/glycol mixture in this solar thermal system. The existing constant flow pump with 5.36 l/s used in the system can be replaced with higher capacity pump or serial connection of another pump. At this stage of the project the flow rate that is required to optimize the system efficiency was not estimated. The second option is a variable flow pump that can be programmed to run at different speeds. This option may suitable than a constant flow pump as the pump speed is unknown for optimum performance.

If the sudden flow rate changes are due to boiling of water/glycol mixture and the water/glycol mixture absorb energy for phase change of liquid from liquid to vapor, then system should temporarily stop to investigate. The system pressure at each point should be estimated and increase the pressure of mixture that supply by the main pump. Secondly, the volume of water/glycol in the mixture should change to increase the boiling point or alternative working fluid should be search.

Chapter Five: **CONCLUSION AND RECOMAMNDATIONS**

5.1 Conclusion

Main objective of this thesis was to install, commission and validate a monitoring system for the solar hot water system at SLC and use collected information to determine the performance of heat pipe evacuated tube solar thermal collector system at Southland Leisure Centre. The main performance indicator is the efficiency of collector which is calculated based on unsteady state heat gain of the working fluid. Long term data monitoring provided the required parameters. Behavior of temperature rises across collectors and flow rate showed unexpected behaviour. Sudden flow rate change was observed and this may have been caused by boiling of the working fluid or the interaction of the flow rate with other panels groups. If the working fluid boiling temperature is lower than 105°C at atmospheric pressure, the system boils and the flow rate changes. It is suggested to carry out a system, flow rate and pressure simulation that should provide the boiling point of working fluid at different areas of the piping network.

The unsteady state efficiency of collector was estimated for clear, cloudy and partly cloudy days which give the performance of collector when the solar energy availability varies. Clear day efficiency is higher than both cloudy day partly cloudy days. In additions the efficiencies calculated for SLC compared with steady state efficiency data provided by Fraunhofer institute where tested same collectors according test standard EN 12975. This comparison was done using efficiency vs. $(T_m-T_a)/G$ graph which are independent of flow rate and T_{out}-T_{in}. According to the comparison, the unsteady state efficiency even on clear days is considerably lower than the steady state efficiency results according to EN 12975. Analysis on frequency of cloudy, partly cloudy and clear days at SLC for 18 months showed that partly cloudy and cloudy days are more frequent. More partly cloudy and cloudy days results in lower

overall efficiency of collectors. The ratio of Unsteady/Steady was introduced to measure the dominance of unsteady heat generation within the collectors. This ratio is high for all categories of days. The high unsteady term implies the lower useful heat gain of working fluid that results in lower efficiencies. The flow rate improvements such as increasing flow rate may increase the useful heat gain. Altering the pump capacity and changing the system control strategy will resolve this issue and an investigation is needed to find the optimum flow rate that will give the optimum efficiency of collectors.

As part of data analysis, the solar availability at SLC was measured to find the strength of solar source in Calgary as well as validate the pyranometer data as a standard for Calgary. SLC gets high solar radiation during winter, up to 800W/m^2, and yearly solar maximum is close 1000 W/m^2 on 45° angle surface. This source is strong enough for future solar thermal applications. The pyranometer data for solar insolation at SLC are slightly higher than Calgary Int'l airport data recorded by NASA. The pyranometer mounted on roof gets much higher reflected radiation from large rooftop and it is much higher in winter due to high reflectivity of snow. Solar radiation data was assessed to be accurate.

5.2 Future Recommendations

Based on the findings in this project, the following are recommended;

1. The internal energy generated within the heat pipes can be included in the calculation and can increase the accuracy of the estimated efficiencies
2. Accuracy of solar radiation data measurements can be increased by mounting multiple pyranometers to measure beam, diffuse and reflected radiation.
3. Flow rate can be adjusted to different values and estimate the efficiencies of collector. This method will help to measure the optimum flow rate that gives best efficiency of HP ETCs at SLC.
4. The flow rate of water/glycol mixture showed sudden changes possibly due to boiling. Boiling of the working fluid should be investigated using a proper simulation of the system.
5. The accurate flow rate and temperatures will be achieved by isolating the section of panels including the tested collectors by allowing working fluid goes only through them.

References

Ayompe, L.M., & Duffy, A. (2013). *Thermal performance analysis of a solar water heating system with heat pipe evacuated tube collector using data from a field trial*. Solar Energy, 90, 17-28. doi:10.1016/j.solener.2013.01.001

Bob, S. (n.d.). *Solar Energy in Canada*. Ontario: Canadian Solar Industries Association (CanSIA) , Ontario: Natural Resources Canada.Retrieved May 4, 2013 from *www.cansia.ca/sites/default/files/161.pdf*

Bragg, S.M., & Reid, R. S. (n.d.). *Transient approximation of SAFE-100 heat pipe operation*. Huntsville (AL) : NASA/MSFC. Retrieved May 4, 2013 from *ntrs.nasa.gov/archive/nasa/casi.ntrs.nasa.gov/20050109882.pdf*

Brunold, S., Frey, R., Frei,U. (1994). *A comparison of three different collectors for process heat applications* . Rapperswil (Swizterland):Institute for Solartechnik.

Campbell Scientific Canada Corp, (2010a).*CR800 Series-Measurements & control systems*. Canada: Campbell Scientific Canada Corp.

Campbell Scientific Canada Corp, (2010b). *R.M. Young wind monitors - Instruction manual.* Canada: Campbell Scientific Canada Corp.

Campbell Scientific Canada Corp, (2010c). *CMP3-L Pyranometer-Instruction manual*. Canada: Campbell Scientific Canada Corp.

Canadian Forest Service, & CanmetENERGY Photovoltaic systems group. (2013). *Photovoltaic potential and solar resource maps of Canada*. Retrieved May12, 2013, from http://pv.nrcan.gc.ca/

CanSIA (2013). *Solar Heat Sustainability Future: Clean energy solutions for Canada*. Ottawa (Canada):Canada Solar Industires Association. Retrieved May4, 2013 from http://www.cansia.ca/sites/default/files/20140129_cansia_solar_heat_sustainable_future.pdf

Chow, T. , Chan, L., Fong, K., Tan, R., & Dong, Z. (2012). *Experimental study of evacuated-tube solar water heaters in hong kong. Proceedings of the Institution of Mechanical Engineers, Part A: Journal of Power and Energy, 226*(4), 447-461. doi:10.1177/0957650912442851

City of Calgary, (2013). *Southland Leisure Centre solar thermal project*. Unpublished manuscript

Dikmen, E., Ayaz, M., Ezen, H. H., Kucuksille, E. U., & Sahin, A. S. (2013). *Estimation and optimization of thermal performance of evacuated tube solar collector system*.1-9. doi:10.1007/s00231-013-1282-0

Duffie, J.A., &Beckman, W.A. (2013). *Solar engineering of thermal processes*. (4th ed). Hoboken (NJ): John Wiley & Sons, Inc.

Dusseldorf .(1991). *VDI-Warmeatlas Dd 17- VDI-Verlag GmbH*. Retrieved October 21, 2013 from: https://detector-cooling.web.cern.ch/detector-cooling/data/Table%208-3-1.htm

European Committee for Standards. (2013). *Thermal solar systems and components — Solar collectors Part 1: General requirements*. Wien (Austria): Austrian Standards Institute. Ref. No. prEN 12975-1:2013: E.

Eggertson, B. (2005). *Green Cool: Using Green Heat Technologies to Offset Cooling Loads*. *Refocus. 6*(4), 58-59. doi:http://dx.doi.org.ezproxy.lib.ucalgary.ca/10.1016/S1471-0846(05)70435-2

Fischer, S., Heidemann, W., Müller-Steinhagen, H., Perers, B., Bergquist, P., & Hellström, B. (2004). *Collector test method under quasi-dynamic conditions according to the european standard EN 12975-2*. *Solar Energy, 76*(1–3), 117-123. doi:http://dx.doi.org.ezproxy.lib.ucalgary.ca/10.1016/j.solener.2003.07.021

Fraunhofer Institute. (2007). *Collector test according to EN 12975-2:2006*. Freiburg (Germany): Fraunhofer-ISE. Test Report: KTB Nr. 2007-07-en.

Ghosh, T.K., &Prelas, M.A. (2011). *Energy Resources and Systems Volume 2: renewable resources*. London (New York): Springer Dordrecht Heidelberg.

Harrison S.J., Rogers . B.A.l,Soltau,H, Wood.B.D. (1993). *The characterization and testing of solar collector thermal performance*.Canada:IEA solar R & D. IEA-SHC-T.3.D.1.Retrieved from http://task03.iea-shc.org/data/sites/1/publications/Characterization%20and%20Testing%20of%20Solar%20Collector%20Thermal%20Performance-April%2019931.pdf

Ineichen, P., Guisan, O., & Perez, R. (1990). *Ground-reflected radiation and albedo*. Solar Energy, 44(4), 207-214. doi:http://dx.doi.org.ezproxy.lib.ucalgary.ca/10.1016/0038-092X(90)90149-7

Islam, M., Fartaj, A., & Ting, D. S. (2004). *Current utilization and future prospects of emerging renewable energy applications in Canada*. *Renewable and Sustainable Energy Reviews, 8*(6), 493-519.

ISO. (2010). *Solar Energy-Test method for solar collector-Part 1: Thermal performance of glazed liquid heating collectors including pressure drop*. ISO TC 180/SC N 165,ISO/WD 9806-1

Jackman, T. (2009). *Solar thermal water heating: An application for Alberta, Canada*.Paper presented at IASTED International Conference Enviorenmental Management and Engineering (EME 2009) Banff (Canada).ISBN-987-1-61567-540-1.

Jagoda, K., Lonseth, R., Lonseth, A., & Jackman, T. (2011). *Development and commercialization of renewable energy technologies in canada: An innovation system perspective*. *Renewable Energy, 36*(4), 1266-1271. doi:http://dx.doi.org.ezproxy.lib.ucalgary.ca/10.1016/j.renene.2010.08.022

Jiangsu Sunrain Solar Energy. (n.d). *Sunrain solar heat pipe collectors: TZ58/1800-R-Series*. Lianyungang (China): Jiangsu Sunrain Solar Energy C. Ltd.

Jiangsu Sunrain Solar Energy. (2008a). *Specifications of collector mounting structure*. China: Jiangsu Sunrain Solar Energy Co. Ltd.

Jiangsu Sunrain Solar Energy. (2008b). *Specifications of collector*. China: Jiangsu Sunrain Solar Energy Co. Ltd.

Kovacs, P. (2012). *A guide to the standard EN 12975*.Sweden: Technical Research Institute. Brussels (Belgium): European Solar Thermal Industry Federation (ESTIF). QAiST - IEE/08/593/SI2.529236, Deliverable D2.3.

Kalogirou, S A.(2014). *Solar Energy Engineering : Processes and Systems* (2nd Edition). Saint Louis, MO, USA: Academic Press, 2014. ProQuest ebrary. Web. 5 August 2014.

MacNish L.(2007). *RASC Calgary Centre - Field Rotation with an Alt-Az Telescope Mount*. Retried February 5, 2014 from http://calgary.rasc.ca/field_rotation.htm.

Mahjouri, F. (n.d.). *Vacuum Tube Liquid Vapor (Heat Pipe) Collector*.Maryland (Colombia):Thermo technologies.Retrieved December 13, 2013. from Thermo Technologies Web site: http://www.thermomax.com/PDF_Files.php.

National Energy Board Canada. (2011). *Canada's Energy Future: Energy supply and demand projection for 2035*.Canada: National Energy Board. Cat. No. NE23-15/2011E-PDF, ISBN 978-1-100-19464-6

National Resources Canada. (2011). *Energy Use Data Handbook 1990 to 2009*. Canada: Government of Canada. Retrieved May 12, 2013, from http://oee.rncan.gc.ca/publications/statistics/trends11/chapter3.cfm?attr=0

National Resources Canada. (2013). *Energy Use Data Handbook 1990 to 2010*. Canada: National Resources Canada . Cat. No. M141-11/2010E (Print),ISSN 1715-3174 . Retrieved from http://oee.nrcan.gc.ca/publications/statistics/handbook2010/handbook2013.pdf

Nielson,J.E. (2010). *European Solar Thermal Standards and Solar Keymark Certification*. Poland: Warzaw University of Technology **.** Retrieved February 20, 2014 from http://typo3.p126074.typo3server.info/fileadmin/Qualicert_Docs/Events/Polish_Validation_Workshop/Nielsen_2.pdf.

Nkwetta, D. N., & Smyth, M. (2012*). Performance analysis and comparison of concentrated evacuated tube heat pipe solar collectors*. *Applied Energy*, *98*(0), 22-32. doi:http://dx.doi.org.ezproxy.lib.ucalgary.ca/10.1016/j.apenergy.2012.02.059

NREL (1992). *Shining On ; A premier on solar radiation data*. NREL/TP-463-4856, DE92010555. Golden(CO): NREL. Retrieved March 6, 2014 from: http://www.nrel.gov/docs/legosti/old/4856.pdf

Onicon Incorparated,(2010).*F-3100 Series-In-line Electromagnetic Flow Meter-Installation & Basic Operation Guide*. USA(FL): Onicon Incorparated.Mnaual 01/10.

Rabl, A.(1985) . *Active Solar Collectors and Their Applications*. Cary, NC, USA: Oxford University Press, Incorporated, 1985. ProQuest ebrary. Web. 14 July 2014.

Ramon, P.N., &Victor, M.M. (2012).*Optical Analysis of the Fixed Mirror Solar Concentrator by Forward Ray-Tracing Procedure*. Journal of Solar Energy Engineering, 134(3). doi:10.1115/1.4006575

RET Screen. (2008). *Solar hot water system schematic*. Retrieved February 2, 2014, from http://www.retscreen.net/ang/solar_hot_water_system_schematic.php

RETScreen. (2008). *Solar pool heating system schematic*. Retrieved February 2, 2014, from http://www.retscreen.net/ang/solar_pool_heating_system_schematic.php

Seimens Industry Inc, (2013a).*PI Bus Interface Module-Owner's manual*.USA: Seimens Industry Inc. Document No. 125-3583.

Seimens Industry Inc, (2013b).*Technical specification sheet-Immersion well temperature sensors*. USA: Seimens Industry Inc**.** Document No. 149-919

Simon, G. , Aaron, G. (2008). *OSEA CANSIA Solar Thermal Community Action Manual.* (2nd ed.). Canada: Canadian Solar Industries Association.

The Dow Chemical Company,(2003).*A Guide to Glycols.* USA:The Dow Chemical Company. Retrieved from http://www.dow.com/webapps/lit/litorder.asp?filepath=propyleneglycol/pdfs/noreg/117-01682.pdf

Trimble H.M.,Walter P. (1935). *Water-Glycol mixtures: Vapour pressure- boiling point - composition relations*.Okla:Industrial and Engineering Chemistry,27(1),66-68

United State Department of Agriculture. (n.d.). *Solar water heating energy self assessment*. Retrieved February 2, 2014, from http://www.ruralenergy.wisc.edu/renewable/solar_thermal/default_solar_thermal.aspx

Walker, A. (2013).*Solar Energy: A Design Guide for Building Professionals*. NJ (USA): RSMeans.

William B.S., & Michael G. (2001). *Power from the sun*. Modified by: http://www.powerfromthesun.net, Retrieved May 4, 2014, from http://www.powerfromthesun.net/book.html

Williams Engineering. (2010a). *Plumbing and control schematics.* Unpublished manuscript.

Williams Engineering. (2010b). *Roof layout and typical details.* Unpublished manuscript.

Williams Engineering. (2010c). *Specifications and controls sequence of operation.* Unpublished manuscript.

Zambolin, E., & Del Col, D. (2010). *Experimental analysis of thermal performance of flat plate and evacuated tube solar collectors in stationary standard and daily conditions*. *Solar Energy, 84*(8), 1382-1396. doi:http://dx.doi.org.ezproxy.lib.ucalgary.ca/10.1016/j.solener.2010.04.020

Zinko, H., Holst, P., Perers, B., & Eriksson, L. (1984). *Comparison of the effective system performance of flat plat and evacuated tube collectors used for district heating purposes.* Sweden: Journal of Solar Energy Research (JSER), 2(1), 17-30.

APPENDIX A: DRAWINGS OF SOUTHLAND LEISURE CENTRE SOLAR THERMAL PROJECT

A.1. Roof Layout(William Engineering, 2010b)

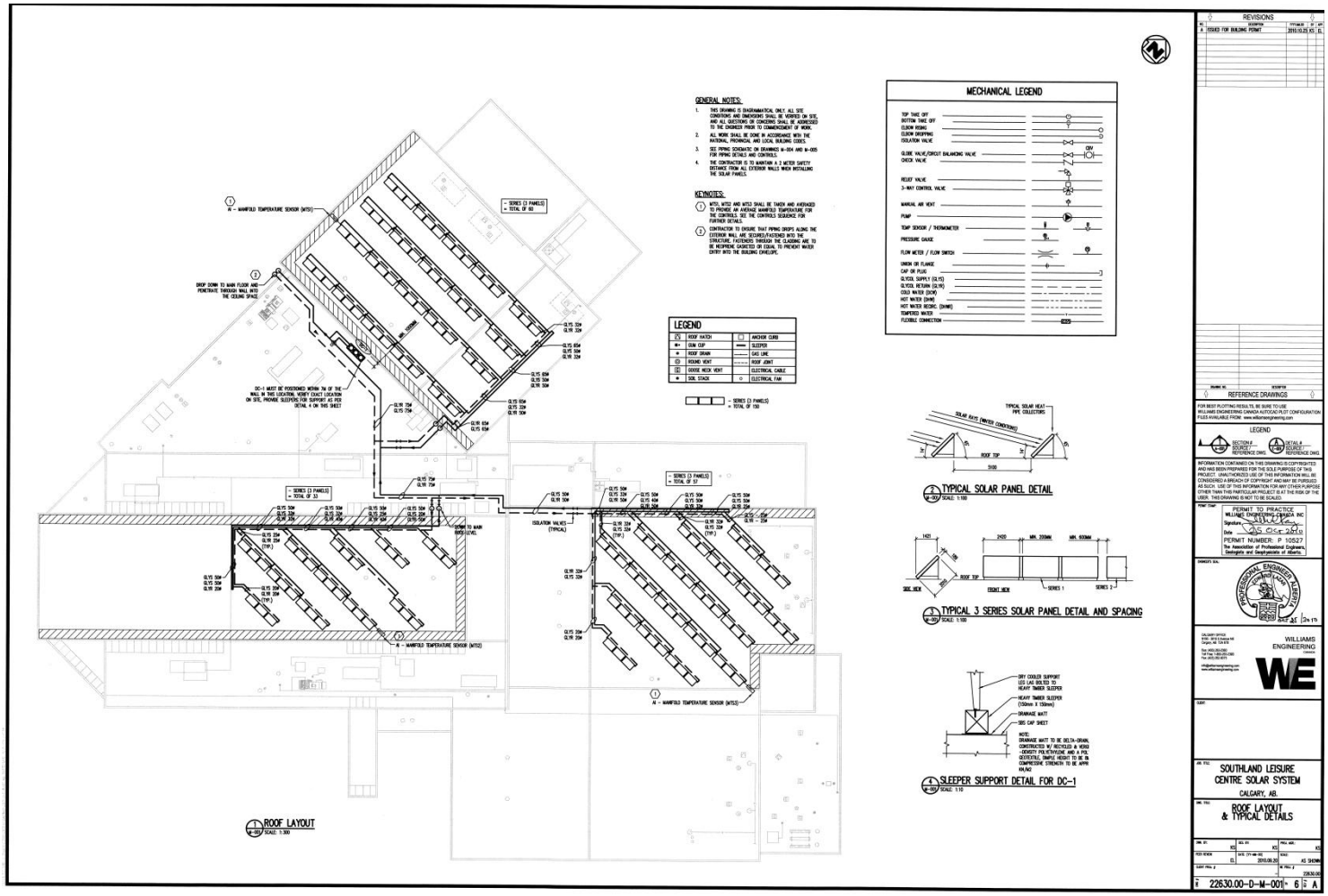

A.2. Plumbing and Control Schematics (William Engineering, 2010a)

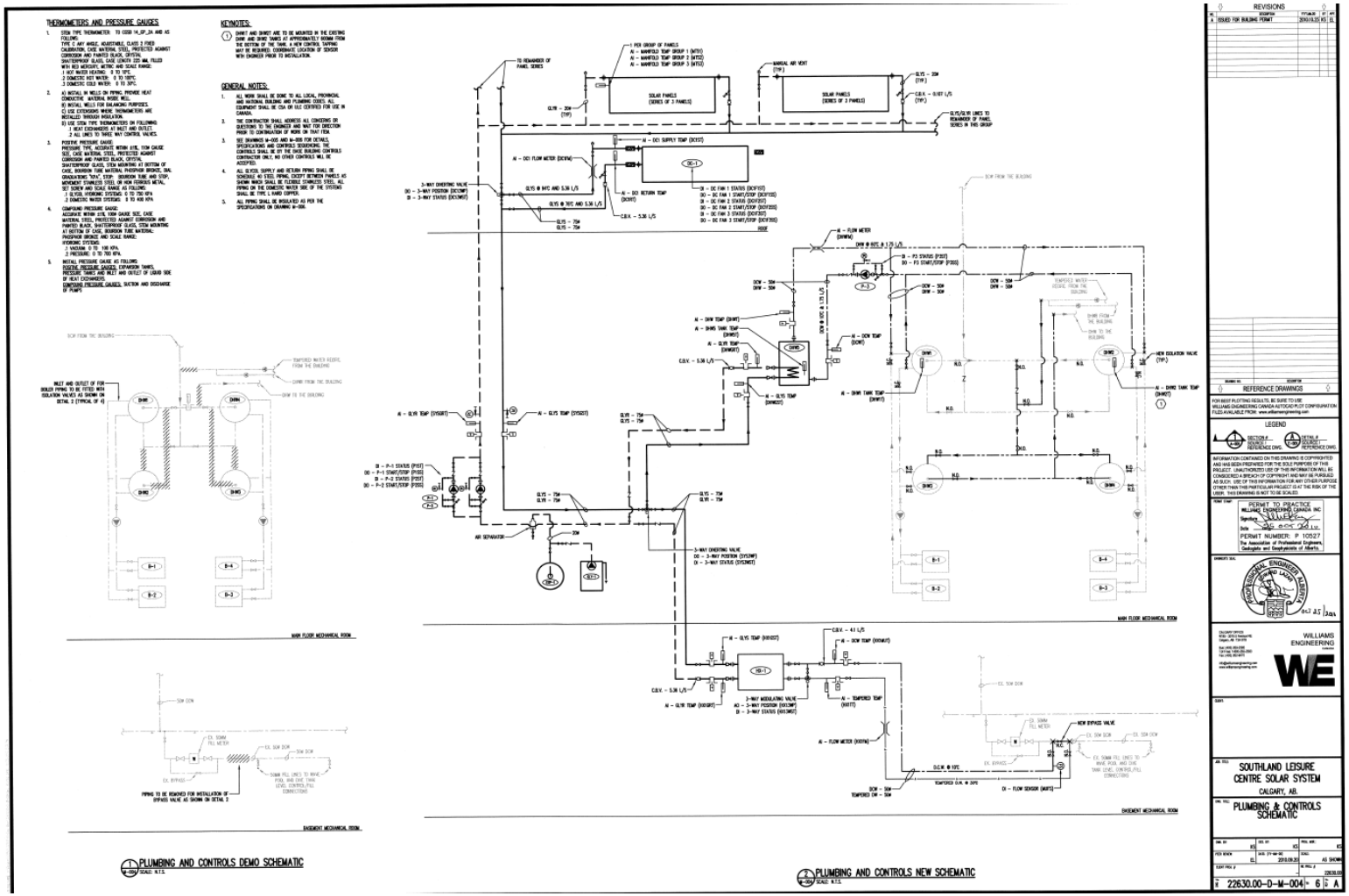

A.3. Heat Pipe Evacuated Tube Collector Specifications (Jiangsu Sunrain Solar Energy, 2008)

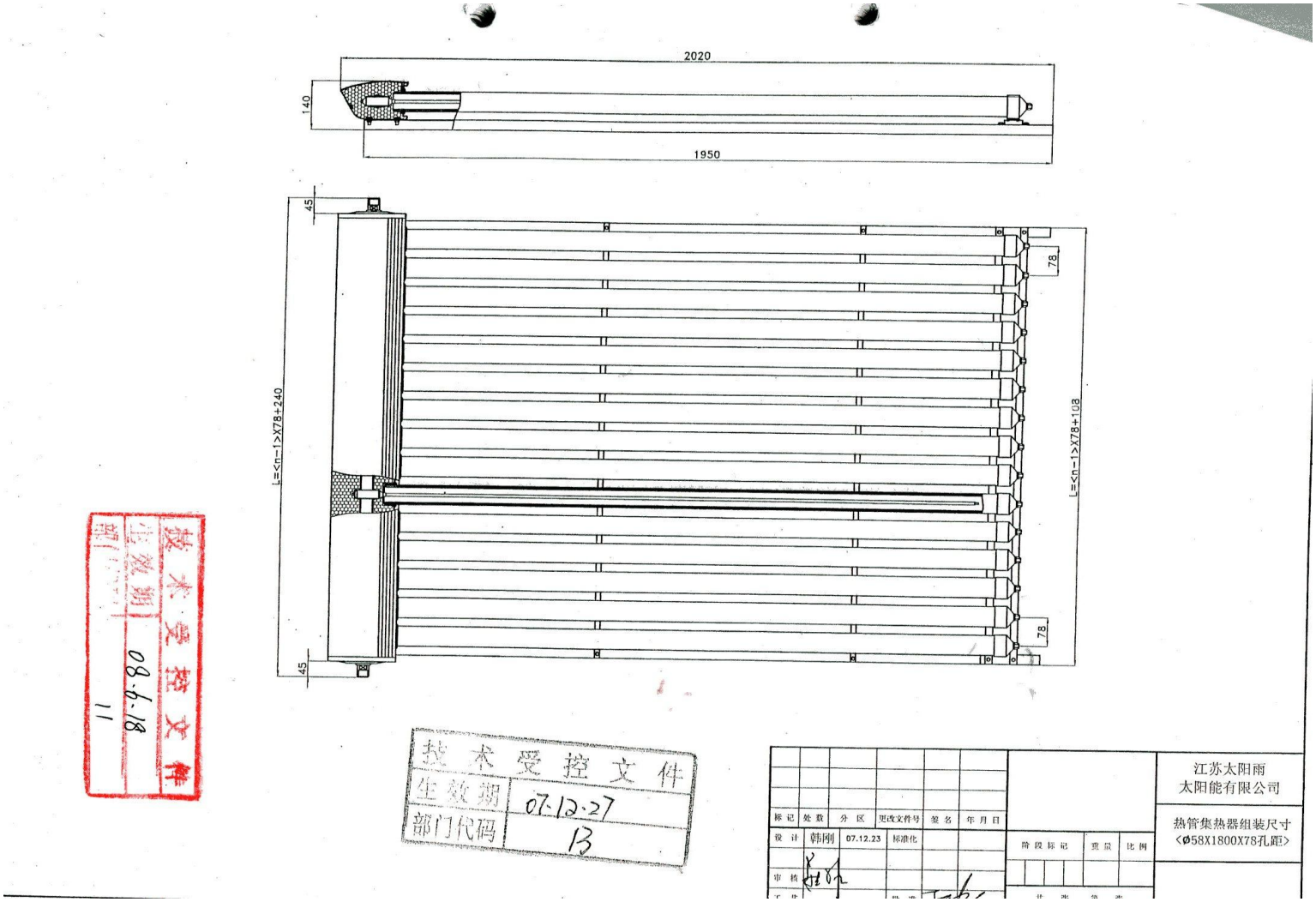

A.4. Solar Collector Mounting Structure((Jiangsu Sunrain Solar Energy, 2008)

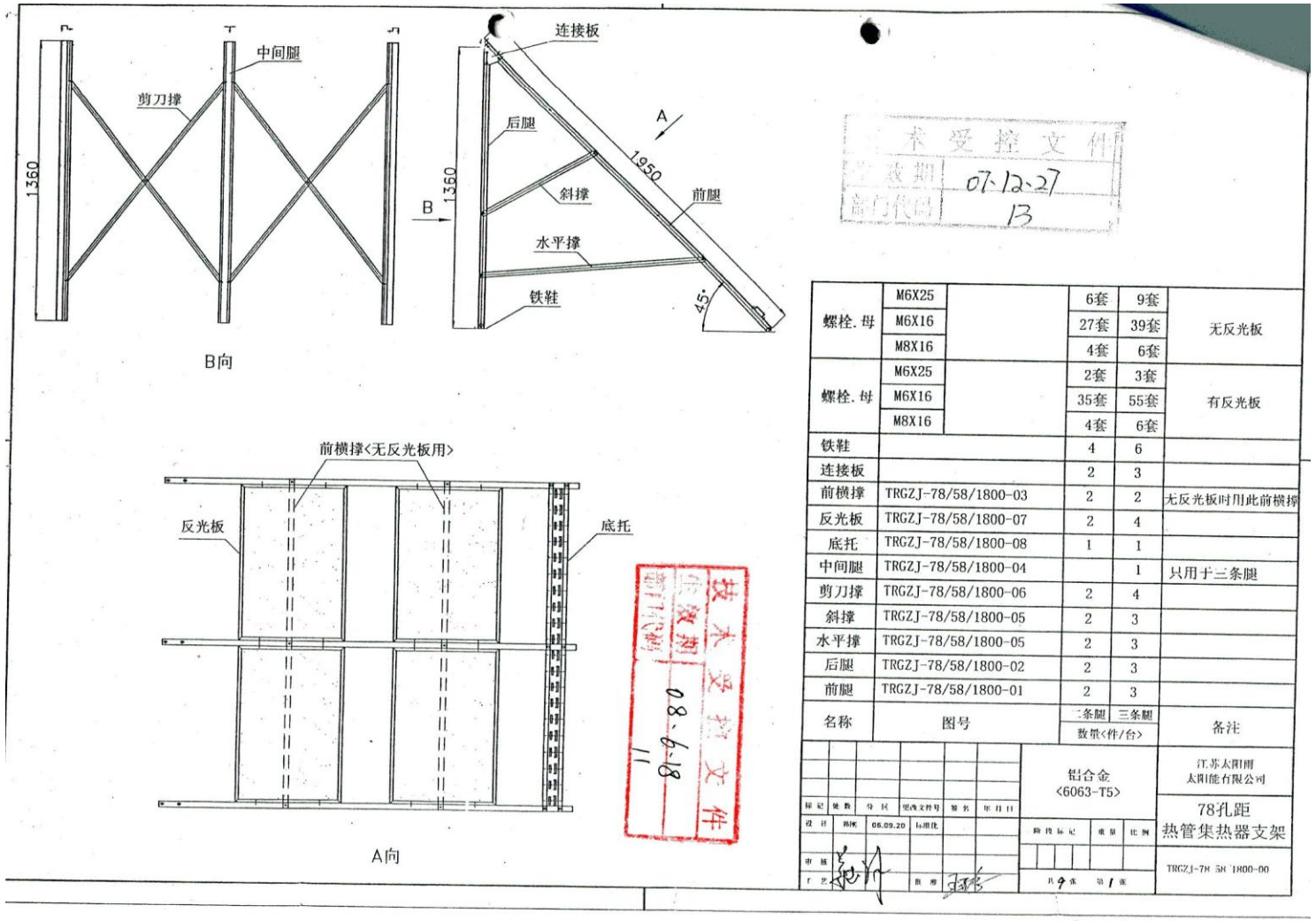

名称	图号	二条腿 数量<件/台>	三条腿 数量<件/台>	备注
螺栓.母	M6X25	6套	9套	无反光板
	M6X16	27套	39套	
	M8X16	4套	6套	
螺栓.母	M6X25	2套	3套	有反光板
	M6X16	35套	55套	
	M8X16	4套	6套	
铁鞋		4	6	
连接板		2	3	
前横撑	TRGZJ-78/58/1800-03	2	2	无反光板时用此前横撑
反光板	TRGZJ-78/58/1800-07	2	4	
底托	TRGZJ-78/58/1800-08	1	1	
中间腿	TRGZJ-78/58/1800-04		1	只用于三条腿
剪刀撑	TRGZJ-78/58/1800-06	2	4	
斜撑	TRGZJ-78/58/1800-05	2	3	
水平撑	TRGZJ-78/58/1800-05	2	3	
后腿	TRGZJ-78/58/1800-02	2	3	
前腿	TRGZJ-78/58/1800-01	2	3	

铝合金 <6063-T5>

江苏太阳雨太阳能有限公司

78孔距 热管集热器支架

TRGZJ-78/58/1800-00

APPENDIX B: SPECIFICATIONS OF SENSORS AND DATA LOGGER

B.1. CR800 Data Logger (Campbell Scientific Canada Corp.,2010a)

3.3 CR800 Specifications

SPECIFICATIONS valid from -25° to +50°C, non-condensing environment, unless otherwise specified. Recalibration recommended every two years. Critical specifications and system configuration should be confirmed with Campbell Scientific before purchase.

PROGRAM EXECUTION RATE
(10) ms to 1 day @ 10 ms increments

ANALOG INPUTS (SE 1-6 or DIFF 1-12)
(3) differential (DF) or 6 single-ended (SE) individually configured input channels. Channel expansion provided by optional analog multiplexers.

RANGES and RESOLUTION: Basic resolution (Basic Res) is the A/D resolution of a single conversion. Resolution of DF measurements with input reversal is half the Basic Res.

Range (mV)[1]	DF Res (µV)[2]	Basic Res (µV)
±5000	667	1333
±2500	333	667
±250	33.3	66.7
±25	3.33	6.7
±7.5	1.0	2.0
±2.5	0.33	0.67

[1] Range overhead of ≈9% on all ranges guarantees full-scale voltage will not cause over-range.
[2] Resolution of DF measurements with input reversal.

ACCURACY[3]:
±(0.06% of reading + offset), 0° to 40°C
±(0.12% of reading + offset), -25° to 50°C
±(0.18% of reading + offset),-55° to 85°C(-XT only)

[3] Accuracy does not include sensor and measurement noise. Offsets are defined as:

Offset for DF w/input reversal = 1.5 x Basic Res+1.0 µV
Offset for DF w/o input reversal = 3 x Basic Res+2.0 µV
Offset for SE = 3 x Basic Res + 3.0 µV

ANALOG MEASUREMENT SPEED:

Integration Type Code	Integration Time	Settling Time	---Total Time[5]--- SE w/ No Rev	DF w/ Input Rev
250	250µs	450µs	≈1ms	≈12ms
60Hz[4]	16.67ms	3ms	≈20ms	≈40ms
50Hz[4]	20.00ms	3ms	≈25ms	≈50ms

[4] AC line noise filter
[5] Includes 250 µs for conversion to engineering units

INPUT NOISE VOLTAGE: For DF measurements with input reversal on ±2.5 mV input range (digital resolution dominates for higher ranges).

250 µs Integration: 0.34 µV RMS
50/60 Hz Integration: 0.19 µV RMS

INPUT LIMITS: ±5 V

DC COMMON MODE REJECTION: >100 dB

NORMAL MODE REJECTION: 70 dB @ 60 Hz when using 60 Hz rejection

SUSTAINED INPUT VOLTAGE W/O DAMAGE: ±16 Vdc max.

INPUT CURRENT: ±1 nA typical, ±6 nA max. @ 50°C; ±90 nA @ 85°C

INPUT RESISTANCE: 20 Gohms typical

ACCURACY OF BUILT-IN REFERENCE JUNCTION THERMISTOR (for thermocouple measurements):
±0.3°C, -25° to 50°C
±0.8°C, -55° to 85°C (-XT only)

PERIOD AVERAGE: Any of the 6 SE analog inputs can be used for period averaging. Accuracy is ±(0.01% of reading + resolution), where resolution is 136 ns divided by the specified number of cycles to be measured.

Input amplitude and frequency:

Voltage Gain	± Input Range mV	Signal Peak-Peak[6] Min mV	Max V	Min Pulse Width µs	Max[7] Freq kHz
1	250	500	10	2.5	200
10	25	10	2	10	50
33	7.5	5	2	62	8
100	2.5	2	2	100	5

spacer
[6] With signal centered at CR800 ground.
[7] The maximum frequency = 1/(Twice Minimum Pulse Width) for 50% of duty cycle signals.

ANALOG OUTPUTS (Vx 1-2)
(2) switched voltage outputs sequentially active only during measurement.

RANGES / RESOLUTION:

Chan	Range	Resolution	Current Source / Sink
V_X	±2.5V	0.67mV	±25 mA

V_X ACCURACY
±(0.06% of setting + 0.8 mV, 0° to 40°C
±(0.12% of setting + 0.8 mV, -25° to 50°C
±(0.18% of setting + 0.8 mV,-55° to 85°C(-XT only)

V_X FREQUENCY SWEEP FUNCTION: Switched outputs provide a programmable swept frequency, 0 to 2500 mV square waves for exciting vibrating wire transducers.

CURRENT SOURCING/SINKING: ±25 mA

RESISTANCE MEASUREMENTS
MEASUREMENT TYPES: Ratiometric measurements of 4- and 6-wire full bridges, and 2-, 3-, and 4-wire half bridges. Precise, dual polarity excitation for voltage excitation eliminates DC errors. Offset values are reduced by a factor of 2 when excitation reversal is used.

VOLTAGE RATIO ACCURACY[8]: Assuming excitation voltage of at least 1000 mV, not including bridge resistor error:

±(0.04% of reading+offset)/V_X

[8] Accuracy does not include sensor and measurement noise. Offsets are defined as:

Offset for DF w/input reversal = 1.5 x Basic Res + 1.0 µV
Offset for DF w/o input reversal = 3 x Basic Res + 2.0 µV
Offset for SE = 3 x Basic Res + 3.0 µV

PULSE COUNTERS (P 1-2)
(2) inputs individually selectable for switch closure, high frequency pulse, or low-level ac. Independent 24-bit counters for each input.

MAXIMUM COUNTS PER SCAN: 16.7×10^6

SWITCH CLOSURE MODE:
Minimum Switch Closed Time: 5 ms
Minimum Switch Open Time: 6 ms
Max. Bounce Time: 1 ms open w/o being counted

HIGH FREQUENCY PULSE MODE:
Maximum Input Frequency: 250 kHz
Maximum Input Voltage: ±20 V
Voltage Thresholds: Count upon transition from below 0.9 V to above 2.2 V after input filter with 1.2 µs time constant.

LOW LEVEL AC MODE: Internal ac coupling removes dc offsets up to ±0.5 V.

Input Hysteresis: 12 mV RMS @ 1 Hz
Maximum ac Input Voltage: ±20 V
Minimum ac Input Voltage:

Sine wave (mV RMS)	Range (Hz)
20	1.0 to 20
200	0.5 to 200
2000	0.3 to 10,000
5000	0.3 to 20,000

DIGITAL I/O PORTS (C 1-4)
(4) ports software selectable as binary inputs or control outputs. Provide edge timing, subroutine interrupts / wake up, switch closure pulse counting, high frequency pulse counting, asynchronous communications (UARTs), SDI-12 communications, and SDM communications

HIGH FREQUENCY MAX: 400 kHz

SWITCH CLOSURE FREQUENCY MAX: 150 Hz

EDGE TIMING RESOLUTION: 540 ns

OUTPUT VOLTAGES (no load): high 5.0 V ±0.1 V; low <0.1

OUTPUT RESISTANCE: 330 ohms

INPUT STATE: high 3.8 to 16 V; low -8.0 to 1.2 V

INPUT HYSTERISIS: 1.4 V

INPUT RESISTANCE: 100 kohms

SERIAL DEVICE/RS-232 SUPPORT: 0 to 5 V UART

SWITCHED 12 V (SW12)
(1) independent 12 V unregulated source is switched on and off under program control. Thermal fuse hold current = 900 mA @ 20°C, 650 mA @ 50°C, 360 mA @ 85°C.

CE COMPLIANCE
STANDARD(S) TO WHICH CONFORMITY IS DECLARED: IEC61326:2002

COMMUNICATION
RS-232 PORTS:
9-pin: DCE (not electrically isolated) for computer or non-CSI modem connection.
COM1 to COM2: Two independent Tx/Rx pairs on control ports (non-isolated); 0 to 5 V UART
Baud Rate: Selectable from 300 to 115.2 kbps.
Default Format: 8 data bits; 1 stop bits; no parity.
Optional Formats: 7 data bits; 2 stop bits; odd, even parity.

CS I/O PORT: Interface with CSI telecommunications peripherals.

SDI-12: Digital control ports 1 or 3 are individually configurable and meet SDI-12 Standard version 1.3 for datalogger mode. Up to ten SDI-12 sensors are supported per port.

PROTOCOLS SUPPORTED: PakBus, Modbus, DNP3, FTP, HTTP, XML, POP3, SMTP, Telnet, NTCIP, NTP, SDI-12, and SDM.

SYSTEM
PROCESSOR: Renesas H8S 2322 (16-bit CPU with 32-bit internal core, running at 7.3 MHz)

MEMORY: 2 Mbytes of Flash for operating system; 4 Mbytes of battery-backed SRAM for CPU usage, program storage and data storage.

RTC CLOCK ACCURACY: ±3 min. per year. Correction via GPS optional.

RTC CLOCK RESOLUTION: 10 ms

SYSTEM POWER REQUIREMENTS
VOLTAGE: 9.6 to 16 Vdc

EXTERNAL BATTERIES: 12 Vdc nominal (power connection is reverse polarity protected)

TYPICAL CURRENT DRAIN: Sleep Mode: ≈0.6 mA
1 Hz Sample Rate (one fast SE meas.): 1 mA
100 Hz Sample Rate (one fast SE meas.): 16.2 mA
100 Hz Sample Rate (one fast SE meas. w/ RS-232 communications): 27.6 mA
optional keyboard display on: add 7 mA to current drain
Backlight on: add 100 mA to current drain

PHYSICAL
DIMENSIONS: 241 x 104 x 51 mm (9.5 x 4.1 x 2 in); additional clearance required for cables and leads.

MASS/WEIGHT (datalogger + base):

MASS: 0.7 kg
WEIGHT: 1.5 lbs

WARRANTY
(3) years against defects in materials and workmanship.

B.2. Flow Meter(Onicon Incorparated, 2010)

1.4 STANDARD FEATURES AND SPECIFICATIONS

- A built-in user interface & display
- A single 4 – 20 mA output for flow rate
- Two programmable open collector pulse outputs. Outputs may be programmed to provide:
  * an indication of flow direction
  * a scaled pulse for totalizing flow
  * a high resolution frequency output to drive peripheral devices
  * an indication of an alarm condition
- Empty pipe detector
- Internal self-diagnostic functions & fault alarms

CALIBRATION
Flow meters are wet calibrated in a flow laboratory against standards that are directly traceable to government standards. A certificate of calibration accompanies every meter.

ACCURACY
± 0.4% of reading from 3.3 to 33 ft/sec
± 0.8% of reading from 1 to 3.3 ft/sec
± 0.0075 ft/s at flows less than 1 ft/s

PROGRAMMING
Factory programmed for specific application

MEMORY
Nonvolatile memory retains all program parameters and totalized values in the event of power loss.

DISPLAY
Alphanumeric LCD displays total flow, flow rate, flow direction & alarm conditions

OUTPUT SIGNALS
Isolated 4 – 20 mA analog output for flow rate
Two programmable open collector pulse outputs (configurable for frequency, pulse or directional flow)

TEMPERATURE RANGE
Liquid temperature range:
Polypropylene liner: 32° to 140°F
Ebonite liner: 23° to 175°F
PTFE liner: -4° to 212° F (300° F with remote electronics)
Ambient temperature range: -4° to 140°F

MAINTENANCE
Periodically inspect the power supply cables, cable glands and the enclosure for signs of damage. Inspect installation and mounting hardware for loose connections.

MECHANICAL
Electronics Enclosure:
Standard: Nylon NEMA 4
Optional: Remote mount transmitter version, maximum distance from the sensor is 65ft.
Outer Body Material:
Standard: Carbon Steel, Painted
Optional: 316 Stainless Steel
Flow Tube (Internal):
304 Stainless Steel

Connection Type:
Standard: ANSI 150 Class Flange
Optional: ANSI 300 Class Flange
Optional: Wafer
Optional: Threaded Process Connection

ELECTRICAL
This equipment is intended for INSTALLATION CATEGORY (OVERVOLTAGE CATEGORY) II applications.

Input Power - Factory Selectable:
Standard - 90 to 265 VAC, 45 to 66 Hz, and 35 mA maximum
Optional - 10 to 63 VDC, 15 to 45 VAC, 45 to 66 Hz and 300 mA maximum
Overcurrent Protective Device Ratings:
Supply mains overcurrent protective devices with the following ratings:
- 120 VAC 50/60 Hz – 15 A
- 230 VAC 50 Hz – 6 A

Wiring:
Flow signals - Use 18-22 AWG shielded cable
Standard input power - Use a three wire service with one wire a protective earth ground. The installation must comply with all local, state and federal building codes.

Optional input power - Use PVC jacketed copper cable with a wire gauge suitable for the length of run and required maximum current carrying capacity. The installation must comply with all local, state and federal building codes.

PRESSURE AND CONDUCTIVITY
Maximum Operating Pressure
(Exclusive of flange rating)
Ebonite: 1000PSI
Polypropylene: 230PSI
PTFE: 580PSI
Minimum Fluid Conductivity:
5 microsiemens/centimeter

Note: Specifications are subject to change without notice.

B.3. Anemometer(Campbell Scientific Canada Corp., 2010b)

2. Specifications

	05103 *05103-10*	*05106* *05106-10* *05106C* *05106C-10*	*05305* *05305-10*
Wind Speed			
Range:	0-100 m/s (0-224 mph)	0-100 m/s (0-224 mph)	0-50 m/s (0-112 mph)
Accuracy:	±0.3 m/s (±0.6 mph)	±0.3 m/s (±0.6 mph)	±0.2 m/s (±0.4 mph)
Starting Threshold:	1.0 m/s (2.2 mph)	1.1 m/s (2.4 mph)	0.4 m/s (0.9 mph)
Distant Constant (63% Recovery):	2.7 m (8.9 ft)	2.7 m (8.9 ft)	2.1 m (6.9 ft)
Output:	A/C Voltage (3 pulses per revolution) 1800 RPM 90 Hz = 8.8 m/s (19.7 mph)	A/C Voltage (3 pulses per revolution) 1800 RPM 90 Hz = 8.8 m/s (19.7 mph)	A/C Voltage (3 pulses per revolution) 1800 RPM 90 Hz = 9.2 m/s (20.6 mph)
Wind Direction			
Range:	0-360° Mechanical, 0-355° Electrical (5° Open)	0-360° Mechanical, 0-355° Electrical (5° Open)	0-360° Mechanical, 0-355° Electrical (5° Open)
Accuracy:	±3°	±3°	±3°
Wind Speed Resolution:	0.2192 mph or 0.098 m/s (scan rate in seconds)		0.2290 mph or 0.1024 m/s (scan rate in seconds)
Starting Threshold at 10° Displacement:	1.1 m/s (2.2 mph)	1.1 m/s (2.2 mph)	0.5 m/s (1.0 mph)
Delay Distance (50% Recovery):	1.3m (4.3 ft)	1.3m (4.3 ft)	1.2m (3.9 ft)
Damping Ratio:	0.25	0.25	0.45
Damped Natural Wavelength:	7.2m (23.6 ft)	7.2m (23.6 ft)	4.4m (14.4 ft)
Output:	Analog D/C Voltage from 10kohm Potentiometer	Analog D/C Voltage from 10kohm Potentiometer	Analog D/C Voltage from 10kohm Potentiometer
Power	Switched Excitation supplied by the Datalogger	Switched Excitation supplied by the Datalogger	Switched Excitation supplied by the Datalogger

	05103 ***05103-10***	***05106*** ***05106-10*** ***05106C*** ***05106C-10***	***05305*** ***05305-10***
Operating Temperature	-50°C to 50°C, assuming non-riming conditions	-50°C to 50°C, assuming non-riming conditions	-50°C to 50°C, assuming non-riming conditions
Dimensions			
Overall:	37 cm H by 55 cm L (14.6 " H by 21.7 " L)	37 cm H by 55 cm L (14.6 " H by 21.7 " L)	38 cm H by 65 cm L (15.0 " H by 25.6 " L)
Main Housing Diameter:	5 cm (2.0 ")	5 cm (2.0 ")	5 cm (2.0 ")
Propeller Diameter:	18 cm (7.1 ")	18 cm (7.1 ")	20 cm (7.9 ")
Mounting Pipe:	34 mm (1.34 ") OD; Standard 1.0 " IPS Schedule 40	34 mm (1.34 ") OD; Standard 1.0 " IPS Schedule 40	34 mm (1.34 ") OD; Standard 1.0 " IPS Schedule 40
Weight			
Sensor:	1.5 kg (3.2 lbs)	1.5 kg (3.2 lbs)	1.1 kg (2.5 lbs)
Shipping (Approximate):	2.3 kg (5.5 lbs)	2.3 kg (5.5 lbs)	2.3 kg (5.5 lbs)
Cable	Supplied by CSC Standard Length 3.3m (10 ft) Custom Lengths Available	Supplied by RMY / CSC Standard Length 3.3m* (10 ft) Custom Lengths Available * 05106C Standard Length 1m (3.3 ft) + Custom Length (with Connectors)	Supplied by CSC Standard Length 3.3m (10 ft) Custom Lengths Available

B.4. Pyranometer(Campbell scientific Canada corp.,2010c)

2. Specifications

The CMP3-L is an ISO Second Class pyranometer. While the worst case accuracy for daily sums given by Kipp & Zonen is ±10%, the typical accuracy is ±5%.

ISO SPECIFICATIONS:

Response Time 95%:	18 seconds
Zero offset due to 200 W/m^2 thermal radiation:	< 15 W m^{-2}
Zero offset due to temperature change of 5ºK / hr:	< ±4 W m^{-2}
Non stability (% change/year):	< ± 1%
Non linearity (0 to 1000 W/m^2):	< ± 2.5%
Directional error (at 80º with 1000 W/m^2 beam):	< ± 20 W m^{-2}
Temperature Dependence of sensitivity:	± 5% (-10º to + 40ºC)
Tilt response (±80º) (at 1000 W/m^2):	< ± 2%

OTHER SPECIFICATIONS

Expected accuracy for daily sums:	± 10%
Spectral range (50% points, nm):	310 to 2800 nm
Sensitivity:	5 to 20 µV W^{-1} m^2
Typical signal output for atmospheric applications:	0 to 15 mV
Impedance:	30 to 100 Ω
Operating Temperature:	-40º to +80ºC
Max. irradiance:	2000 Wm^{-2}
Detector:	Copper-constantan multi junction thermopile
Level accuracy:	1 degree

DIMENSIONS / SHIPPING DIMENSIONS

CMP3-L:	3 in dia x 4 in / 8x12x4 in

WEIGHT/SHIPPING WEIGHT

CMP3-L:	1.2 lbs / 1.8 lbs

B.5. Immersion Well Temperature Sensor(Seimens Industry Inc. 2013)

Immersion Well Temperature Sensors

Description

The Immersion Well Temperature Sensors monitor and transmit changes in temperature to the building control system. Specific devices within the range are compatible with whatever North American manufactured building automation system you may be installing. They thread into a well in a pipe and sense the medium temperature in the pipe. All sensors incorporate precision temperature sensing elements to accurately and reliably measure temperature.

Features

- Variety of sensing elements
- Suitable for hot or chilled medium
- Responsive to temperature change
- Accurate and reliable indication of temperature
- Familiar installation requires no special tools

Figure 1. Immersion Well Temperature Sensor.

Specifications

Temperature Range	Controller dependent
Output Signals	Changing resistance
Sensing Element Type	NTC Thermistor, Platinum RTD, or Nickel RTD
Accuracy	
NTC Thermistors, mid-range	±1.0°F (±0.5°C)
Pt RTD and Ni RTD, mid-range	±0.75°F (±0.4°C)
Installation	
Wiring	2-conductor: 18 to 22 AWG twisted pair (per code requirements)
Calibration Adjustments	NTC: None required RTD: Adjust for increased temperature offset (a constant) as required, related to added resistance of the field wiring
External Installation Threads	1/2-inch – 14 NPT
Conduit Connection Threads	1/2-inch – 14 NPSMI
Housing Material	Cast zinc
Immersion Well Material	300 Series Stainless Steel

APPENDIX C: SHORTCUT PROGRAM (ATHAUDAGE DONA, 2011)

C.1. Short Cut Program Codes

```
'CR800 Series 'Created by Short Cut (2.8)

'Declare Variables and Units
Public BattV
Public SlrkW
Public SlrkJ
Public WS_ms
Public WindDir
Public SEVolt

Units BattV=Volts
Units SlrkW=kW/m^2
Units SlrkJ=kJ/m^2
Units WS_ms=meters/second
Units WindDir=Degrees
Units SEVolt=mV

'Define Data Tables
DataTable(OneMin,True,-1)
      DataInterval(0,1,Min,10)
      Average(1,SlrkW,FP2,False)
      Totalize(1,SlrkJ,IEEE4,False)
      Average(1,WS_ms,FP2,False)
      Sample(1,WindDir,FP2)
      Sample(1,SEVolt,FP2)
EndTable

'Main Program
BeginProg
      Scan(5,Sec,1,0)
            'Default Datalogger Battery Voltage measurement BattV
            Battery(BattV)
            'CMP3 Pyranometer measurements SlrkJ and SlrkW
            VoltDiff(SlrkW,1,mV25,1,True,0,_60Hz,1,0)
            If SlrkW<0 Then SlrkW=0
            SlrkJ=SlrkW*0.3056235
            SlrkW=SlrkW*0.06112469
            '05103 Wind Speed & Direction Sensor measurements WS_ms and
WindDir
            PulseCount(WS_ms,1,1,1,1,0.098,0)
            BrHalf(WindDir,1,mV2500,3,1,1,2500,True,0,_60Hz,355,0)
            If WindDir>=360 Then WindDir=0
            'Generic Single-Ended Voltage measurements SEVolt
```

```
            VoltSE(SEVolt,1,mV5000,4,True,0,_60Hz,1,0)
            'Call Data Tables and Store Data
            CallTable(OneMin)
      NextScan
EndProg
```

C.2. Programming Steps

C.2.1. Select Sensors

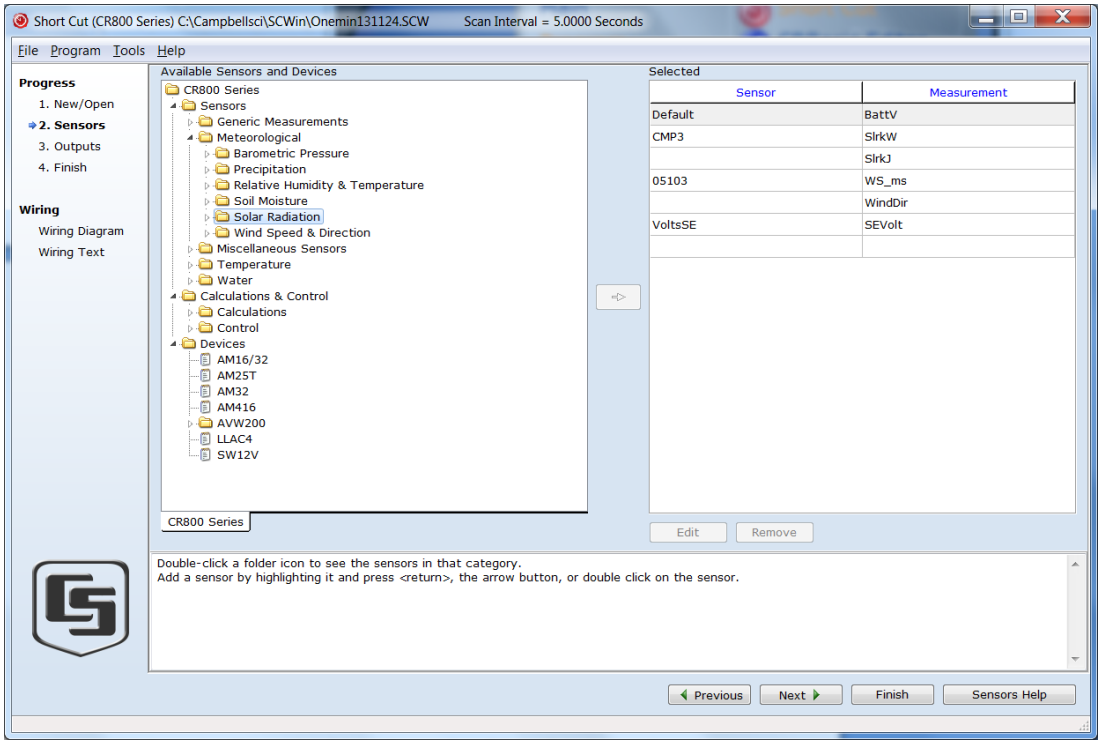

C.2.2. Select Output Units

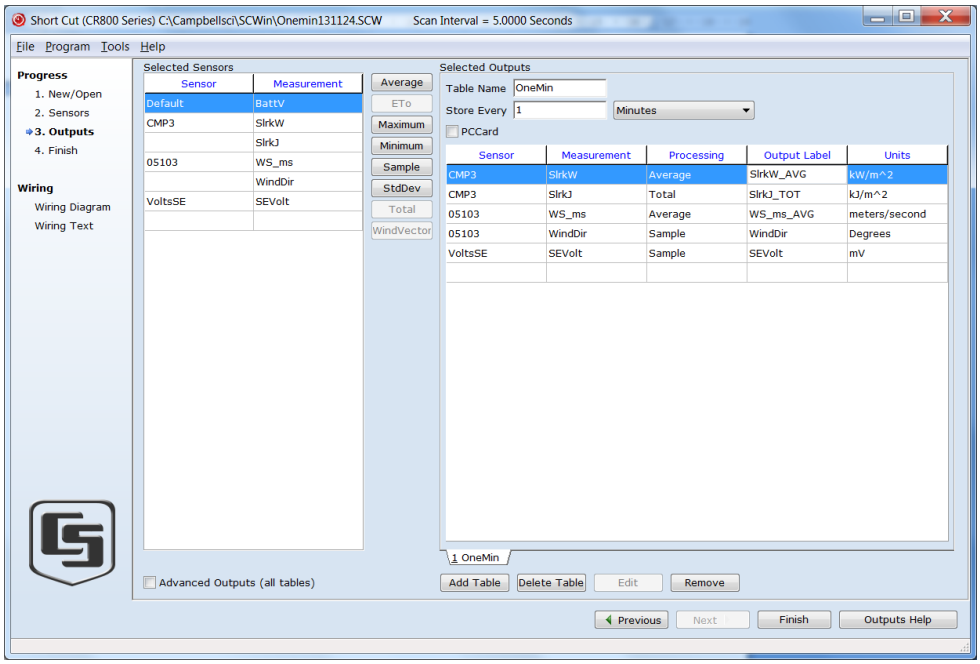

C.2.3. Draw Wiring Diagram

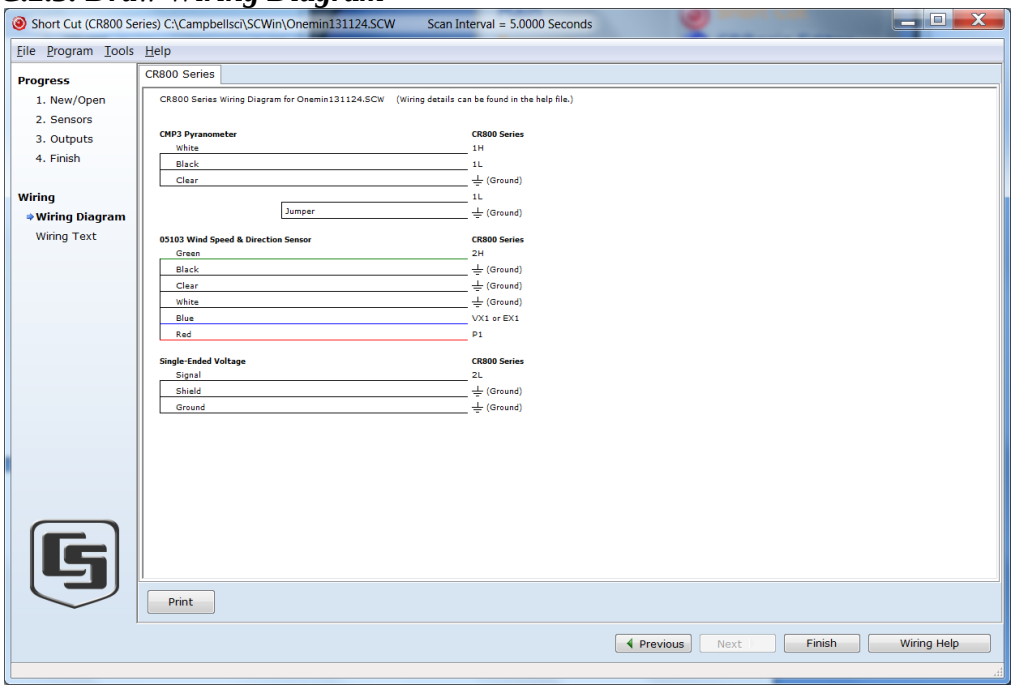

APPENDIX D: BOILING POINT(THE DOW CHEMICAL COMPANY,2003)